Long term HelioClim-3 global, beam and diffuse irradiance validation

Ineichen, Pierre

UNIVERSITÉ DE GENÈVE
INSTITUTE FOR ENVIRONMENTAL SCIENCES

solarXdat //

Long term HelioClim-3 global, beam and diffuse irradiance validation

Pierre Ineichen
University of Geneva
February 2016

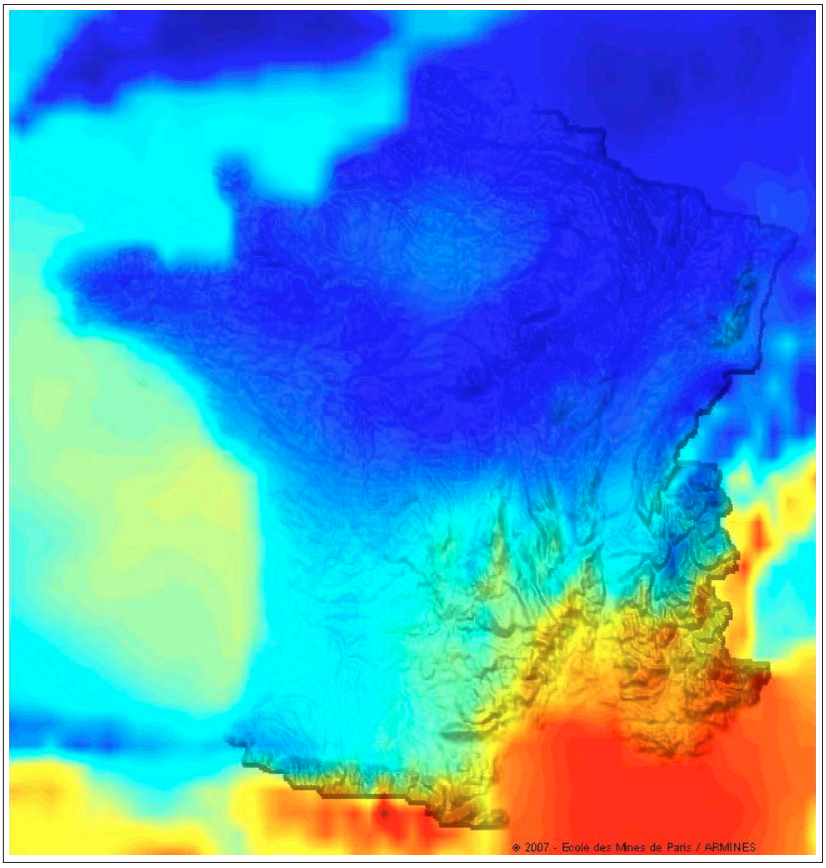

Long term HelioClim-3 global, beam and diffuse irradiance validation

Pierre Ineichen
University of Geneva
February 2016

Abstract

Satellite derived solar radiation is nowadays a good alternative to ground measurements for renewable energy applications. It has the advantage to provide data with a good accuracy, the best time and space granularity, in term of real time series and average year such as TMY.

This report presents results of a long term validation in the European and Mediteranean regions of the irradiance evaluated by the HelioClim-3 scheme in hourly, daily and monthly values, and seven average products on an annual basis. The performance is also put forward with the natural interannual variability.

The main results are:

- the accuracy of the derived hourly global irradiance reaches 20% (standard deviation) with no bias, and 46% for the beam component with a 6% to 9% mean bias,
- the main improvement from version 4 to version 5 comes from the use of a new clear syk model with sub-daily aerosol data as input,
- some systematic patterns are pointed out, depending on the sky type, the site latitude, the aerosol optical depth and the ground snow cover,
- the overall annual uncertainty of the HelioClim-3 scheme is situated within one interannual variability standard deviation for the global component, and within two standard deviations for the beam irradiation,
- the overall performance for the beam component is slightly worse for version 5, but the frequency distributions are improved, particularly for high irradiance values.

Table of content

Nomenclature

G_h or *GHI*	global horizontal solar irradiance or irradiation
G_{hc}	clear sky global horizontal solar irradiance or irradiation
B_n or *DNI*	normal beam (or direct) solar irradiance or irradiation
D_h or *DIF*	diffuse horizontal solar irradiance or irradiation
B_{nc}	clear sky normal beam solar irradiance or irradiation
G_{sat}	modeled solar irradiance or irradiation
G_{mes}	measured solar irradiance or irradiation
I_o	extra-atmospheric solar irradiance
K	clearness or clear sky index
K_t	global clearness index (G_h normalized by $I_o \sin h$)
K_t'	modified global clearness index
K_c	global clear sky index (G_h normalized by G_{hc})
K_d	diffuse clearness index
K_b	beam clearness index
K_{bc}	beam clear sky index (B_n normalized by B_{nc})
T_L	Linke turbidity coefficient
T_{Lam2}	Linke turbidity coefficient at air mass = 2
aod	atmospheric aerosol optical depth
w	atmospheric water vapor content or column
δ_{cda}	aerosol optical depth of a clean and dry atmosphere
δ_w	water vapor atmospheric optical depth
T_a	ambiant temperature at 2m
RH	relative humidity at 2m
h	solar elevation angle
AM	atmospheric air mass
n	cloud index
ρ	planetary albedo
ρ_g	overcast sky planetary albedo
ρ_c	clear sky planetary albedo
mbd	mean bias difference
rmsd	root mean square difference
sd	standard deviation
bsd	bias standard deviation (standard deviation of the bias)
R	correlation coefficient
KSI%	second order Kolmogorov-Smirnov test

1. Introduction

Meteorological satellite images as data sources to evaluate the ground irradiance components become the state of the art in the field of solar energy systems. The strongest argument is the high spatial coverage, and the fifteen minutes temporal granularity. They also have the advantage to provide nowcast data used for example to assess the proper operation of a solar plant. On the other hand, long term ground data are very scarce concerning the beam irradiance. The use of secondary inputs such as polar satellite data and ground information increases significantly the precision of the algorithms, mainly for the beam component. Following a paper from Zelenka et al. (1998) concerning the nuggets effect, the interpolation distance to the nearest ground measurement site is limited to 10 to 30 km, depending on the irradiance parameter; this strengths the satellite derived data argument.

Many universities and private companies provide satellite derived data, freely or for pay, averaged over up to 12 years (Meteosat second generation is operational since April 2004) or in real time (nowcasting), and integrated over different time ranges. The aim of this document is to conduct a long term validation (2004 - 2013) of HelioClim-3 satellite scheme against ground measurements, for both the global and the beam components, and based on hourly, daily and monthly values.

2. Ground data

Data acquired at 22 ground sites are used for the validation, with up to 10 years of continuous measurements; for the validation itself, due to the satellite variability, only data from 2004 to 2013 are used. The data acquired before 2004 are used to illustrate the interannual variability. The list of the stations is given in Table I, with their characteristics. The climate range covers desert to oceanic, the latitude from 20°N to 60°N (with one site at 25°S), and the altitudes from sea level to 1580 meters.

The concerned parameters are the global irradiance on a horizontal plane G_h (or GHI), the normal beam irradiance B_n (or DNI) and the horizontal diffuse irradiance D_h (or DIF). For some sites, only the beam

Table I List of the ground sites with the latitude, longitude, altitude, climate, the acquired parameters and the origin of the data

Site	GHI	DNI	DIF		Lat	Long	altitude	Climate	Data source
Almeria (Spain)	x	x	x	2004 - 2011	37.092	-2.364	491	dry, hot summer	PSA
Bratislava (Slovakia)	x		x	2004 - 2007	48.166	17.083	195	semi-continental	CIE
Cabauw (the Netherlands)	x	x	x	2005 - 2013	51.970	4.930	70	temperate maritim	BSRN
Camborne (Great Britain)	x	x	x	2004 - 2013	50.220	-5.310	88	oceanic	GAW
Carpentras (France)	x	x	x	2004 -2013	44.083	5.059	100	mediternean	BSRN
Davos (Switzerland)	x	x	x	2004 - 2011	46.813	9.844	1586	alpine	PMO/SLF
Geneva (Switzerland)	x	x		2004 - 2013	46.199	6.131	420	semi-continental	CIE
Kassel (Germany)	x	x	x	2004 - 2011	51.312	9.478	173	temperate humide	FhG
Kishinev (Moldavia)	x	x	x	2004 - 2013	47.000	28.817	205	continental humid	GAW
Lerwick (Great Britain)	x	x	x	2004 - 2013	60.133	-1.183	82	cold oceanic	GAW
Lindenberg (Germany)	x	x	x	2004 - 2010	52.210	14.122	125	moderate maritim	BSRN
Madrid (Spain)	x	x	x	2004 - 2011	40.450	-3.730	650	semi-arid	UMP
Nantes (France)	x		x	2004 - 2010	47.254	-1.553	30	oceanic	CSTB
Payerne (Switzerland)	x	x	x	2004 - 2011	46.815	6.944	490	semi-continental	BSRN
Sede Boqer (Israel)	x	x	x	2004 - 2012	30.905	34.782	457	dry steppe	BSRN
Skukuza (South Africa)	x			2006 - 2007	-25.020	31.497	365	steppe, hot arid	CSIR
Tamanrasset (Algeria)	x	x	x	2004 - 2011	22.780	5.510	1400	hot, desert	BSRN
Toravere (Estonia)	x	x	x	2004 - 2013	58.254	26.462	70	cold humid	BSRN
Valentia (Ireland)	x		x	2004 - 2013	51.938	-10.248	14	oceanic	GAW
Vaulx-en-Velin (France)	x	x	x	2004 - 2013	45.778	4.923	170	semi-continental	ENTPE
Wien (Austria)	x		x	2004 - 2013	48.250	16.367	203	continental	GAW
Zilani (Letonia)	x	x	x	2004 - 2009	56.520	25.920	107	cold humid	GAW

or the diffuse component is acquired; the third component is then calculated by difference following the closure equation, the equation connecting together the three irradiance components: $G_h = D_h + B_h$. For one site, the South African site of Skukuza, only the global component is available. For comparison purpose, the beam component is evaluated with the help of the DirIndex model (Perez et al. 1992).

The ground data are kindly provided by the Plataforma Solar de Almeria (PSA & DLR, Spain), the Baseline Surface Radiation Network (BSRN), the Aerosol Robotic Network (Aeronet), the Global Aerosol Watch project (GAW), the CIE International Daylight Measurements Program (Commission internationale de l'éclairage IDMP), the Universidad Politecnica de Madrid (UMP, Spain), the Ecole Nationale des Travaux Publiques (ENTPE, Lyon, France), the Centre Scientifique et Technique du Bâtiment (CSTB, Nantes, France), the Institut für Schnee- und Lawinenforschung (SLF) and the Physikalisch-Meteorologisches Observatorium Davos (PMOD/WRC, Switzerland), the Frauenhofer Institute für Winderergie und Energisystemtechnik (IWES, Kassel, Germany), and the Natural Resources and the Environment, Global Change and Ecosystem Dynamics Research Group (CSIR, South Africa).

High precision instruments (WMO standards) such as Kipp+Zonen CMP10, Eppley PSP pyranometers, and Eppley NIP pyrheliometers, are used to acquire the data. A stringent calibration, characterization and quality control was applied on all the data by the person in charge of the measurements; the coherence of the data for all the stations was verified by the author and is described in section 5.

3. Satellite data: HelioClim-3

Meteosat Second Generation (MSG) images are routinely processed with the Heliosat-2 method (Rigollier 2004) every 15' to update the HelioClim-3 (HC3) database. Heliosat-2 combines a clear sky model with a "cloud index". The cloud index approach is based on the assumption that the appearance of a cloud over a pixel results in an increase of reflectance in visible imagery; the attenuation of the downwelling shortwave irradiance by the atmosphere over a pixel is related to the magnitude of change between the reflectance that should be observed under a cloud-free sky and that is currently observed. This magnitude of change is quantified by the cloud index.

Versions 4 and 5 are the two most advanced versions of HelioClim-3. Version 4 (HC3v4) uses the climatological European Solar Radiation Atlas clear-sky model (ESRA 2000, Rigollier et al. 2000), based on the Linke Turbidity Factor T_L. The climatological database of Linke Turbidity Factor has been estimated using ground measurements worldwide (Remund et al. 2003), and led to one map per month which have been temporally interpolated to generate one map per day. The major drawback of this climatological database is that it was never updated to take into account the attenuation or increase of the atmosphere turbidity due to local effects such as maritime inputs, volcanoes, fires, evolution of the water vapor content, pollution, etc. Version 5 of HelioClim-3 (HC3v5) (Lefèvre et al. 2013) is an attempt to overcome this limitation, by exploiting the new McClear clear sky model (Qu et al. 2014), outcome of the MACC projects (Kaiser et al. 2012). McClear provides updated sub-daily information on the content of the atmosphere, combining both in-situ and satellite inputs.

HelioClim-3 estimates of the Surface Solar Irradiance (SSI) are available at integration periods (or time steps) of 15 minutes, one hour, one day and one month. The temporal coverage of data is from February 2004 up to current day-2 for the version 5, and day-1, real time and even d+1 forecast data for version 4.

HelioClim-3 provides 15 minutes GHI values, on which decomposition models (ESRA 2000) are applied to compute all the components of the radiation over an horizontal, fix-tilted and normal plane for the actual weather conditions. When a request is launched, post-processing layers are applied for instance to modulate the radiation values inside the MSG pixels to take into account the actual elevation of the required location, or to compute the shadowing effect of the far horizon. HelioClim-3 time series can be retrieved either via the SoDa website (www.soda-is.com), or automatically via a machine-to-machine access. Several other value-added services based on this resource are also available as a one-shot request, such as the purchase of a volume of HelioClim-3 time series or Typical Meteorological Years (TMY) on a given area, irradiation maps, measurement completion, etc.

4. Data quality control

Sensor calibration is the key point for precise data acquisition in the field of solar radiation. The radiation sensors should be calibrated by comparison against a sub-standard before the beginning of the acquisition period, and then every year. Due to possible errors and inaccuracies, a post-calibration is difficult to conduct.

The validity of the results obtained from the use of measured data is highly correlated with the quality of the data bank used as reference. Controlling data quality is therefore the first step to perform in the process of validating models against ground data. This essential step should be devised properly and automated in order to rapidly detect significant instrumental problems like sensor failure or errors in calibration, orientation, leveling, tracking, consistency, etc. Normally, this quality control process should be done by the institution responsible for the measurements. Unfortunately, it is not always the case. Even if some quality control procedures have been implemented, it might not be sufficient to catch all errors, or the data points might not be flagged to indicate the source of the problem. A stringent control quality procedure must therefore be adopted in the present context, and its various elements are described in what follows.

If the three solar irradiance components -beam, diffuse and global- are available, a consistency test can be applied, based on the closure equation that link them:

$$B_n = \frac{G_h - D_h}{\sin(h)}$$

where B_n, G_h and D_h are respectively the normal beam irradiance, the horizontal global and diffuse irradiance, and h the solar elevation angle over the horizon.

An a posteriori automatic quality control cannot detect all acquisition problems that could have happened, however. The remaining elements to be assessed are threefold:

- the measurement's time stamp (needed to compute the solar geometry),
- the sensors' calibration coefficient used to convert the acquired data into physical values,
- the coherence between the parameters.

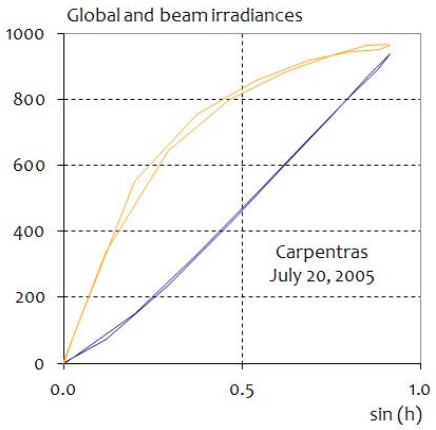

Figure 1 above: G_h and B_n represented versus the sinus of the solar elevation angle for a clear day.

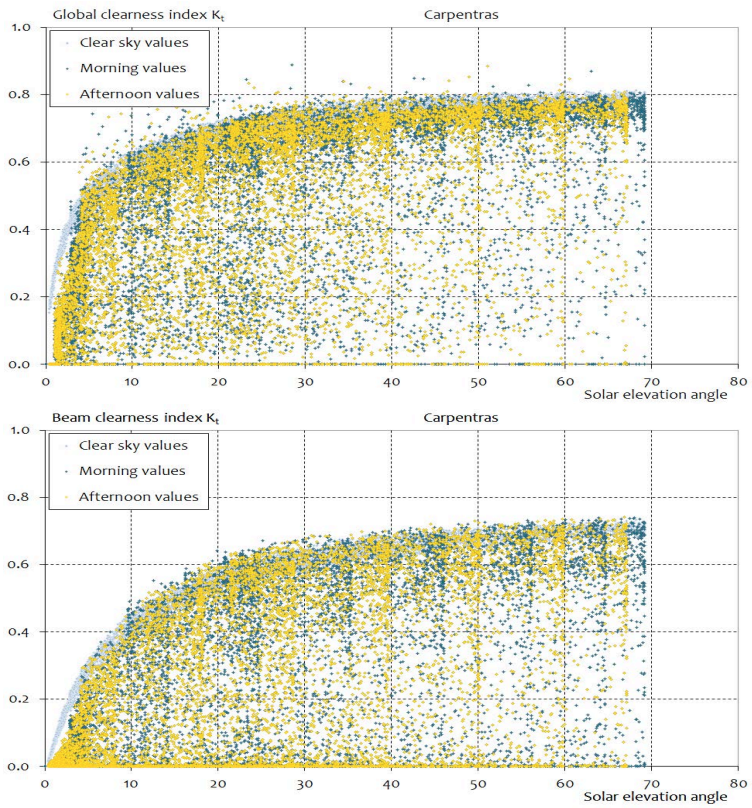

Figure 2 right: K_t and K_b represented separately for the morning (dark blue) and the afternoon (yellow) data, versus the solar elevation angle for hourly values acquired in Carpentras.
Corresponding clear sky model data are represented in light blue.

4.1 Time stamp

To detect a possible time shift in the data, the symmetry (with respect to solar noon) of the irradiance for very clear days is visually checked. The global horizontal and direct normal irradiances are plotted versus the sine of the solar elevation angle for specific clear days. If the time stamp is correct, the afternoon curve should normally lie over the morning curve as visualized in Figure 1. Exceptions do occur, however, at sites where the atmospheric turbidity changes during the day, due for example to topography-induced effects, where the clear-sky irradiance can be significantly different in the afternoon than in the morning. As the global irradiance is less sensitive to turbidity, the accordance morning/afternoon is of more importance for the global component.

If this test is positive, verification can be done with the help of the global clearness indices K_t and K_b defined respectively as:

$$K_t = \frac{G_h}{I_o \cdot \sin(h)} \qquad K_b = \frac{B_n}{I_o}$$

where I_o is the extraterrestrial solar irradiance (i.e. the solar constant corrected for the actual sun-earth distance). The clearness index is then plotted for the morning and afternoon data separately, e.g. using different colors. The upper limit, representative of clear-sky conditions, should lie over for the morning and the afternoon data as represented in Figure 2 for 3 years of global and beam irradiance data acquired at Carpentras (France). Ideal hourly clear-sky values, calculated with the Solis model (Müller et al 2004, Ineichen 2008), are plotted in light blue on the same graph. This test is very sensitive since a time shift of only a few minutes will conduct to a visible asymmetry.

When these two conditions (symmetry around solar noon and consistency of envelope) are fulfilled, the time stamp of the data bank can be considered correct, and the solar geometry can be precisely calculated.

4.2 Sensor calibration

The sensors' calibration can be verified for clear sky conditions by comparison against data from a nearby station or with the help of additional measurements. To conduct this test, for each day, the highest hourly values of G_h and B_n are selected from the measurements and plotted against the day of the year as illustrated on Figure 3. These points are representative of the clearest daily conditions. As the highest value for each day is selected, the upper limit normally represents clear-sky conditions (for G_h, it happens that higher-than-clear-sky values are obtained under partly cloudy or scattered clouds, high-sun conditions, this is why this test should not be applied for data with time granularity lower than hourly). On such graphs, data from nearby sites, or from different years for the same site can be compared.

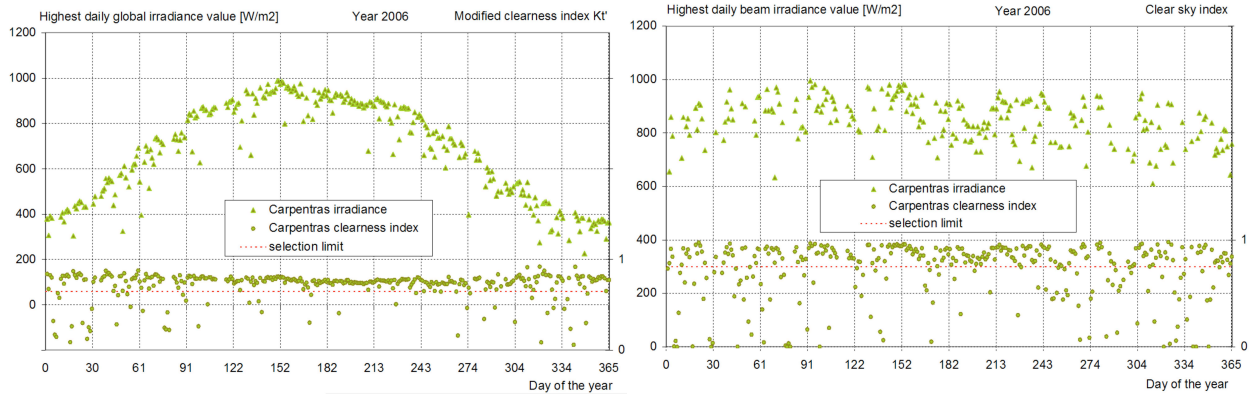

Figure 3 Daily highest value of respectively the global and the beam irradiances reported versus the day of the year for the station of Carpentras. The corresponding modified clearness index and clear sky index are also represented.

The G_h graphs can be augmented by superimposing the modified clearness index K_t', which was defined by Perez and Ineichen (1990) as:

$$K_t' = \frac{K_t}{(1.031 \cdot \exp(-1.4 / (0.9 + 9.4 / AM)) + 0.1)}$$

where *AM* is the optical air mass as defined by Kasten (1980). This modified clearness index has the advantage of being relatively more independent from the solar elevation angle than K_t. Therefore, it is possible to delineate three K_t' zones to characterize the sky condition (Ineichen 2009):

clear-sky conditions	$0.65 < K_t' \leq 1.00$
intermediate sky conditions	$0.30 < K_t' \leq 0.65$
cloudy sky conditions	$0.00 < K_t' \leq 0.30$

In the upper part of Figure 3, only values with $K_t' > 0.65$ are represented.

For B_n, the clear-sky index is defined as:

$$K_{bc} = \frac{B_n}{I_o \, e^{-MA \cdot (\delta_{cda} + \delta_w)}}$$

where δ_{cda} is the broadband clean and dry atmosphere optical depth, and δ_w is the atmospheric water vapor optical depth. These two broadband optical depths can be evaluated following Molineaux et al. (1998) with simplified expressions:

$$\delta_{cda} = -0.101 + 0.235 \cdot AM^{-0.16} \qquad \delta_w = 0.112 \cdot AM^{-0.55} \cdot w^{0.34}$$

The denominator of K_{bc} is representative of the beam irradiance transmitted by a clean atmosphere. K_{bc} is represented on the right graph of Figure 3. On the upper part, only values for K_{bc} higher than 0.8 are represented.

The sensor calibration's correctness can then be assessed by comparison if data from a nearby site are available. If not, this can alternatively be done with the help of a clear-sky radiative transfer model when the atmospheric aerosol optical depth (*aod*) and the total water vapor column (*w*) are known. The long term stability of the calibration can also be assessed with this method by plotting on the same graph several years of data in different colors.

In the first case, it can be assumed that clear conditions result in similar irradiances if the sites are not too far one from the other, and are in similar climate situations. The upper limits of the compared plots should therefore coincide. This is illustrated on Figure 4 for the sites of Toravere and Zilani, situated at 200 km one from the other and under similar climates.

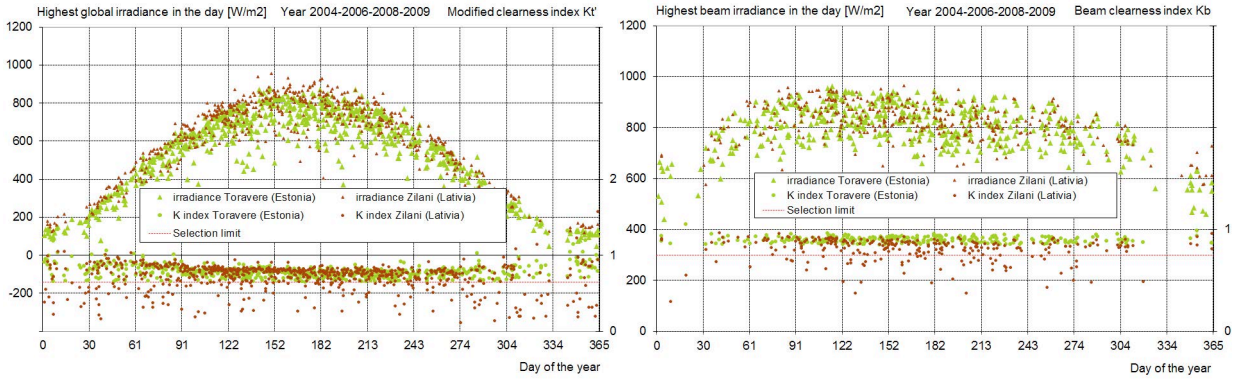

Figure 4 Comparison of measurements from two nearby (200km) sites: daily highest value of the global irradiance reported versus the day of the year for the station of Toravere and Zilani, for the irradiance components and the corresponding modified clearness index.

In the second case, *aod* and *w* data may be retrieved from independent ground-based sunphotometer networks such as the AErosol RObotic NETwork (Aeronet), if a station is close to that of the radiometric station being investigated. These quantities are measured automatically at 15-minute intervals by Aeronet stations. Since only data acquired under direct sun conditions are valid, the original data stream (Level-1) is analyzed to filter out non-sun conditions (Level-1.5). Further corrections are applied to reflect any change in calibration or quality-control issues (Level-2). Level-2 data should be used whenever possible since they are of the best possible quality. Individual values are then averaged to obtain a daily value. The same procedure can be done for *the* total water vapor column *w*. In case it is not measured by a nearby Aeronet or similar network, it can be evaluated from the ground ambient temperature T_a and relative humidity *RH* by the use of an empirical model, such as Atwater's model (Atwater and Ball 1976). The latter method is approximate, but spatially extrapolating actual measurements also introduces errors, so that there is no perfect method in most cases. When temperature and/or humidity data are missing, the data from a neighboring station can be used, or as a last resort (and much larger errors), monthly average from climatic data banks. These *aod* and *w* values are then used with a clear sky model (Solis clear-sky radiative model (Muller et al. 2004, Ineichen 2008), or CPCR2 (Gueymard 1989)) to evaluate the clear-sky hourly G_h and B_n values. These are plotted on the same graphs than above, as shown in

Figure 5 for measurements from Carpentras. On these graphs, the upper limits of the irradiance values and of the clearness indices obtained with the two methods should show similar upper limits.

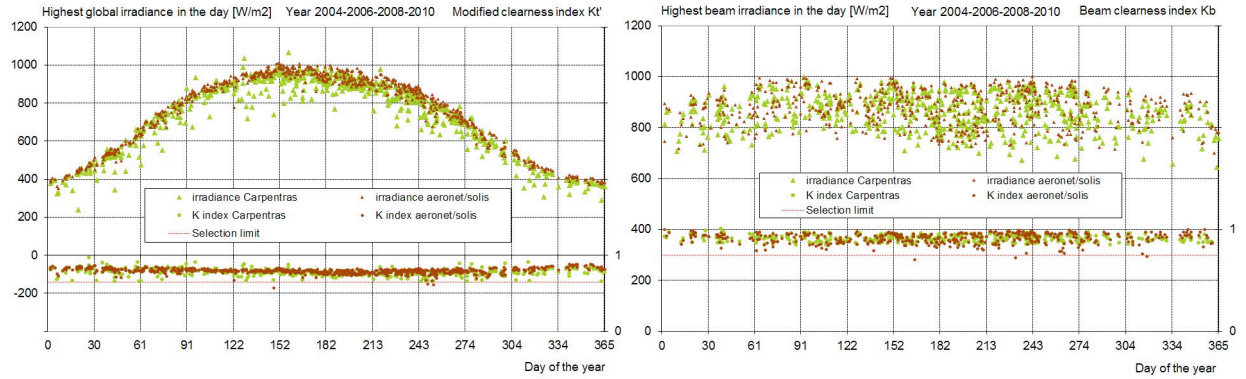

Figure 5 Comparison of the clear sky irradiance obtained from BSRN measurements and evaluated with the solis model with aeronet data.

To quantitatively assess the correctness of the calibration factor, a linear regression is applied on the clear condition selected hourly values (as defined in section 5.2) , between the two sets to be compared. This is illustrated in Figure 6 for the two components. The regression line is also shown for each case, its slope is representative of the calibration error.

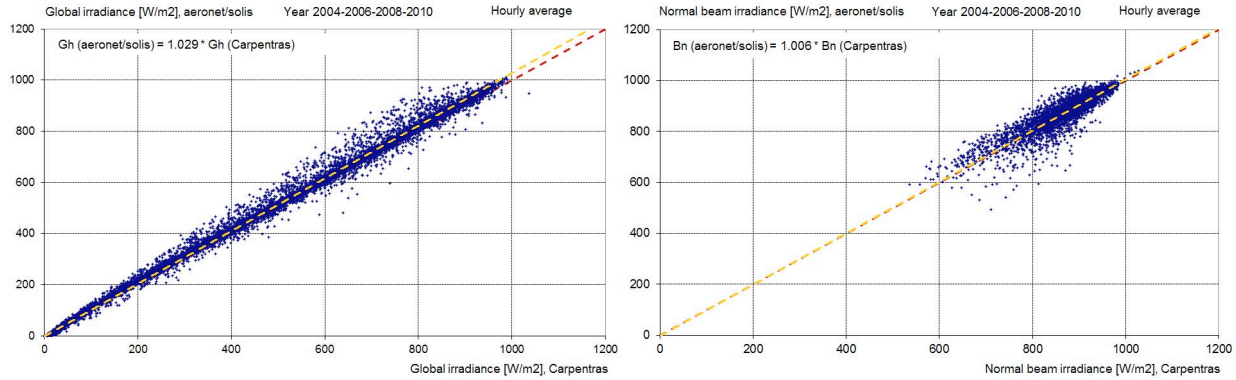

Figure 6 Scatter plots of the two data sets for the global and the beam components. The red dashed line given on the graph is representative of the calibration coefficient discrepancy.

In the latter case, the irradiance components can be compared year by year for the same site in order to assess the stability of the measurements. Here again, the upper boundary should not change from one year to the other, if there are no significant changes in the turbidity and/or the humidity. An example is given on Figure 7 for measurements acquired in 2006 and 2010 at Carpentras. Considering the whole period used in the validation, a calibration coefficient shift can be pointed out by this method.

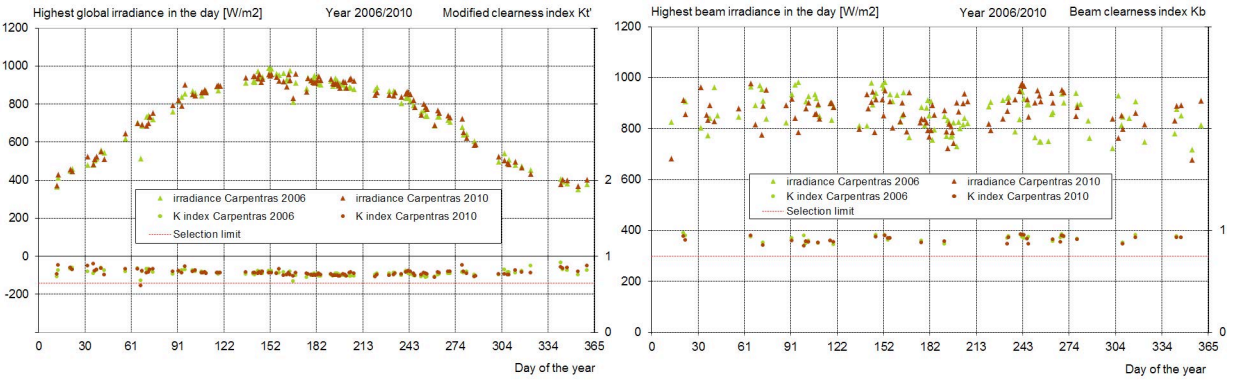

Figure 7 Comparison between two different years of BSRN measurements: same representations as in Figure 3 and 5

4.3 Components consistency

The consistency test between the G_h and B_n components can be verified with the help of the global and beam clearness indices.

The hourly beam clearness index K_b is plotted versus the corresponding global index K_t as illustrated for the site of Carpentras on Figure 8. On the same graph, the clear-sky predictions from the Solis radiative model are represented for four different a priori values of *aod*. The corresponding Linke turbidity coefficient T_{Lam2} is then calculated from the B_n thus obtained:

$$B_n = I_o \cdot e^{(-\delta_{cda} \cdot T_{Lam2} \cdot AM)}$$

T_{Lam2} is evaluated for $AM = 2$ and its correspondence with *aod* is also indicated on the graph (Ineichen 2008c)
. Any important deviation between the predicted and measured clear-sky values indicates calibration uncertainties, pyrheliometer misalignment, soiled or shaded sensors, or miscategorization of clear-sky conditions.

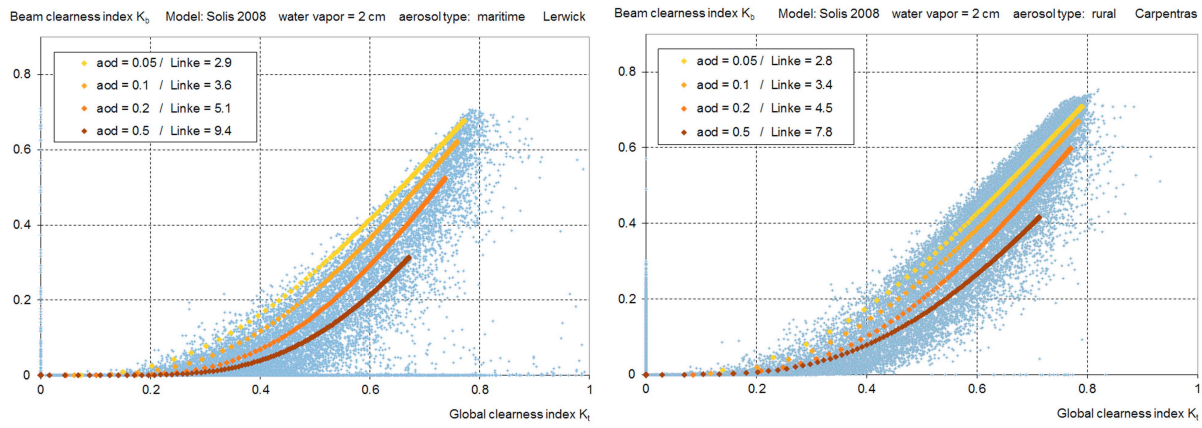

Figure 8 The beam clearness index is plotted against the global clearness index for Lerwick (maritime) and Carpentras (rural). On the same graph, clear sky modelled values are represented for 4 different aerosol loads. The corresponding Linke turbidity coefficients are also indicated

When the three components, global, diffuse and beam, are available, the closure equation can be applied. Due to the measurement methods for each of the components, the strict equality cannot be verified for all the values and acceptability limits are to be defined. For example:

- the BSRN quality control is the following:

$$\frac{G_h}{[D_h + B_n \sin(h)]}$$ should be within 8% for $h > 15°$ and 15% for $h \le 15°$

for $$D_h + B_n \sin(h) > 50 \left[\frac{W}{m^2}\right]$$

- the SERI quality control for the closure is defined as follow

$$K_t = K_d + K_b \pm 0.03$$

- closure equation applied in this report:

if $$B_{ncalc} = \frac{G_h - D_h}{\sin(h)} \quad \text{and} \quad B_{limit} = 1.1 \cdot B_n + 50 \left[\frac{W}{m^2}\right]$$

then $B_n + \text{abs}(B_n - B_{ncalc}) < B_{limit}$

These different quality controls are illustrated in the Figure 9 where the kept hourly values are represented in blue.

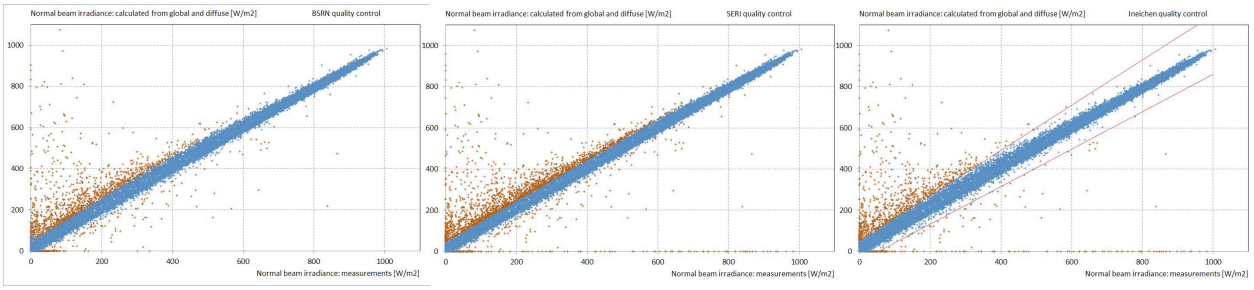

Figure 9 Closure equation: quality control applied on the beam irradiance when the three components are available. The selected hourly values are represented in blue. For the QC applied in this report, the limit is also reported on the graph.

5. Model-measurements hourly, daily and monthly comparison indicators

5.1 *First order statistics*

The most conventional comparison indicators are the mean bias difference (*mbd*), the root mean square difference (*rmsd*), the standard deviation (*sd*) and the determination coefficient (*R*); they represent a quantification of the model dispersion and are defined as follow:

$$mbd = \frac{\sum(G_{sat} - G_{mes})}{N} \qquad rmsd = \sqrt{\frac{\sum(G_{sat} - G_{mes})^2}{N}}$$

$$sd = \sqrt{\frac{\sum\left(G_{sat} - \overline{G_{mes}}\right)^2}{N}} \qquad R = \frac{\sum\left(G_{sat} - \overline{G_{sat}}\right)\cdot\left(G_{mes} - \overline{G_{mes}}\right)}{\sqrt{\left(\sum\left(G_{sat} - \overline{G_{sat}}\right)^2\right)\cdot\left(\sum\left(G_{mes} - \overline{G_{mes}}\right)^2\right)}}$$

where G_{mes} and G_{sat} represent respectively the measured and the modeled irradiance. The *mbd* gives an indication of the systematic bias of a model. Even if the average bias over all the sites is small, it can be highly variable from one site to the other. Therefore, the standard deviation of the biases (bias standard deviation *bsd*) is evaluated, it give an indication of the spatial stability of the model.

Comparison can also be done in terms of frequency of occurrence and cumulated frequency of occurrence: for the irradiance, it gives an indication of the repartition for each level of radiation, and for the clearness index for hourly values, it assesses that the modeled level of radiation occurs at the right time during the day. The obtained graph is a line (or a bar chart) representative of the relative frequency of occurrence of the considered parameter. This is illustrated on Figure 10 (left) for the normal beam clearness index K_t. On the same graph, the frequency of occurrence of the ground measurements is represented as grey bars, and the two version of HelioClim-3 in color lines. On the right graph, the cumulated frequency of occurrence is represented.

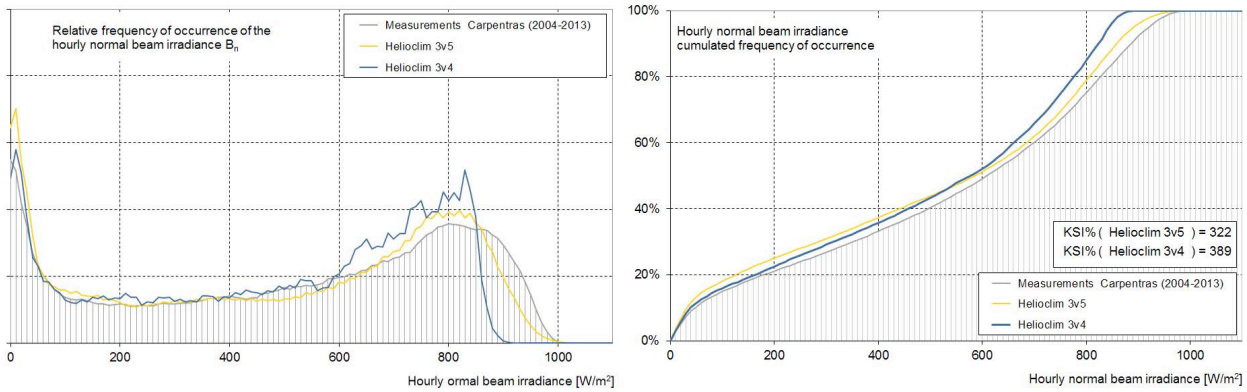

Figure 10 Relative frequency of occurrence of the clearness index (left) and the cumulated frequency of occurrence of the beam irradiance for the measurements (grey) and the two version of the model (right).

5.2 *Second order statistics*

A second order statistic, the Kolmogorov-Smirnov test (Massey et al. 1951, Espinar et al. 2009), is also applied on the data. It represents the capability of the model to reproduce the frequency of occurrence at each of the irradiance level. In order to avoid a peak at the zero level of the beam irradiance, these values are excluded from the statistic. A visualization is given on Figure 10 (right) where the irradiance cumulated frequency of occurrence is represented against the irradiance for the same site than above. The quantitative value representative of the Kolmogorov Smirnov test Integral (*KSI*) is defined as:

$$KSI = \int_{G_{\min}}^{G_{\max}} \left| F_c\left(G_{sat}\right) - F_c\left(G_{mes}\right) \right| \cdot dG_{mes}$$

where $F_c(G_{mes})$ and $F_c(G_{sat})$ are respectively the irradiance ground measurements and the corresponding modelled cumulated frequencies of occurrence. *KSI%* is then obtained by normalizing *KSI* by a critical value depending on the number of events, the lower the value is, the closest the model is to the measurements. The obtained *KSI%* values are given on the graph in Figure 10 (right).

These statistical parameters include dispersions introduced by:

- the retrieval procedure,
- the comparison of point measurements (ground data) with area measurements (pixels),
- the comparison of the average of four instantaneous measurements with 60 minutes integrated values.

5.3 *Model-measurements difference distribution*

In terms of validation, when evaluating satellite derived parameters with the same time step, the comparison can be done by means of scatter plots; these give a visual evaluation of the capability of the model to reproduce the measurements. On such graphs, the 1:1 diagonal line is representative of an ideal model, and the points should lie around this line. An illustration is given on Figure 11 for hourly and daily values.

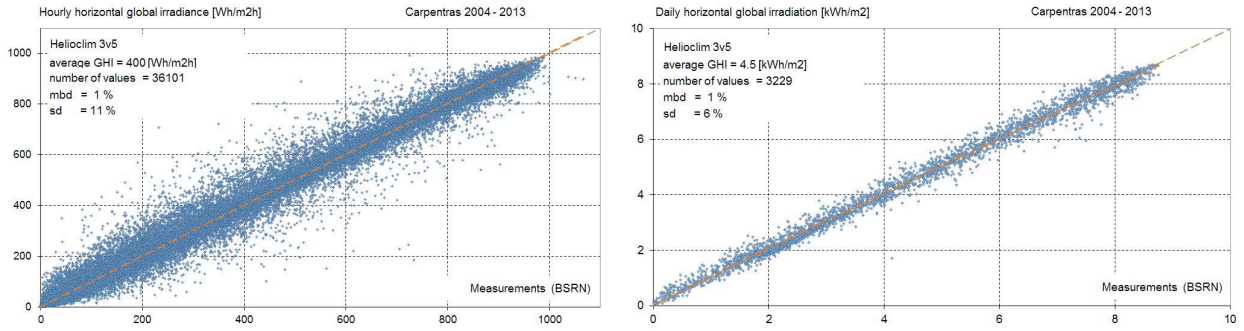

Figure 11 Hourly and daily modeled against measured global irradiance at the site of Carpentras for the whole considered period.

On Figure 12, the distribution of the difference between the model and the measurements around the 1:1 axis for hourly values is represented in term of frequency of occurrence for the whole period (in addition, inthe annex, for the months of April and August). On the same graph, the cumulated frequency of occurrence is also represented. For good results, this curve should be as steep as possible, and cross the 50% value on the zero axis of the horizontal scale. The cumulated frequency is given every two months on a separate graph (Figure 12, right). The same representations are given for the three radiation components and all the sites in the annex where *n* referes to the three irradiance components: global (g), normal beam (b) and diffuse (d) (see Figures a-10n to a-13n in the annex).

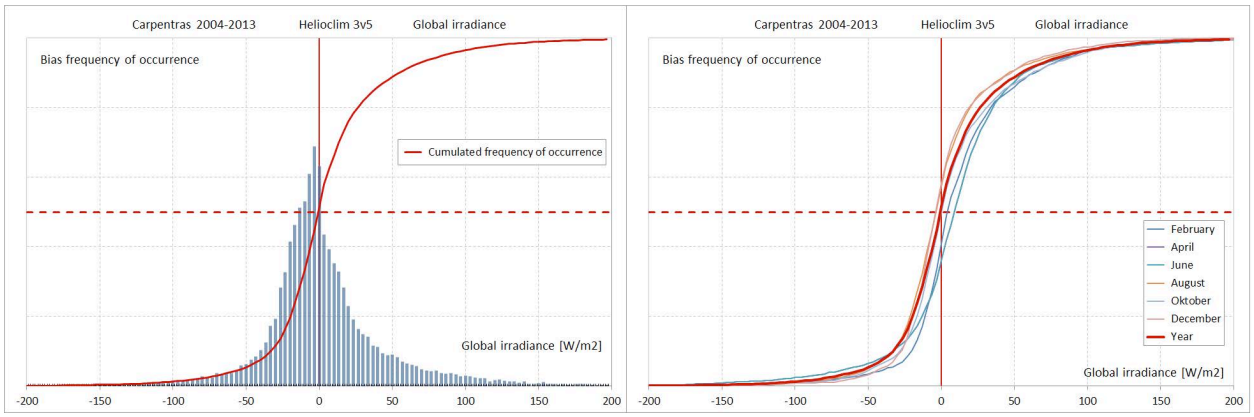

Figure 12 Model-measurements difference distribution (left) between model and measurements for the HelioClim-3v5 model and the site of Carpentras. On the right graph, the cumulated frequency of occurrence is given for 6 months.

6. Interannual variability analysis method

The annual global and beam irradiation values are analyzed year by year. A reference period covering the years 2004 to 2010 will guide the evaluation of the different products. The yearly total determined by the average over this reference period is used as normalization value for all the annual totals. This normalized average (= 100%) is represented on the Figure 13 by the first blue bar from the left and labelled *2004-2010 average*. A standard deviation is calculated over the 8 years reference period, it is represented on the graph by the light orange zone surrounding the 100% line.

The following values are represented on Figure 13:

- the year per year annual ground irradiation measurements are represented by blue bars,
- the average or typical data banks values, satellite based or ground measurements, are represented by the yellow bars on the left part of the graph,
- the year per year HelioClim-3v4 data are represented by the orange bars,

- the year per year HelioClim-3v5 data are represented by the green bars,
- the annual deviation from the 100% reference period average is represented by the red bars for the typical year data, left part of the graph,
- the ground measurements annual deviation from the reference period are represented by the brown bars, right part of the graph.

This method implies that there are no missing values in the evaluation of the yearly total. As this is not always the case, and to circumvent the elimination of too many data, a correction has to be applied as described in section 7.4.

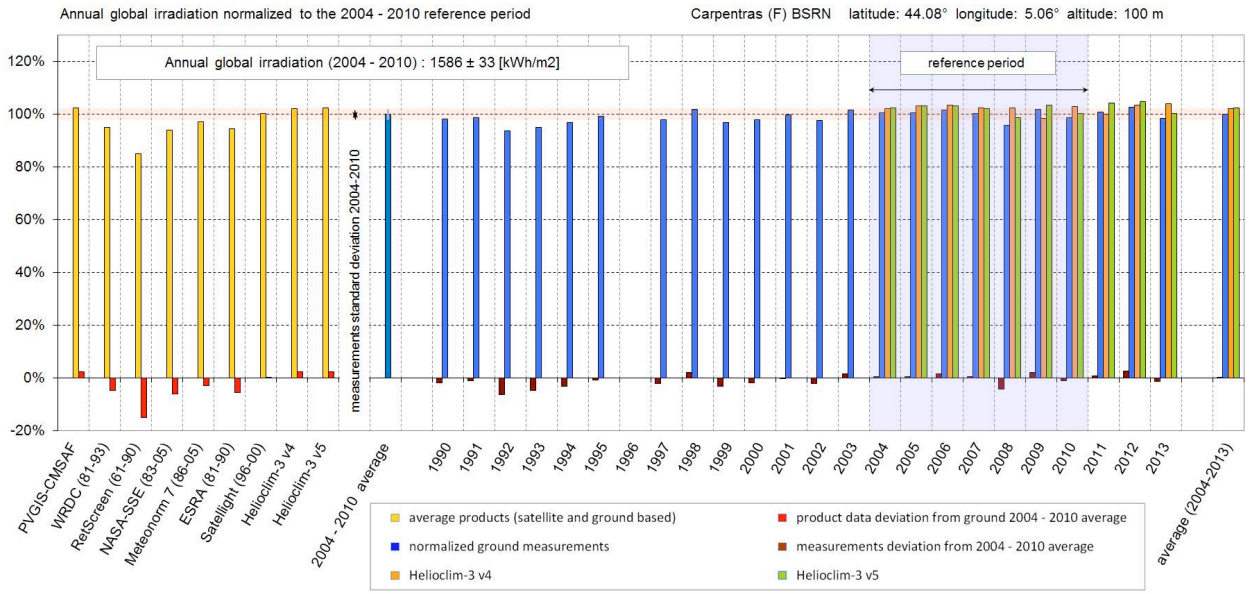

Figure 13 Total annual irradiation normalized to the average annual value over the reference period (2004-2010) for the site of Carpentras.

7. Ground data validity assessment, calibration and stability

The first step in a model validation procedure is to assess the validity of the ground measurements. This can be done by applying a stringent quality control. If some simple errors like a time shift in the data can be corrected, the suspicious data should be discarded. After having confirmed the time stamp in the data banks (see section 4.1), the following tests are applied on the time series.

7.1 Comparison with Aeronet network

For 6 of the 22 ground measurements sites, data from a nearby Aeronet station are used to assess the calibration coefficient of the instruments. These are Carpentras (France), Davos (Switzerland), Madrid (Spain, only for 2012), Sede Boqer (Israel), Tamanrasset (Algeria) and Toravere (Estonia). The Solis clear sky model (Müller et al. 2004, Ineichen 2008) is used to evaluate the global and beam irradiance from the aerosol optical depth *aod* and the water vapor content *w* of the atmosphere.

To validate the calibration coefficient applied during the measurements, the clear sky values are selected from the measured data (see section 4.2), and compared with the corresponding values derived from the Aeronet data and the Solis model.

For all the sites except Davos, Table II shows small differences between the sets of data, less than 2% in the average, these effects are not significant enough to consider a calibration adaptation (see for example, Figure 7 for the site of Carpentras).

The site of Davos shows differences of the order of 5% between spring and autumn, probably due to snow effects.

Table II List of the ground sites with year by year period of comparison, the aeronet convergent period, the results of the closure test, and the percentage of acquired monthly values considered for the interannual variability.

Site	year per year comparison		aeronet comparison	Remark	Closure equation	Interannual	
	global irradiance	beam irradiance	G_n and B_n			Gh	Bn
Almeria (Spain)	1997-2013	2001-2012	n/a	none	96%	100%	99%
Bratislava (Slovakia)	1994-2013	1993-2013	n/a	none	n/a	100%	100%
Cabauw (the Netherlands)	2005-2013	2005-2013	2005-2013	Gh(aero/solis) > Gh(bsrn) [around 2%] Bn(aero/solis) ≈ Bn(bsrn)	91%	99%	99%
Camborne (Great Britain)	1990-2013	2005-2013	n/a	none	93%	99%	93%
Carpentras (France)	1990-2013	1997-2013	2003-2011	Gh(aero/solis) > Gh(bsrn) [around 2%]	85%	99%	99%
Davos (Switzerland)	1995-2013	1995-2011	2006-2011	Bn 20% to high from Dec. 1999 to Feb 2000 Aeronet Gh 5% higher in spring than in autumn	69%	97%	91%
Geneva (Switzerland)	1990-2013	1998-2013	n/a	Gh compatible with Payerne and Vaulx-en-Velin	n/a	97%	95%
Kassel (Germany)	2003-2012	2003-2012	n/a	none	95%	98%	98%
Mt Kenya (Kenya)	2004-2007	2004-2007	n/a	no continuous data	n/a	n/a	n/a
Kishinev (Moldavia)	2003-2013	2003-2013	n/a	none	97%	100%	100%
Lerwick (Great Britain)	2001-2013	2001-2013	n/a	none	99%	94%	90%
Lindenberg (Germany)	1995-2010	1995-2006	n/a	none	92%	100%	100%
Madrid (Spain)	2004-2013	2004-2013	2012	Gh and Bn within 2-3% with aeronet Bn: low amount of data for interannual validation	87%	98%	87%
Nantes (France)	1995-2013	1995-2010	n/a	none	n/a	99%	94%
Payerne (Switzerland)	1993-2013	1994-2009	n/a	Gh compatible with Geneva	78%	100%	97%
Sede Boqer (Israel)	2003-2011	2003-2011	1996-2010	Bn(aero)<Bn(bsrn) [2% summer] Gh 2% to high from 2005-2008	91%	100%	94%
Skukuza (South Africa)	2004-2007	n/a	2004-2007	Gh(aero/solis) > Gh(bsrn) [around 2%]	n/a	n/a	n/a
Tamanrasset (Algeria)	1995-2013	1995-2013	2006-2009	Gh, very clear conditions, at noon, 5% underestimation by aeronet/solis 1% overestimation by aeronet/cpcr2	93%	100%	99%
Toravere (Estonia)	1999-2013	1999-2013	2002-2009	none	90%	100%	99%
Valentia (Ireland)	1996-2013	1996-2013	n/a	none	98%	100%	100%
Vaulx-en-Velin (France)	1993-2013	1993-2013	n/a	1995-2004 Gh and Bn to high (5-9%)	94%	97%	96%
Wien (Austria)	1994-2013	1994-2013	n/a	none	n/a	100%	97%
Zilani (Letonia)	1991-2009	1991-2009	n/a	Gh 10% to low in 1999 Gh 15% to high in 2003	90%	99%	98%

7.2 Long term stability

For the long term stability test, one can assume that the highest global and beam irradiance values do not vary significantly from one year to the other, and that a steep variation should be an issue of a calibration drift, more particularly when the effect disappears abruptly, i.e. in the case of a re-calibration of the sensors.

The long term stability is verified by comparing year by year the highest values of the hourly global and beam irradiance (see Figure 7). This analysis pointed out some significant drifts given in Table II for the following data:

- Davos: the beam irradiance is 20% too high from December 1999 to February 2000. This period is not included in the validation, but is integrated in the interannual variability analysis,
- Vaulx-en-Velin: the irradiance is 5% to 9% too high from 1995 to 2004,
- Zilani: the global irradiance is 10% too low in 1999, and the beam is 15% too high in 2000. Here also, it is not included in the validation period.

After applying the corresponding coefficients on the data, the quality control show normal behavior.

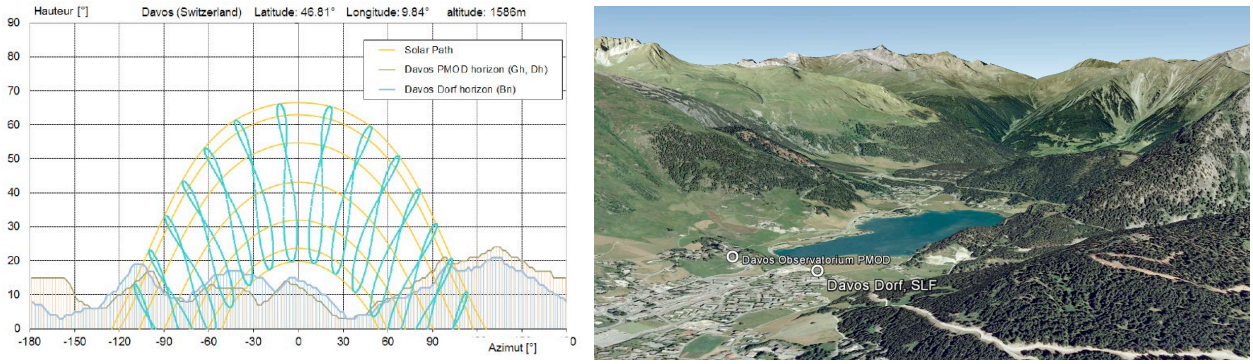

Figure 14 Horizon of the two sites of Davos PMOD and Davos SLF. The sky view factors do not differ, but slight differences can occur on the beam component.

7.3 Components coherence

The component coherence is verified according to section 4.3 with the help of the closure equation when the three components are available. The results of the coherence test are given in Table II in term of a percentage of data kept after the test. This percentage stays between 69% and 100%.

The lowest value, 69%, is the result for Davos, where the beam component is not acquired in the same location than the global and the diffuse; a slight difference in the time stamp is also possible. In addition, the distance between two sites is about 300 meters, Davos is in a valley and the two horizons are slightly different as shown on Figure 14. If the effect on the global irradiance is not visible, the sky view factors are similar, the beam component can be influenced by this difference.

The closure equation is applied on the normal beam component which is very sensitive for low solar elevations, and therefore, values of 90% are satisfactory.

Some sites like Leerwick shows a very high percentage of kept data, even if the three components are stamped as separate measurements at the WRDC server. It is probable that the third component is retrieved from the two others.

For the sites where only two components are available, the closure equation is not applicable, and 100% of the data are kept.

The second coherence test is done on only the global and the beam component by comparing the corresponding clearness indices (Figure 8 in section 4.3). This test is applied indifferently on beam measurements, or beam evaluated from global and diffuse irradiances. For this test, only two sites show singularities:

- as shown on Figure 15, the beam clearness index in Lerwick (A) shows values that seems too low compared with the clear sky model Solis which is also represented on the Figure for four different aerosol optical depths. For comparison, the same graph is given for the site of Almeria (B). This is confirmed with the diffuse fraction (G_h / D_h) test given on (C) where the fraction is high compared to the clear sky model. This test is applied on only the global and the diffuse components and is independent from the beam. This can be a result of very high permanent turbidity. The closure test is coherent.

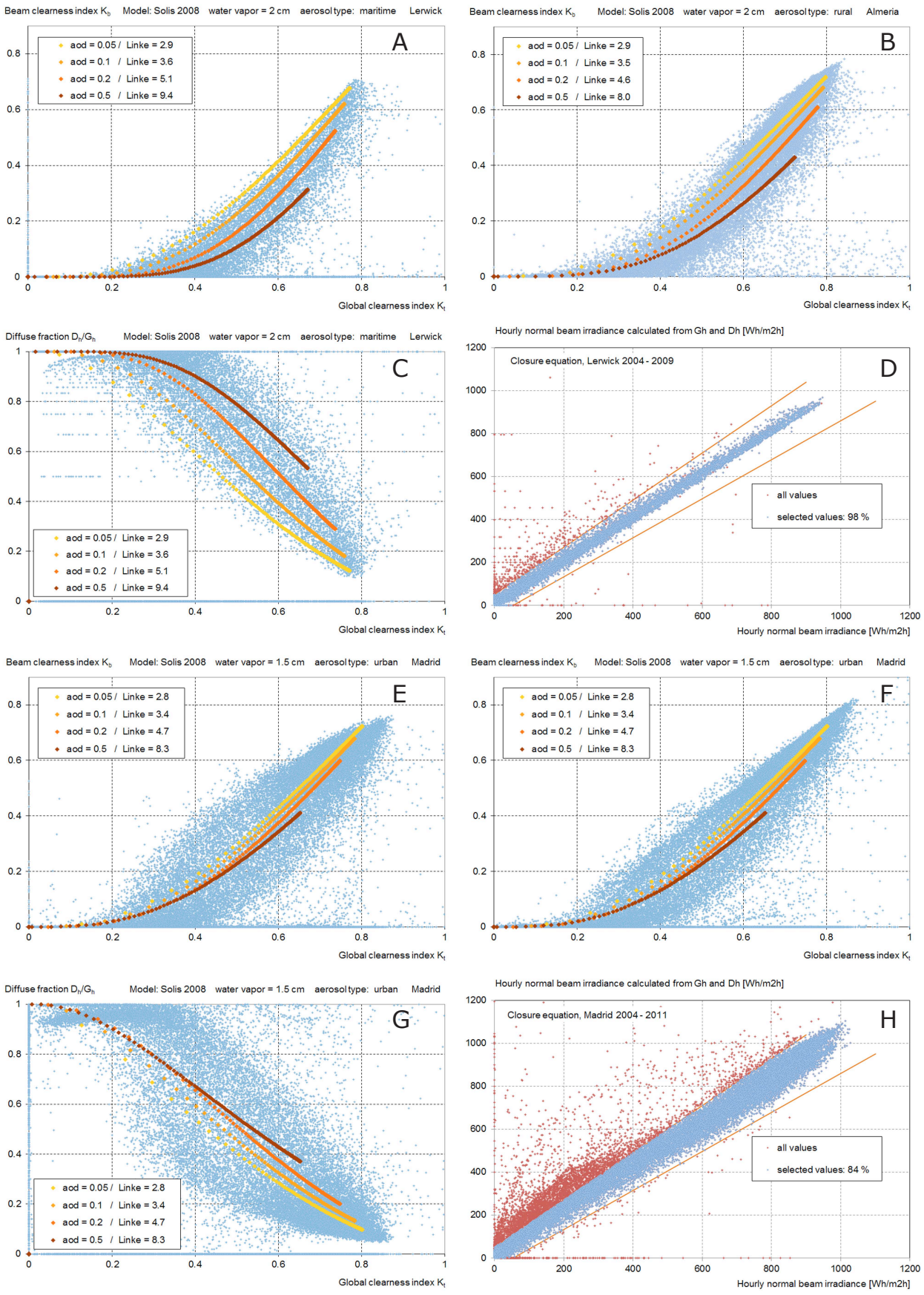

Figure 15 Components coherence test. Site of Lerwick: (A) K_b versus K_t, slightly too low beam component compared to the Solis clear sky, and (C) diffuse fraction versus K_t, slightly too high diffuse. The closure equation (D) gives good results. (B) Site of Almeria is given for comparison purpose.
(E) to (G) Site of Madrid: (E) and (G) it is the only site with these specific shapes. Slight improvement when representing the beam evaluated from the global and the diffuse (F). The closure equation (H) shows high discrepances.

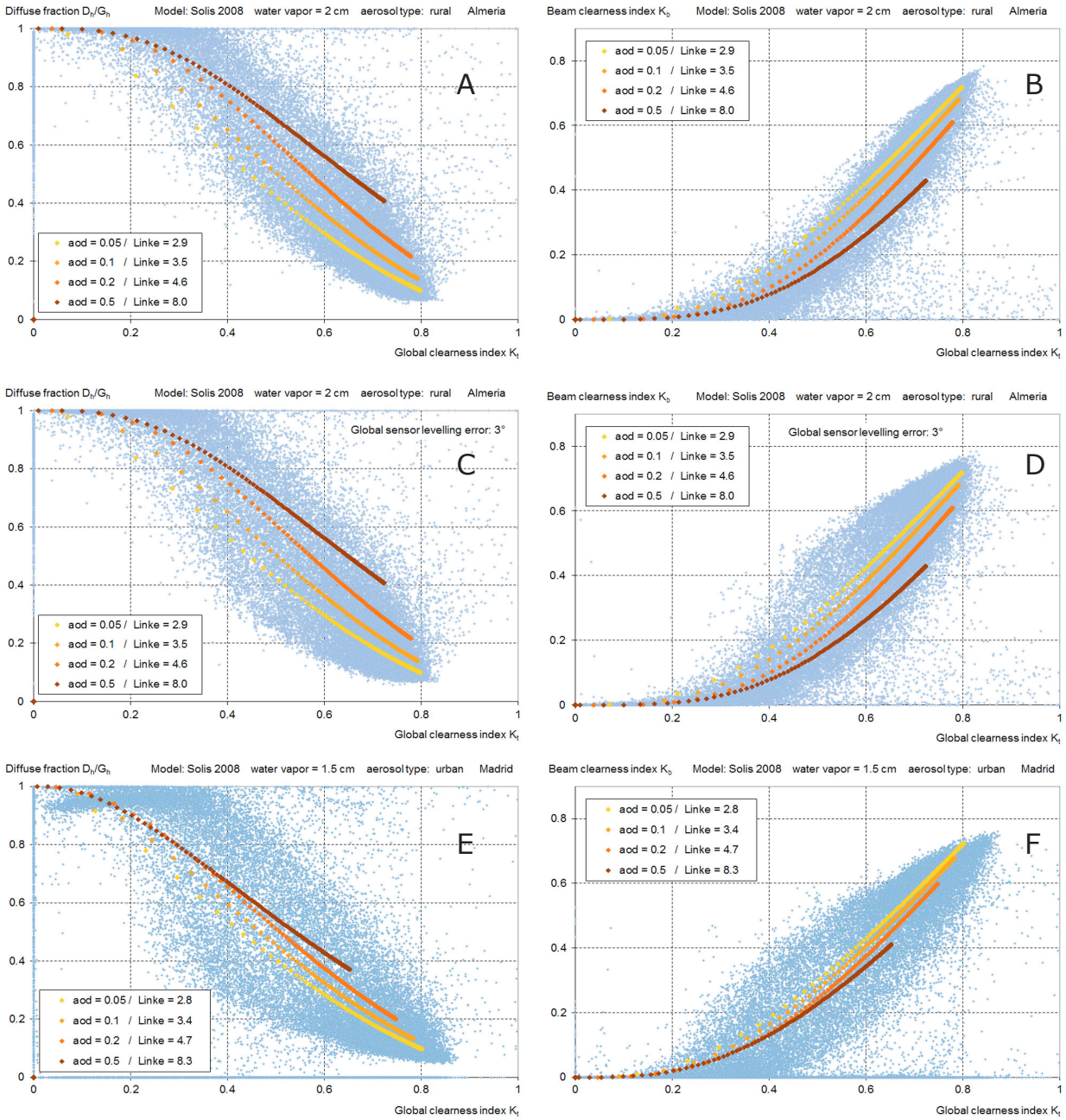

Figure 16 Components coherence test. Global irradiance sensor levelling sensitivity study on the data from Almeria. (A) and (B) Diffuse fraction and clearness index tests applied on the measurements of Almeria. (C) and (D) effect on data from Almeria for a 3° sloped global sensor. The shape of the data on (C) and (D) looks similar to (E) and (F).

- for the site of Madrid, the shape of Figure 16E is not common, it is the only site showing such a behavior. Replacing the beam component in the clearness index by the global/diffuse difference improves slightly the shape, but it is still not common (F). Another issue can be a levelling default of the global sensor. A sensitivity test is conducted on the data of Almeria and given on Figure 16. The reference graphs drawn from the measurements are given in (A) and (B). When an levelling error of 3° is artificially introduced in the measurements, the result given on (C) and (D) show a similar behavior compared to the corresponding graphs for Madrid (E) and (F). This could be an explanation of this singularity.

7.4 Data validation for the interannual variability

The aim of the analysis of the interannual variability is to take into account the natural variation of the

irradiation from one year to the other in the model uncertainty. To conduct a significant interannual variability analysis, a long period of data is needed. These long time series have to be as continuous as possible and with no missing data. As the majority of the ground measurements time series are not complete and as it is not possible the fill the gaps, a strategy has to be developed to circumvent the problem.

The following corrections are applied on the data: to obtain a yearly total, the data are taken month by month and added. For each month, the missing share of ground measurements is evaluated in term of a number of missing data percentage. When the gaps' length represents less than 5% of the month, a linear extrapolation is applied on the monthly values based on the normalized number of hourly values aggregated in the considered month. When more than 5% of the data are missing, the monthly value is replaced by the average of all the corresponding months of the considered time series. The missing share statistics are given in Table II.

In Lerwick, the 10% missing data for the beam component occur mainly in 2011. For the site of Madrid too many data are missing for the beam component, so that the interannual variability analysis is not significant.

Due to these corrections, the results given in the interannual variability bar charts do not correspond exactly to the hourly validation results. As the hourly comparison is restricted to validated values, some differences may also occur depending on the length of the comparison period. Nevertheless, the results are significant when considered as a general overview the tendency of a model to reproduce the data.

8. Validation results

8.1 Hourly, daily and monthly validation

The total amount of points included in the comparison and the corresponding irradiance and irradiation averages are the following:

- 700'000 hourly values $G_h = 317$ $B_n = 322$ $D_h = 129$ [W/m²]
- 60'000 daily values $G_h = 3.73$ $B_n = 3.78$ $D_h = 1.51$ [Wh/m².day]
- 2'000 monthly values $G_h = 108$ $B_n = 109$ $D_h = 44$ [Wh/m².month]

The number of ground or satellite derived values differ from one site to the other, and the covered periods are not of the same length for all the sites (see Table II).

Table III Results of the hourly, daily and monthly validation. The standard deviation calculated on the mean bias differences over all the 18 sites.

	HelioClim-3v4						HelioClim-3v5					
	Gh		Bn		Dh		Gh		Bn		Dh	
	mbd	sd	mbd	sd	mbd	sd	mbd	sd	mbd	sd	mbd	sd
hourly [Wh/m2h]	317		322		129		319		323		129	
	0	65	18	155	-12	58	4	64	28	150	-16	55
	0%	21%	6%	48%	-10%	45%	1%	20%	9%	46%	-12%	43%
Daily [kWh/m2]	3.73		3.78		1.51		3.73		3.78		1.51	
	0.00	0.45	0.22	1.24	-0.15	0.47	0.04	0.42	0.33	1.08	-0.18	0.44
	0%	12%	6%	33%	-10%	31%	1%	11%	9%	29%	-12%	29%
Monthly [kWh/m2]	85.7		80.2		41.0		88.4		82.7		42.2	
	8.2	8.8	23.8	21.3	-2.4	5.1	2.8	6.5	10.3	14.2	-2.4	3.7
	0%	6%	6%	16%	-10%	15%	1%	5%	9%	13%	-12%	15%
bias sd	4.4%		13.1%		16.2%		3.4%		13.7%		16.2%	

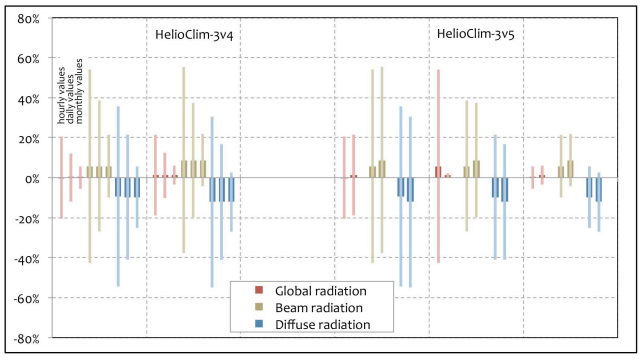

Figure 17 Corresponding graphical representation of the results.

Table III and Figure 17 give the main results of the validation (the complete results, site by site, for the two versions of HelioClim-3, component by component, in hourly, daily and monthly, absolute and relative values are given in the annex, Tables a-I, a-II and a-III). A general observation is that the hourly global irradiance is retrieved with a zero average bias and a standard deviation around 20% (65 [W/m²]), the beam component around 47% (150 [W/m²]) with a +6% to +9% bias, and the diffuse around 45% (56 [W/m²]) with a -10% bias. If the overall bias for the global irradiance is zero, it can be highly variable from one site to the other (-8% to +9%) . This is highlighted by the standard deviation of the mean bias deviation *bsd*; it stays around 3.5% for the global component. For the beam component (and a fortiori for the diffuse irradiance), the bias varies from site to site, especially for northern sites (i.e. Lerwick).

8.1.1 Model-measurements difference distribution

In a general way, for the global component and both versions, the bias distribution around the 1:1 axis follows a un- or slightly skewed normal distribution, so that the standard deviation indicator is significant (see Figures 11 & 12, a-1g to a-4g and a-10g to a-13g in the annex). This is not the case for the normal beam irradiance, where bimodal (i.e. Nantes), skewed or not normal distributions can occur depending on the site. No common rule can be drawn from the Figures a-10b to a-13b in the annex, the shape of the distribution depends on the clear sky model used and the specificities of the input parameters. For some sites with sunny conditions like Almeria, Carpentras, Tamanrasset or Sede Boqer, the dispersion of the hourly bias is so high that the distribution cannot be considered as normal. In this case, the standard deviation has to be considered with precaution. Concerning the diffuse component, even if the values on the model/measurements graphs are not aligned on the 1:1 axis, the frequency of occurrence distribution is not too far from a normal distribution; this makes the standard deviation representative of the uncertainties (see Figures a-1d to a-4d and a-10d to a-13d in the annex)

8.1.2 Improvement from HelioClim-3 version 4 to version 5

The improvement between HelioClim-3 version 4 and version 5 is the use of a new clear sky model. In version 4, the used clear sky is evaluated with the ESRA model, developed by Rigollier and Geiger (Rigollier et al. 2000, Geiger et al. 2002). Validation of this model (Ineichen 2016) shows clearly an underestimation for both global an beam components. This is illustrated on Figure 18 (upper graphs) where the clearness index is represented versus the solar elevation angle for both components. The measurements are plotted in yellow dots, and the model in blue. The upper limit, representative of clear conditions, is never reached by the modelled values, especially for the beam component (see Figures a-1b to a-4b in the annex). The consequence on the irradiance modelled values is that the highest values are never reached. In HelioClim-3 v5, an adaptation of the clear sky model is done using the McClear model (Lefèvre 2013) with MACC-II aerosol sub-daily data (Kaiser et al. 2002). The improvement is illustrated on Figure 18 lower graphs, where the same parameters than for version 4 are represented. For the new version, the clear sky measurements are reached by the modelled values, except for low solar elevation angle values where a slight underestimation is visible (see Figures a-9g and a-9b in the annex).

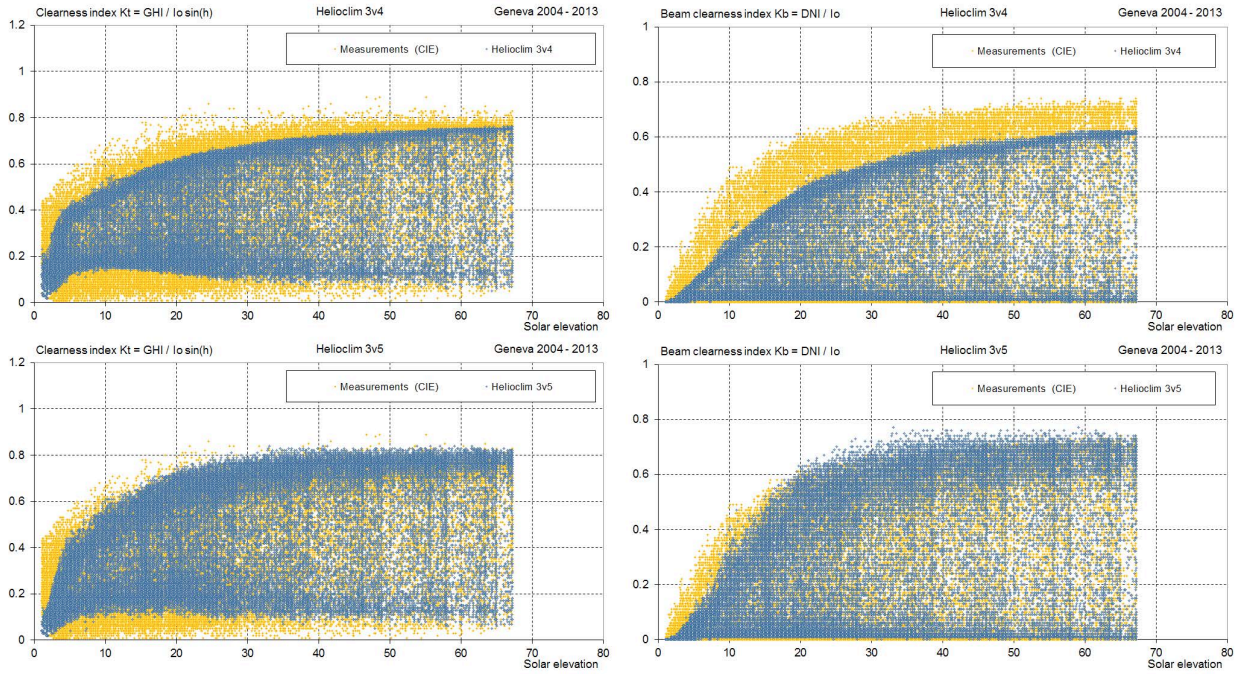

Figure 18 Global and beam clearness index (K_t *and* K_b) plotted versus the solar elevation angle for the two versions of helioclim-3.

8.1.3 Time resolution of the input parameters

When representing the clearness index versus the solar elevation angle, the time resolution effect of the *aod* and *w* input to the model can be pointed out. In version HelioClim-3 v4, monthly climatic values are used to evaluate the clear sky, whereas sub-daily values obtained from the MACC-II project are used in HelioClim-3 v5. This is illustrated on Figure 19 where aggregates of points are visible only on the left graph. This effect can be seen on the graphs for all the sites (see Figures a-9n in the annex), more particularly on sites where *aod* and *w* are highly variable (i.e. Lerwick and Nantes).

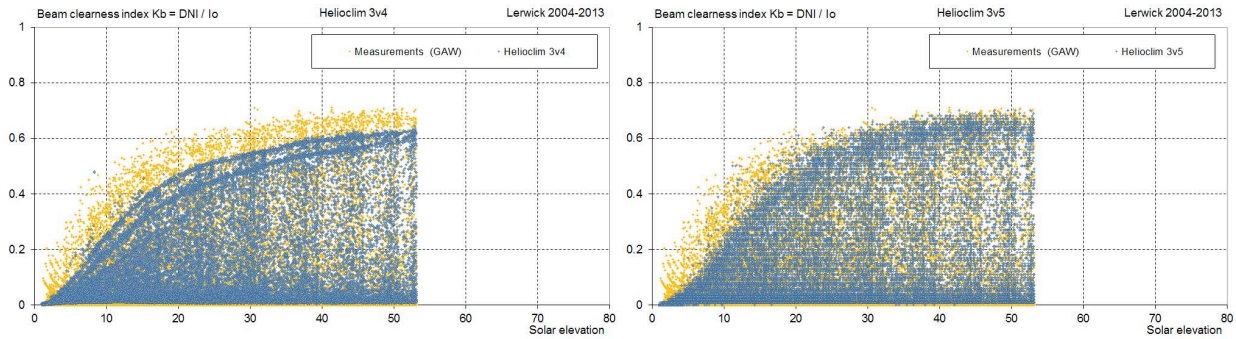

Figure 19 Beam clearness index K_b plotted versus the solar elevation angle for the two versions of helioclim-3 for the site of Lerwick.

8.1.4 Sky condition effect

The observation of the bias versus the modified clearness index K_t' (or the sky type, see Figures a-5g and a-5b in the annex) shows the same general tendency for all the models and both components: a slight overestimation for cloudy conditions and an underestimation for clear skies. The highest effect is a beam component overestimation for intermediate conditions. This is illustrated on Figure 20. For clear conditions, the dispersion is due to an approximate knowledge of turbidity. In the case of inter-

mediate cloud cover, the model does not identify with enough precision the type and thickness of the clouds (see Figures a-5g and a-5b in the annex).

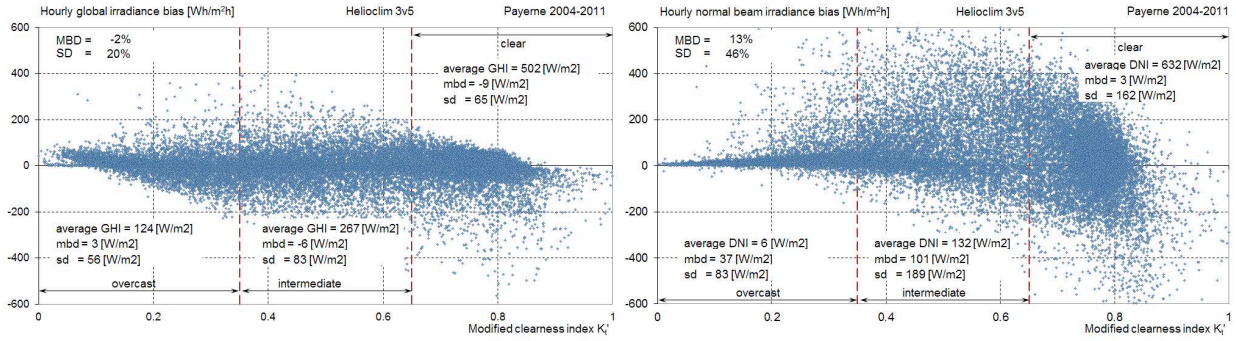

Figure 20 Model bias versus the clearness K_t (or sky conditions) for the global and beam components.

8.1.5 Snow effect

For the site of Davos, the snow cover during the winter period has a significant effect on the modeled irradiance. Indeed, if no particular attention is payed in winter, the high reflectance of the snow cover can change the determination of the ground albedo, and during the process, can be interpreted as cloudy conditions. The result is an overestimation of the irradiance for cloudy condition conditions due to the underestimation of the ground albedo. Moreover, the variability of the snow cover induces a higher dispersion of the irradiance, especially for the beam component. The effects are visible on Figure 21 where the model bias is represented versus the modified clearness index, or sky conditions, for the global and the normal beam components.

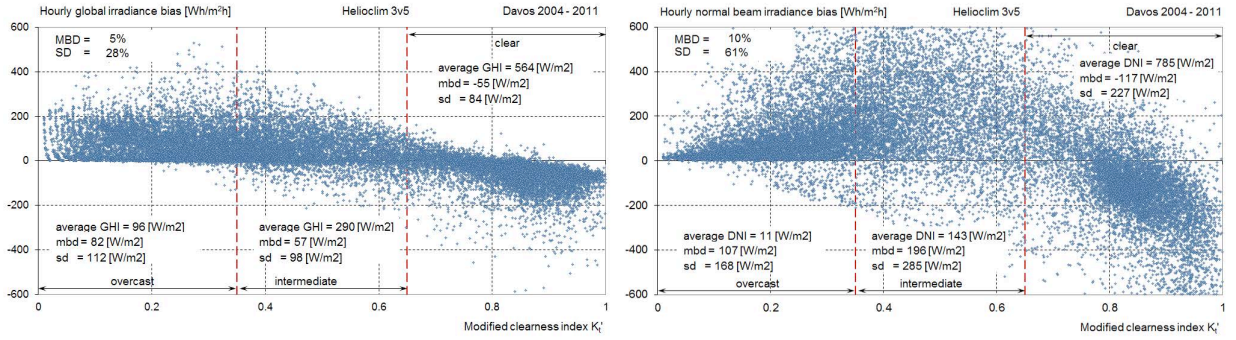

Figure 21 Model bias versus the clearness K_t (or sky conditions) for the global and beam components and the site of Davos.

8.1.6 Latitude effect

Due to the angle of view of the ground surface by the satellite, the size of the image pixel increases with the latitude of the site. This means that the reflectance of the ground includes also a higher variety of ground albedo values, and cloud types and altitudes. The small view angle of the satellite with respect to the ground increases the parallax effect on the cloud position (Schutgens 2009, Marie-Joseph 2013). The result on the modeled irradiance is a higher dispersion (standard deviation) for both components as illustrated on Figure 22 where the standard deviation of the modeled values are represented against the latitude of the station.

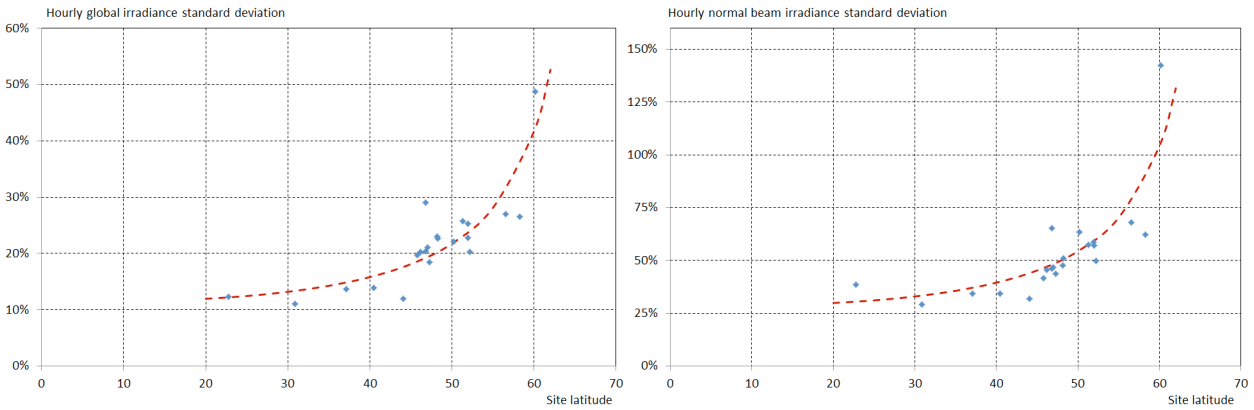

Figure 22 HelioClim-3 relative standard deviation versus the latitude of the station for the global and the normal beam irradiance.

8.1.7 Aerosol effect

The graphs on Figure 23 represent the hourly bias of the beam component versus the aerosol optical depth. A clear dependance can be pointed out for all the sites (see Figures a-6b in the annex), the model shows a negative bias for clean atmosphere condition, and going more or less to an overestimation for higher turbidity. The effect is less market for the version 5 of HelioClim-3. For the global component, as it is less sensitive to the aerosol load, the effect is smaller, even negligible.

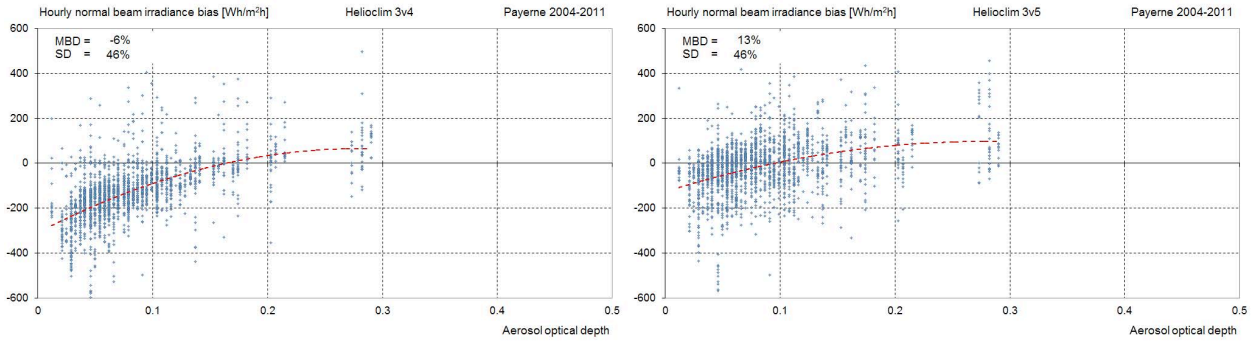

Figure 23 Model bias versus the clearness K_t (or sky conditions) for the beam component and the two version of HC-3.

When representing the daily model-measurements bias versus the day of the year, the general tendency is a summer/winter pattern for the beam component as it is illustrated on Figure 24 left. This effect is certainly correlated with the atmospheric turbidity ; it follows the aerosol load seasonal dependency. The right graph on Figure 24 represents the monthly bias surrounded by ± one standard deviation: the monthly modeled average and the measurements average are represented (for all the sites, see Figures a-7n and a-8n in the annex).

Figure 25 is a graphical illustration of the monthly validation. On the left graph, the monthly values of the two version of HelioClim-3 model, and on the right graph, all the average models are shown; the measurements are in red, the dashed red lines represent ± one standard deviation around the monthly value. Figures a-21n in the annex give a graphical representation for all the sites and models. For the global component, 96% of the monthly HelioClim-3 v5 modeled values are situated between the two dashed lines, 92% for version 4; for the normal beam component, 88% of the monthly HelioClim-3 v5 modeled values are situated between the two dashed lines, 84% for version 4. From these graphs, it

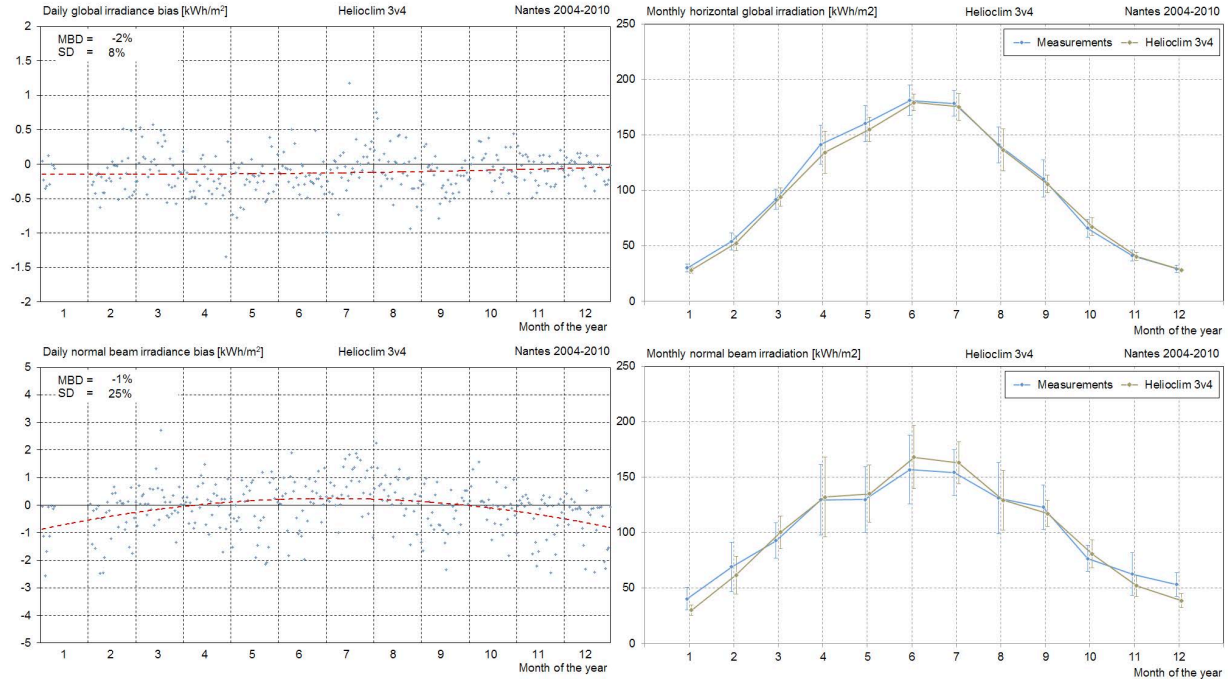

Figure 24 Left graphs: Model-measurements difference for daily normal beam irradiation values versus the day of the year. Right graphs: Monthly averaged values surrounded by ± one standard deviation for the modeled and the measured values of the global irradiation.

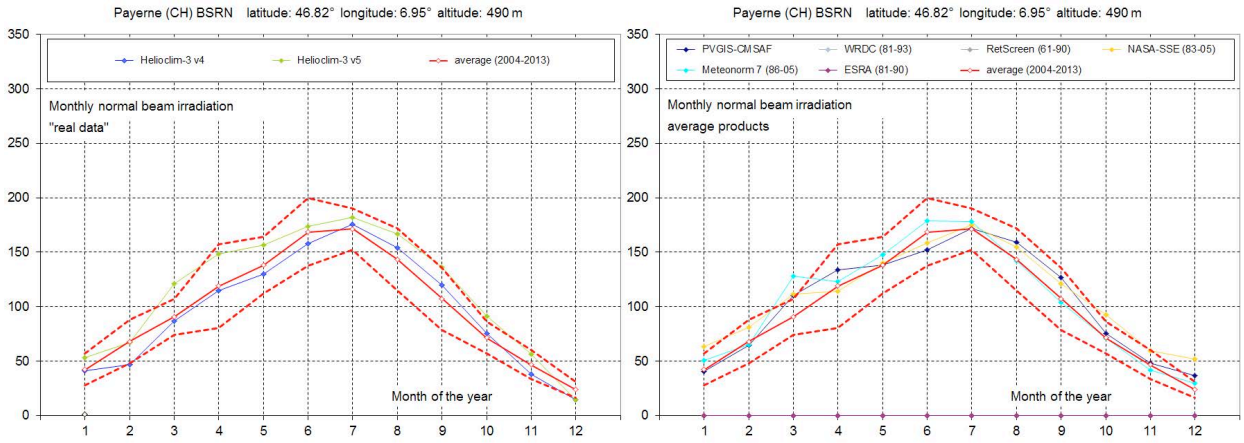

Figure 25 Comparison of the monthly values for all the models. In red, the measurements, the red dashed lines represent ± one standard deviation.

arises that the only site where all the average modelled monthly values are apart from one standard deviation around the average monthly measured values is Sede Boqer (see annex).

8.2 Frequency distribution

The correspondence between the frequency distribution of the modeled values and the measurements is as important as a low bias and standard deviation. It is the guaranteeing of a realist representation of the solar resource by the satellite models.

The general observation is that the two versions of the models, for all the sites, present a coherent frequency distribution representation of the global irradiance level (with the exception of Davos for the snow periods, Figures a-12g and a-13g). When considering the global clearness index frequency distribu-

tion, for all non-arid climate sites, a peak of overestimation can be seen for K_t values around 0.15. The peak is slightly smoothed on version 5 values, but still present. For the beam component, the general pattern is an overestimation for very low beam or clearness index values, and an underestimation for intermediate values. For both components, as stated in section 8.1.2, the high irradiance and clearness index values are better modeled with version 5. These two effects are illustrated on Figure 26 for the site of Kassel. The Figures for all the sites are given in the annex, Figures a-14n to a-19n.

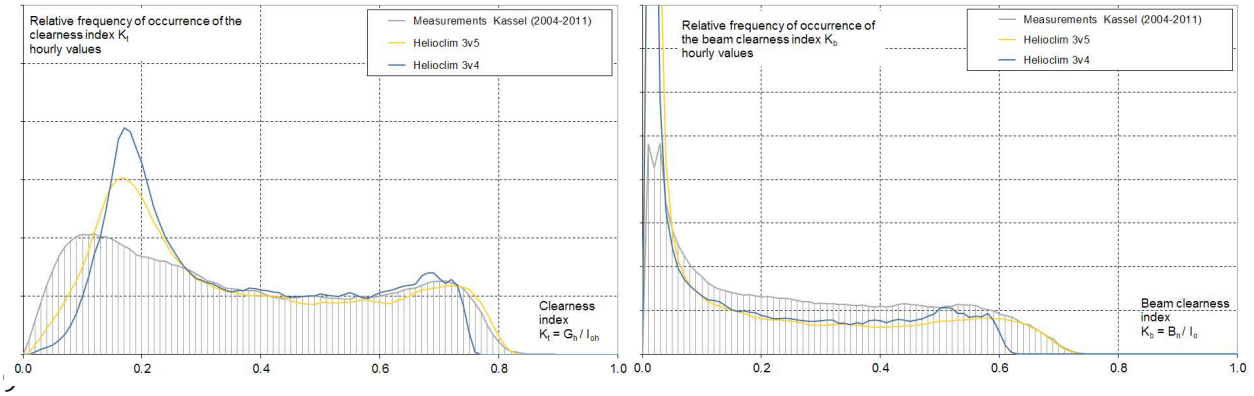

Figure 26 Frequency distribution of occurrence versus the clearness index for the site of Kassel.

8.3 Interannual variability

Beside the visual analysis of Figure a-20g and a-20b, it is interesting to compare the bias of the models with the interannual variability expressed by the standard deviation around the annual irradiation average for both the global and the beam components. The comparison results are given in Table IV. The blue columns represent the annual average for each site and the corresponding standard deviation over the reference period 2004-2010. The results are expressed as mean bias differences; if the *mbd* is less than one standard deviation *sd*, the cell background is represented in green. These *mbd* are hig hly variable from site to site and from model to model, even if the combined results for all sites are relatively good. On the last lines, the absolute bias and the standard deviation of the bias *bsd* is given for all models. These values express the spatial «smoothness» of the model.

From Table IV, the following points can be underlined for the global component:

- if version 4 has a lower overall mean bias, the absolute bias and the standard deviation of the bias are lower for version 5,
- considering the site by site results, half of the sites present a bias within ± one standard deviation of the interannual variability, 23% within ± two standard deviations, and 14% with a higher bias. The results are slightly better for version 5

and for the beam component:

- the average bias over all sites is relatively high, but as stated in previous sections, the clearness index distribution is better represented by version 5, especially for high values,
- version 4 gives slightly better results for all the annual indicators,
- the worst results arise for high latitude sites (size of the pixels view angles), and for dry climate sites (albedo determination difficulties, aerosol and clear sky model uncertainties),

- considering the site by site results, around half of the sites have a bias within ± one standard deviation of the interannual variability. The site to site and version to version comparison of the bias shows a high variability.

Table IV Results of the yearly validation and interannual variability analysis.

	Yearly total [kWh/m2] 2004-2010	standard deviation 2004-2010	PVGIS-CM SAF	WRDC (1981-1993)	RetScreen (1961-1990)	NASA-SSE (1983-2005)	MN 7 (1980-2000)	ESRA (1981-1990)	Satellight (1996-2000)	Helioclim-3 v4	Helioclim-3 v5	Yearly total [kWh/m2] 2004-2010	standard deviation 2004-2010	PVGIS-CM SAF	NASA-SSE (1983-2005)	MN 7 (1980-2000)	Satellight (1996-2000)	Helioclim-3 v4	Helioclim-3 v5
Sites	Global irradiation, annual mean bias difference											Beam irradiation, annual mean bias difference							
Almeria	1850	2.5%	3.2%		-8.1%	-8.1%	-3.0%		4.9%	4.8%	2.0%	2126	5.5%	7.5%	-3.8%	-11.1%	15.1%	11.8%	3.6%
Bratislava	1197	3.5%	1.4%	-0.7%	-0.6%	-2.7%	-0.1%	2.5%	-5.2%	-0.2%	1.6%	1191	7.4%	-1.3%	-4.0%	-7.5%	-11.9%	0.6%	6.9%
Cabauw	1085	2.3%	1.1%		-5.2%	-5.2%	-0.7%			-4.0%	-2.4%	908	4.7%	5.5%	2.7%	5.9%		12.7%	17.4%
Camborne	1121	3.6%	3.5%		1.5%	1.5%	-2.0%			-0.4%	1.2%	875	5.2%	20.9%	29.3%	15.8%		25.5%	31.4%
Carpentras	1587	2.1%	3.5%	-4.8%	-15.0%	-6.0%	-2.8%	-5.4%	0.4%	2.3%	2.3%	1884	4.1%	5.7%	0.4%	-10.1%	4.9%	2.9%	4.4%
Davos	1383	1.3%	-18.5%		-2.7%	-7.9%	2.1%	-2.9%	-17.5%	9.7%	5.6%	1420	8.4%	-38.5%	-8.0%	18.1%	-26.2%	25.8%	16.6%
Geneva	1282	2.3%	3.8%	-6.3%	0.1%	0.1%	-4.9%	-5.5%	-0.6%	-0.3%	5.7%	1274	3.3%	0.7%	4.3%	-9.8%	-0.9%	1.5%	19.6%
Kassel	1048	2.7%	0.6%		-5.6%	-5.6%	-5.8%	-6.6%	-5.9%	-4.7%	-1.4%	874	6.4%	-0.4%	1.0%	-7.9%	-5.1%	6.8%	17.0%
Lerwick	810	4.7%	-2.9%	-4.3%	9.2%	9.1%	-3.5%	-4.4%	-2.5%	3.4%	5.3%	580	13.3%	15.2%	55.5%	18.2%	0.8%	38.8%	46.4%
Lindenberg	1110	2.7%	0.5%	-2.9%	-2.9%	-8.9%	-3.0%	-11.5%	-3.6%	-3.5%	-3.8%	1026	9.6%	-1.0%	-8.1%	1.4%	-0.4%	2.9%	4.3%
Madrid	1697	4.9%	4.2%		-5.2%	-5.2%	-3.1%	-2.5%	1.7%	3.4%	5.2%	1798	5.2%	16.1%	10.0%	-0.8%	14.1%	16.3%	20.9%
Nantes	1271	3.4%	5.3%	-5.6%	-3.8%	-7.1%	-2.6%	-1.3%	-3.2%	-2.6%	-0.9%	1307	6.7%	2.7%	-12.1%	-9.6%	-8.8%	-3.5%	0.4%
Payerne	1278	2.2%	2.9%	-8.4%	-2.5%	0.4%	-1.8%	-8.3%	-2.8%	-5.6%	0.1%	1191	4.4%	5.5%	11.1%	5.9%	2.0%	-3.1%	14.8%
Sede Boqer	2114	1.2%	0.3%	0.5%	-6.7%	-3.9%	-4.0%			-7.1%	-5.7%	2382	3.6%		4.6%	-5.4%		-16.0%	-12.5%
Tamanrasset	2345	1.8%	-3.4%	0.8%	2.6%	-8.1%	0.9%			2.1%	2.3%	2355	4.0%		6.1%	18.1%		18.5%	19.1%
Toravere	981	3.8%	-0.7%		3.1%	3.1%	-0.1%		4.6%	2.4%	0.7%	1028	8.8%	-12.0%	8.4%	2.4%	7.2%	4.9%	2.2%
Valentia	1021	4.6%	8.6%	-3.9%	-4.8%	8.0%	-5.3%	-4.7%	-4.2%	-0.8%	0.7%	992	13.4%	2.9%	10.7%	-21.5%	-21.3%	-4.7%	0.4%
Vaulx-en-Velin	1304	4.4%	2.7%	-7.8%	-4.0%	-3.0%	-6.3%	-3.3%	0.4%	-0.5%	2.8%	1359	5.3%	-2.1%	-2.1%		-0.5%	-1.4%	8.0%
Wien	1175	2.7%	3.5%	-6.8%	-6.0%	-0.8%	1.0%	-7.0%	-1.4%	-2.1%	0.1%	1112	8.0%	-1.1%	2.9%	-3.1%	-2.5%	0.8%	8.7%
Zilani	1024	3.3%	-6.5%	-3.2%	2.5%	2.5%	-2.6%		6.0%	7.7%	1.6%	1000	9.1%	-13.0%	13.4%	-0.1%	20.5%	21.2%	5.7%
All sites	1334	2.8%	0.6%	-3.6%	-3.2%	-3.3%	-2.3%	-4.6%	-1.7%	0.2%	1.1%	1334	6.2%	0.9%	4.8%	0.0%	-0.2%	7.4%	10.7%
All sites absolute bias			3.8%	4.0%	4.8%	5.0%	2.8%	4.9%	4.0%	3.5%	2.7%			8.5%	7.9%	9.1%	9.5%	10.8%	12.1%
Standard deviation of mbe			5.5%	4.6%	6.3%	6.2%	3.3%	5.5%	5.9%	4.6%	3.6%			13.7%	9.9%	12.0%	13.2%	14.9%	15.2%
MBD within one standard deviation							MBD within two standard deviations							MBD higher than two standard deviations					

9. Conclusions

The first conclusion is that the quality control is a key point in any model validation. Even if the data are highly qualified by the organization in charge of the acquisition, uncertainties can remain in the data and influence the validation. The best case is when independent data such as aerosol optical depth are also available.

The conclusions of the present study are the following:

- for latitude from 20° to 60°, altitude from sea level to 1600 m and various climate, the hourly global irradiance is retrieved with a negligible bias and an average standard deviation around 20% for both versions of HelioClim-3 scheme. For the beam irradiance, the bias is around 6% to 9%, and the standard deviation around 47%,
- as expected, the main improvement from version 4 to version 5 comes from the clear sky model and the knowledge of the aerosol optical depth, better results are obtained with daily (our sub daily) turbidity instead of monthly climatic values,
- the intermediate sky conditions are more difficult to model: the type and altitude of the clouds are not easy to determine precisely,
- the snow cover has to be taken into account, especially in the alps region,
- a general pattern with the atmospheric aerosol load is visible for all sites. Even if the pattern is present for the two versions of HelioClim-3, it is less marked for the latest version. Some seasonal effects can be related to the aerosol variability during the year,

- the standard deviation is increasing with the latitude, i.e. the size of the pixels and the angle of view of the satellite,
- a peak of discrepancy in the frequency distribution is present for all the non-arid sites around K_t = 0.15 for both versions. On the other hand, version 5 presents a much better representation of high clearness index values,
- even if the overall results for the beam component are slightly worst for the HelioClim-3 v5, the frequency distribution are improved.

10. Acknowledgements

The ground data are kindly provided by the Plataforma Solar de Almeria (PSA & DLR, Spain), the Baseline Surface Radiation Network (BSRN), the Aerosol Robotic Network (Aeronet), the Global Aerosol Watch project (GAW), the CIE International Daylight Measurements Program (Commission internationale de l'éclairage IDMP), the Universidad Politecnica de Madrid (UMP, Spain), the Ecole Nationale des Travaux Publiques (ENTPE, Lyon, France), the Centre Scientifique et Technique du Bâtiment (CSTB, Nantes, France), the Institut für Schnee- und Lawinenforschung (SLF) and the Physikalisch-Meteorologisches Observatorium Davos (PMOD/WRC, Switzerland), the Frauenhofer Institute für Winderergie und Energisystemtechnik (IWES, Kassel, Germany), and the Natural Resources and the Environment, Global Change and Ecosystem Dynamics Research Group (CSIR, South Africa).

11. References

Aeronet. Aerosol Robotic Network. Available from <http://aeronet.gsfc.nasa.gov/> (last access in August 2015)

Atwater M A, Ball J T (1976) Comparison of radiation computations using observed and estimated precipitable water. J. Appl. Meteorol. 15, 1319-1320.

BSRN. Baseline surface radiation network. Available from: <http://www.bsrn.awi.de/> (last access in August 2015)

Espinar B, Ramirez L, Drews D, Beyer H G, Zarzalejo L F, Polo J and Martin L (2009) Analysis of different comparison parameters applied to solar radiation data from satellite and German radiometric stations, *Solar Energy* 83 (2009) 118–125

ESRA (2000) European Solar Radiation Atlas, 2000. Fourth edition, includ. CD-ROM. Edited by Greif J, Scharmer K. Scientific advisors: Dogniaux R, Page J K. Authors : Wald L, Albuisson M, Czeplak G, Bourges B, Aguiar R, Lund H, Joukoff A, Terzenbach U, Beyer H G, Borisenko E P. Published for the Commission of the European Communities by Presses de l'Ecole, Ecole des Mines de Paris, France, France

Geiger M, Diabaté L, Ménard L, Wald L (2002) A web Service for Controlling the Quality of Measurements of Global Solar Irradiation. Solar Energy, 73 (6), 475-480.

Gueymard C (1989) A two-band model for the calculation of clear sky solar irradiance, illuminance, and photosynthetically active radiation at the earth surface. Solar Energy, Vol. 43, N° 5, 253-265.

Ineichen P (2008) A broadband simplified version of the Solis clear sky model, Solar Energy 82, 758–762.

Ineichen P (2008a) Comparison and validation of three global-to-beam irradiance models against ground measurements. Sol. Energy , doi:10.1016/j.solener.2007.12.006

Ineichen P (2008b) A broadband simplified version of the Solis clear sky model, Excel tool. Available from: <http://www.unige.ch/energie/fr/equipe/ineichen/solis-tool/> (last access in August 2015)

Ineichen P (2008c) Conversion function between the Linke turbidity and the atmospheric water vapor and aerosol content. Solar Energy 82, 1095–1097

Ineichen P (2016) Validation of Models that Estimate Clear Sky Global and Beam Solar Irradiance. In press in *Solar Energy*

Ineichen P, Barroso C, Geiger B, Hollmann R, Marsouin A, Mueller R (2009) Satellite Application Facilities irradiance products: hourly time step comparison and validation over Europe. International Journal of Remote Sensing, Vol. 30, No. 21, 5549–5571.

Kaiser J W, Peuch V H, Benedetti A, Boucher O, Engelen R J, Holzer-Popp T, Morcrette J J, Wooster M J (2012) The MACC-II Management Board: The pre-operational GMES Atmospheric Service in MACC-II and its potential usage of Sentinel-3 observations, ESA Special Publication SP- 708, Proceedings of the 3rd MERIS/(A)ATSR and OCLI-SLSTR (Sentinel-3) Preparatory Workshop, held in ESA-ESRIN, Frascati, Italy, 15–19 October

Kasten F.(1980) A simple parameterization of two pyrheliometric formulae for determining the Linke turbidity factor. Meteor. Rdsch. 33, 124–127.

Lefèvre M, Oumbe A, Blanc P, Espinar B, Gschwind B, Qu Z, Wald L, Schroedter-Homscheidt M, Hoyer-Klick C, Arola A, Benedetti A, Kaiser J W and Morcrette J J (2013) McClear: a new model estimating downwelling solar radiation at ground level in clear-sky conditions, Atmos. Meas. Tech., 6, 2403-2418, doi:10.5194/amt-6-2403-2013.

Marie-Joseph I, Linguet L, Gobinddass M-L and Wald L (2013) On the applicability of the Heliosat-2 method to assess surface solar irradiance in the Intertropical Convergence Zone, French Guiana, International Journal of Remote Sensing, 34:8, 3012-3027

Massey Jr F J, (1951) The Kolmogorov–Smirnov test for goodness of fit. Journal of the American Statistical Association 4, 68–78.

Meteonorm 6.1 (2009) Global Meteorological Database for Engineers, Planners and Education, <http://www.meteonorm.com> (last access in August 2015)

Molineaux B, Ineichen P, O'Neill N T (1998) Equivalence of pyrheliometric and aerosol optical depth at a single wavelength. Appl. Opt., 37, 7008-7018.

Müller R et al. (2004) Rethinking satellite-based solar irradiance modelling – the solis clear-sky module, Remote Sensing of Environment, 91(2), 160–174, doi:10.1016/j.rse.2004.02.009.

Perez R, Ineichen P, Seals R, Zelenka A (1990) Making full use of the clearness index for parametrizing hourly insolation conditions. Solar Energy 45, N° 2, 111-114.

Perez R, Ineichen P, Maxwell E, Seals R, Zelenka A (1992) Dynamic global to direct irradiance conversion models. *ASHRAE Transactions-Research series*, pp354-369.

Qu Z, Gschwind B, Lefevre M and Wald L (2014) Improving HelioClim-3 estimates of surface solar irradiance using the McClear clear-sky model and recent advances in atmosphere composition, Atmos. Meas. Tech., 7, 3927-3933, doi:10.5194/amt-7-3927-2014 (Creative Commons Attribution 3.0 License)

Remund J, Wald L, Lefèvre M, Ranchin T, Page J (2003) Worldwide Linke turbidity information, Proceedings of ISES Solar World Congress, 16-19 June 2003, Göteborg, Sweden.

Remund J (2009): Aerosol optical depth and Linke turbidity climatology, Description for final report of IEA SHC Task 36, Meteotest Bern

Rigollier C, Bauer O, Wald L (2000) On the Clear Sky Model of the ESRA - european Solar Radiation Atlas - with Respect to the Heliosat Method. Solar Energy **68** (1), 33-48.

Rigollier C, Lefèvre M, Wald L (2004) The method heliosat-2 for deriving shortwave solar irradiance radiation from satellite imagesSolar Energy, 77(2), 159-169

Schutgens N A J, Roebeling R A (2009) Validating the Validation: The Influence of Liquid Water Distribution in Clouds on the Intercomparison of Satellite and Surface Observations. Journal of Atmospheric and Oceanic Technology 26: 1457–74. doi:10.1175/2009JTECHA1226.1.

Zelenka, A, Perez R, Seals R and Renné D (1998) Effective accuracy of models converting atellite radiances to hourly surface insolation. Proc. 9th Conference on Satellite Meteorology and Oceanography, Paris, 25-29 May, 1998, 710–713.

UNIVERSITÉ DE GENÈVE
INSTITUTE FOR ENVIRONMENTAL SCIENCES

solarXdat //

Long term HelioClim-3 global, beam and diffuse irradiance validation

Annex

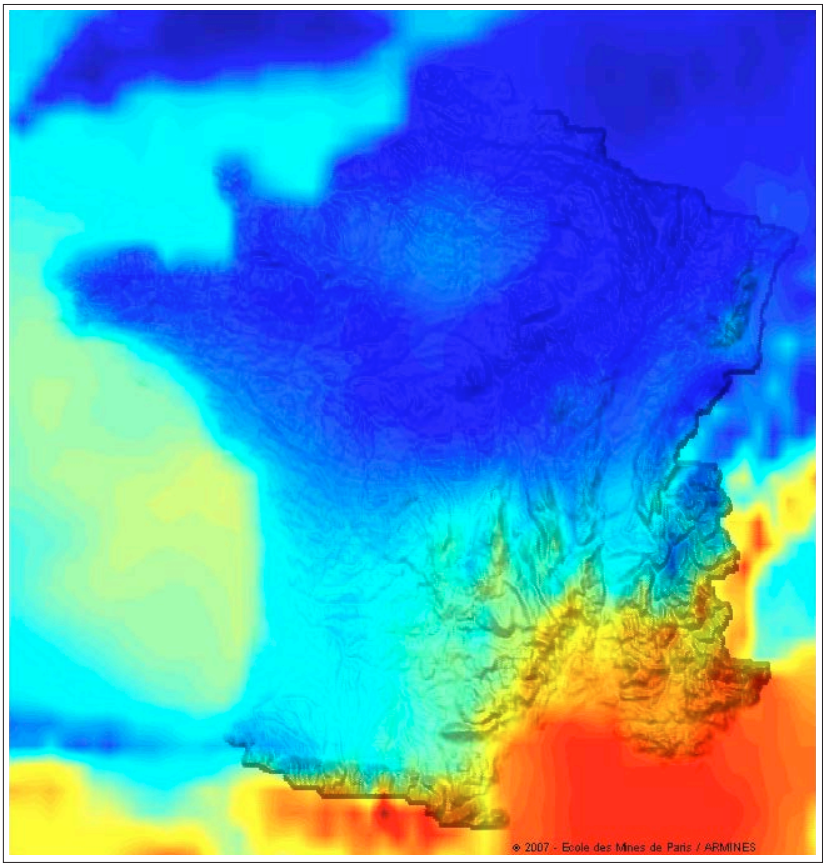

Figures and Tables

The *n* referes to the three irradiance components: global (g), normal beam (b) and diffuse (d)

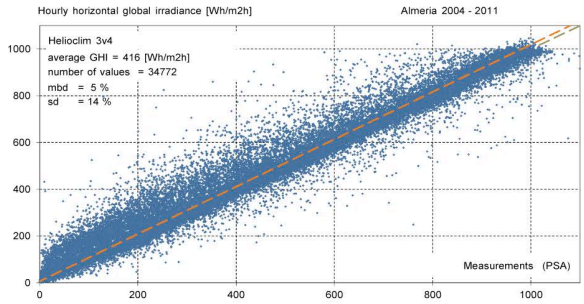

Figure a-1g Model versus measurements for hourly global irradiance

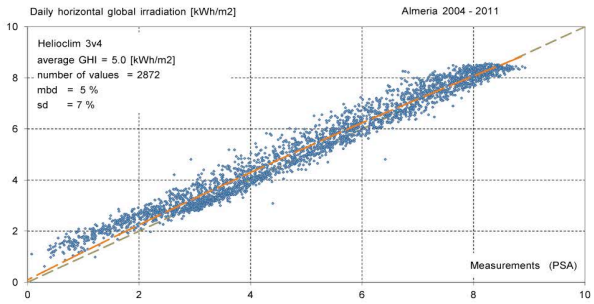

Figure a-2g Model versus measurements for daily global irradiation

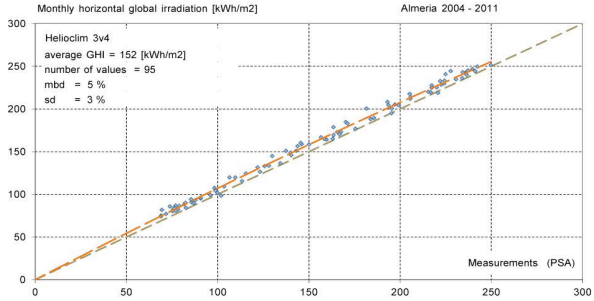

Figure a-3g Model versus measurements for monthly global irradiation

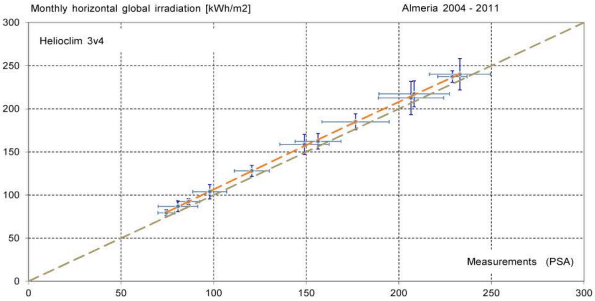

Figure a-4g Model versus measurements for monthly average global irradiation, surrounded by ± one standard deviation on each axis

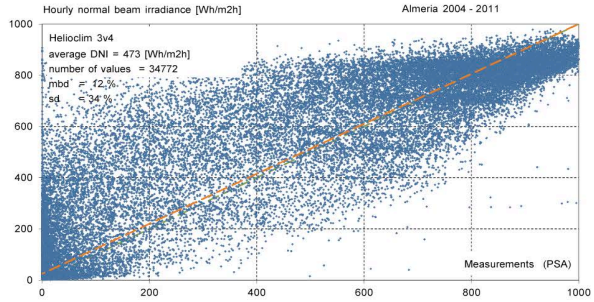

Figure a-1b Model versus measurements for hourly normal beam irradiance

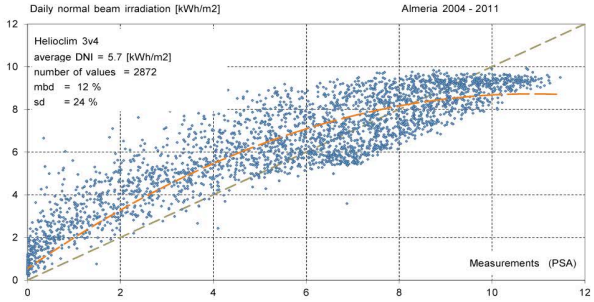

Figure a-2b Model versus measurements for daily normal beam irradiation

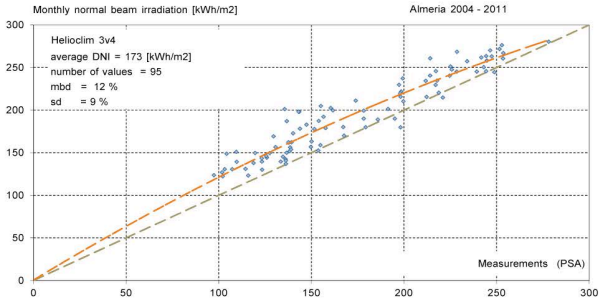

Figure a-3b Model versus measurements for monthly normal beam irradiation

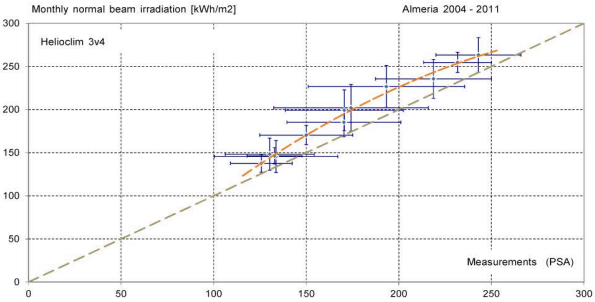

Figure a-4b Model versus measurements for monthly average normal beam irradiation, surrounded by ± one standard deviation on each axis

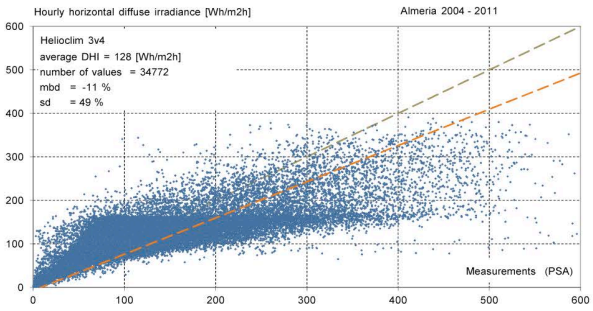

Figure a-1d Model versus measurements for hourly diffuse irradiance

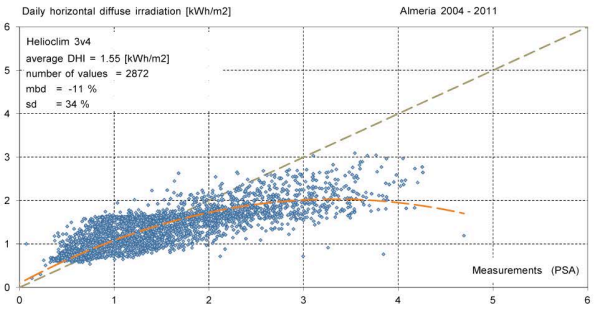

Figure a-2d Model versus measurements for daily diffuse irradiation

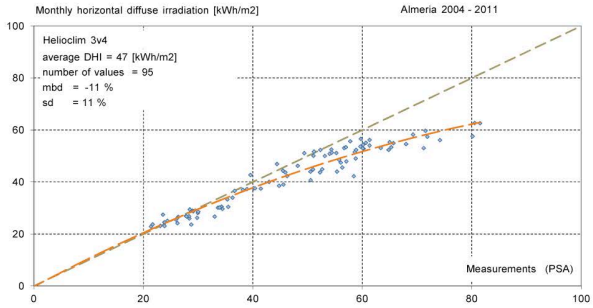

Figure a-3d Model versus measurements for monthly diffuse irradiation

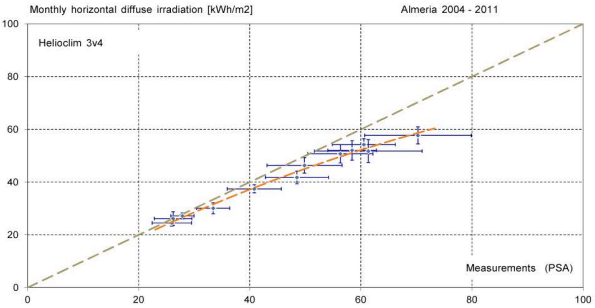

Figure a-4d Model versus measurements for monthly average diffuse irradiation, surrounded by ± one standard deviation on each axis

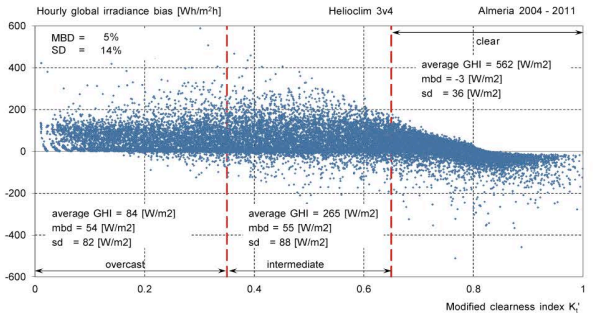

Figure a-5g Model-measurements difference for hourly global irradiance values versus the modified clearness index K_t'

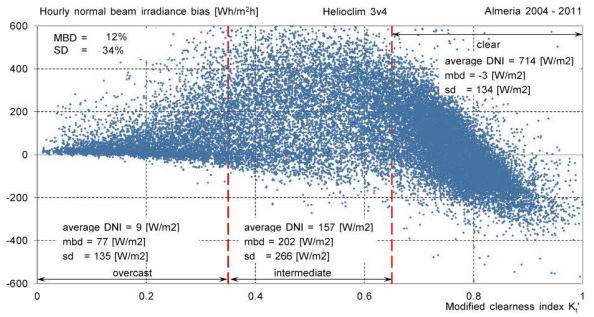

Figure a-5b Model-measurements difference for hourly normal beam irradiance values versus the modified clearness index K_t'

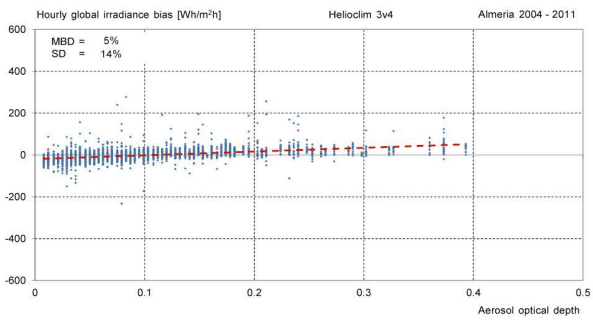

Figure a-6g Model-measurements difference for hourly global irradiance values versus the aerosol optical depth

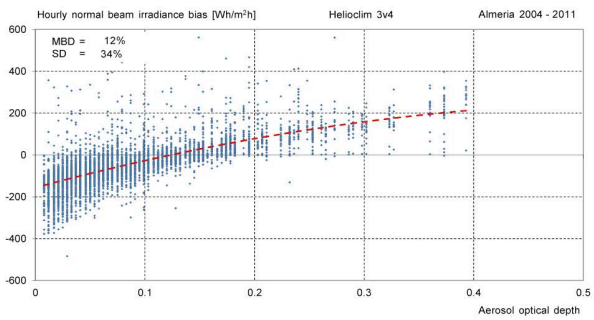

Figure a-6g Model-measurements difference for hourly normal beam irradiance values versus the aerosol optical depth

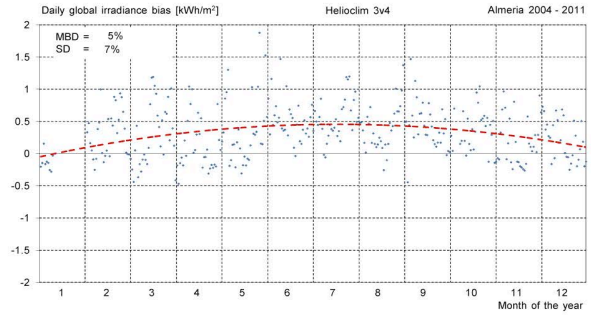

Figure a-7g Model-measurements difference for daily global irradiation values versus the day of the year

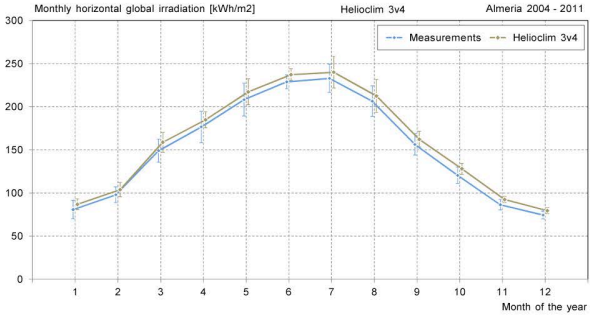

Figure a-8g Monthly averaged values surrounded by ± one standard deviation for the modeled and the measured values of the global irradiation.

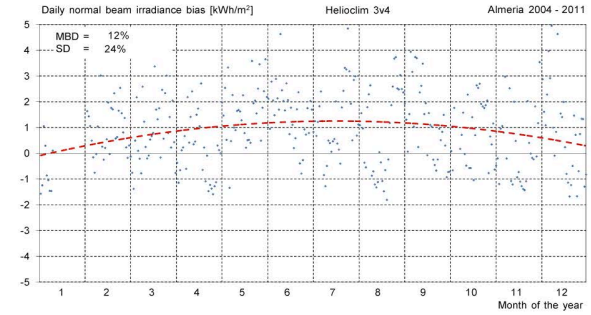

Figure a-7b Model-measurements difference for daily normal beam irradiation values versus the day of the year

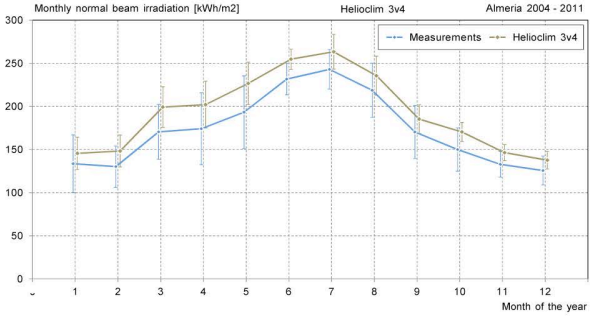

Figure a-8b Monthly averaged values surrounded by ± one standard deviation for the modeled and the measured values of the global irradiation.

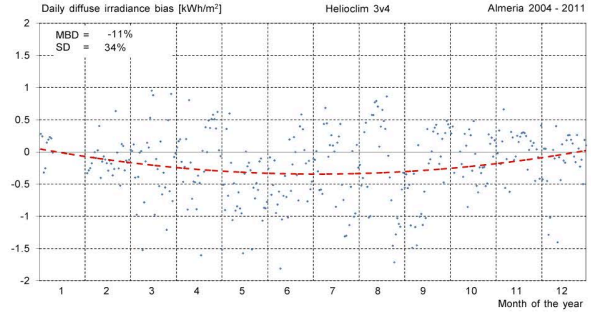

Figure a-7d Model-measurements difference for daily diffuse irradiation values versus the day of the year

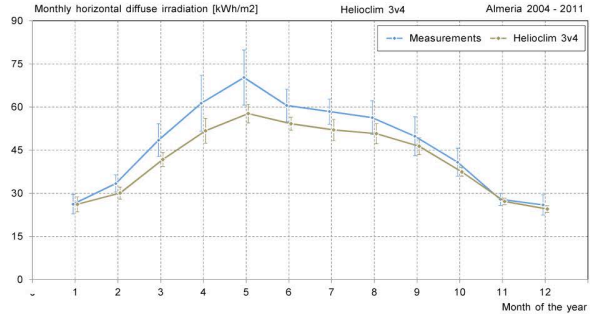

Figure a-8d Monthly averaged values surrounded by ± one standard deviation for the modeled and the measured values of the global irradiation.

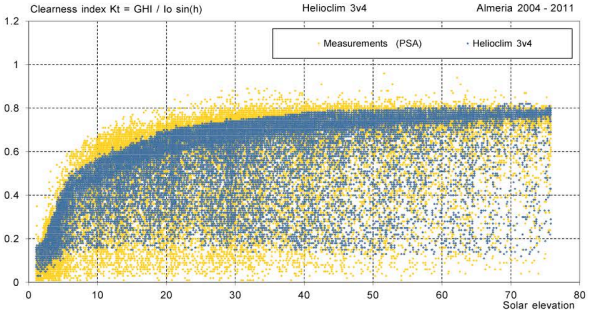

Figure a-9g Clearness index K_t versus the solar elevation angle for the measurements (yellow) and the modeled (blue) hourly values

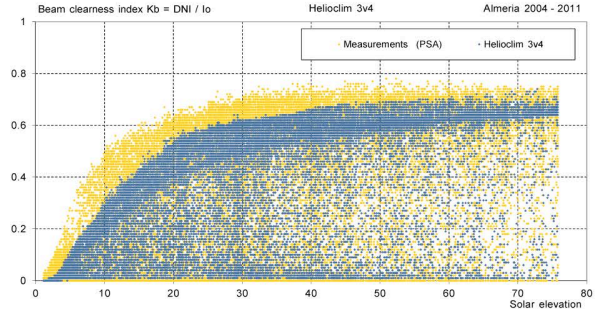

Figure a-9b Normal beam clearness index K_b versus the solar elevation angle for the measurements (yellow) and the modeled (blue) hourly values

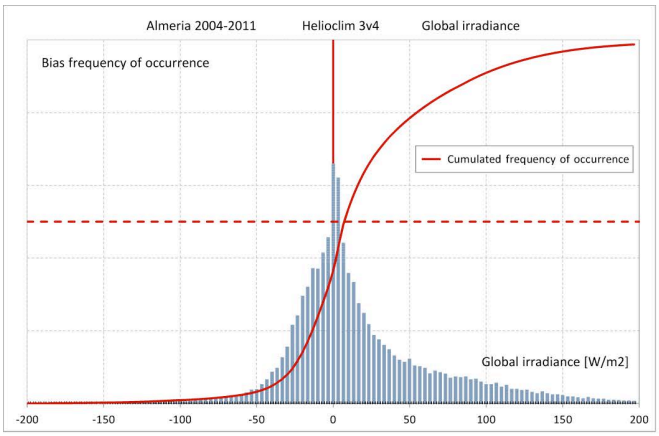

Figure a-10g Hourly values distribution of the model-measurements difference around the 1:1 axis of Fig a-1g for the all the data. The corresponding cumulated curve is also represented

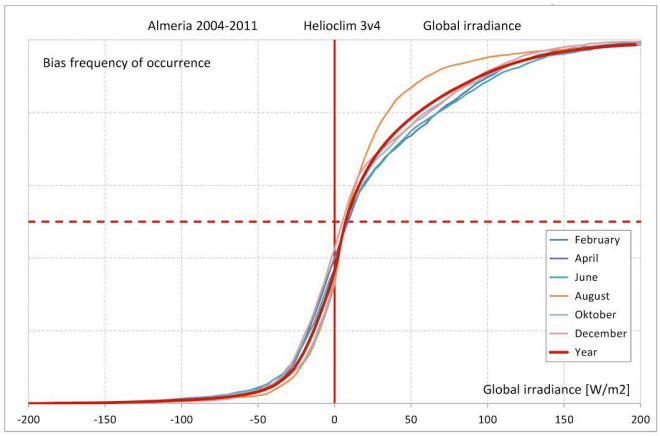

Figure a-11g Cumulated frequency of occurrence of the model-measurements difference versus the model-measurements difference

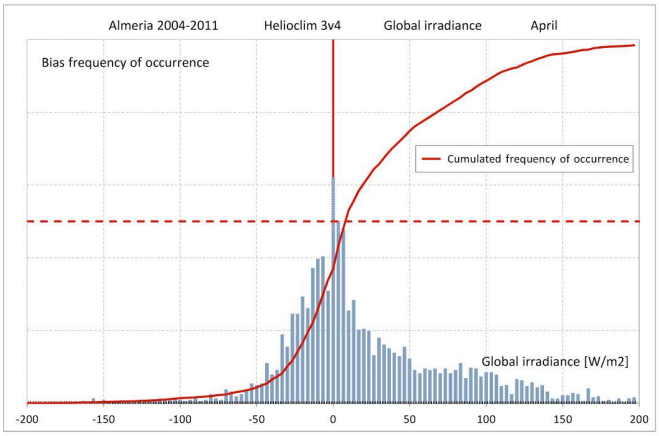

Figure a-12g same as Fig a-10g for April

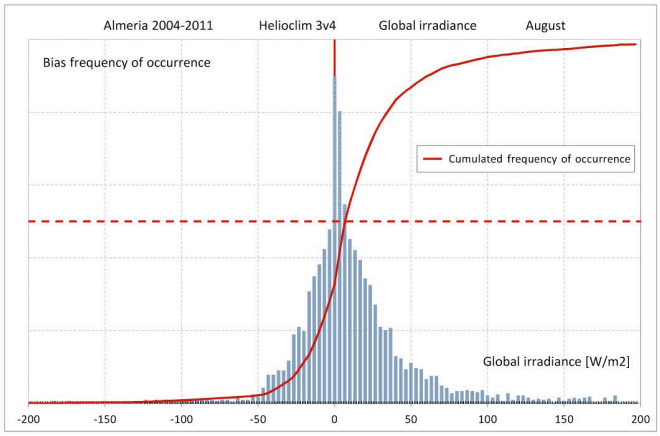

Figure a-13g same as Fig a-10g for August

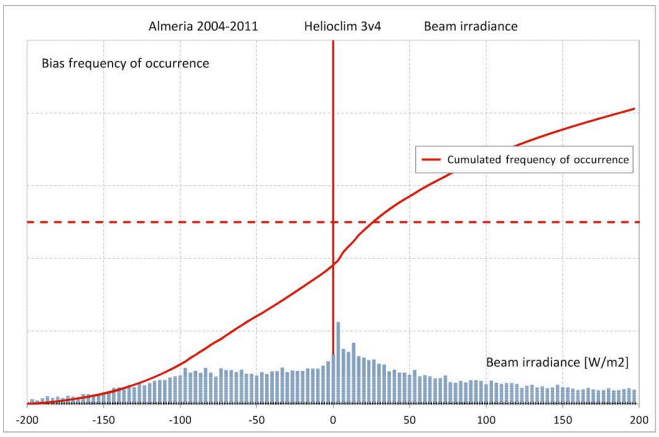

Figure a-10b Hourly values distribution of the model-measurements difference around the 1:1 axis of Fig a-1b for the all the data. The corresponding cumulated curve is also represented

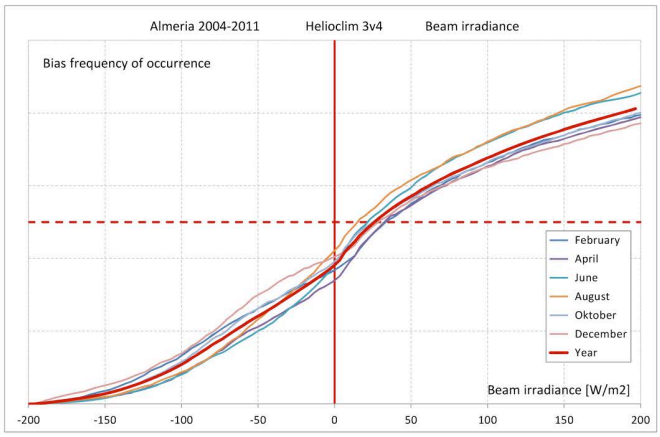

Figure a-11b Cumulated frequency of occurrence of the model-measurements difference versus the model-measurements difference

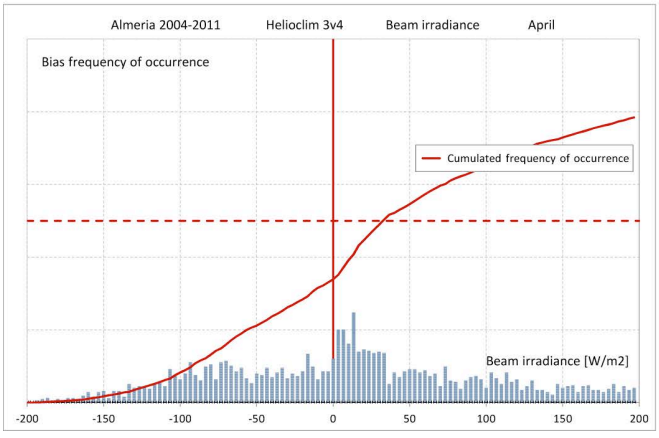

Figure a-12b same as Fig a-10b for April

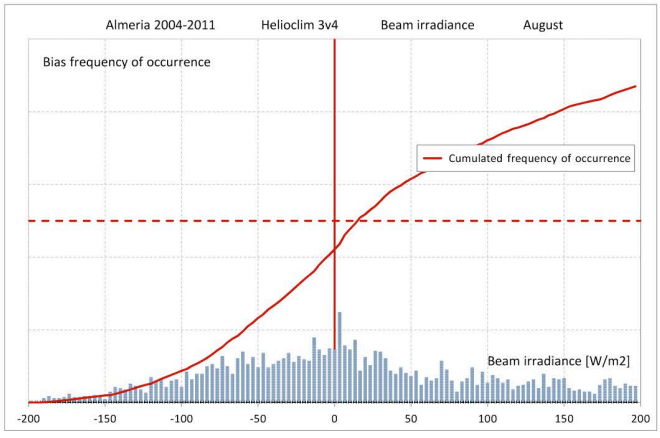

Figure a-13b same as Fig a-10b for August

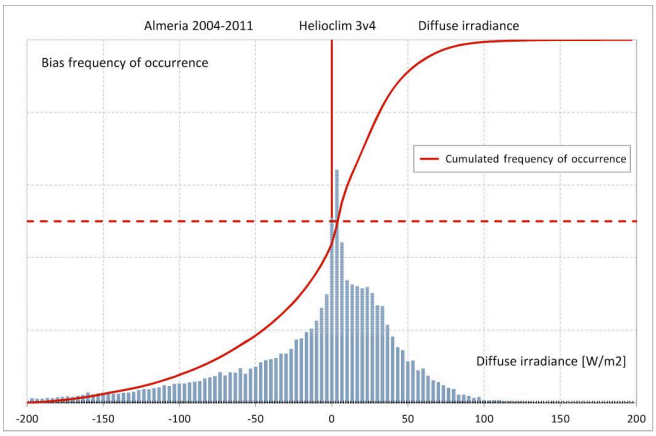

Figure a-10d Hourly values distribution of the model-measurements difference around the 1:1 axis of Fig a-1d for the all the data. The corresponding cumulated curve is also represented

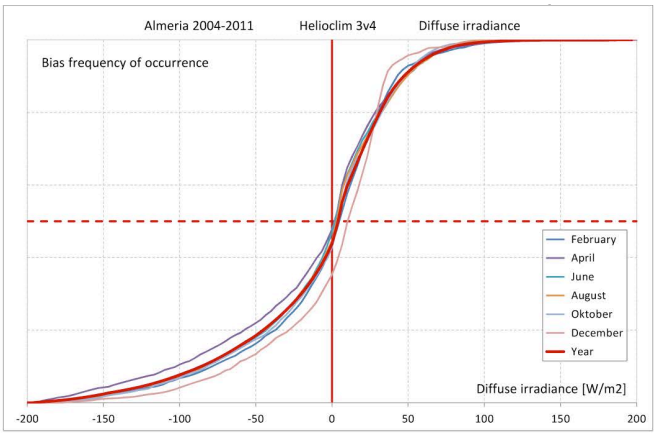

Figure a-11d Cumulated frequency of occurrence of the model-measurements difference versus the model-measurements difference

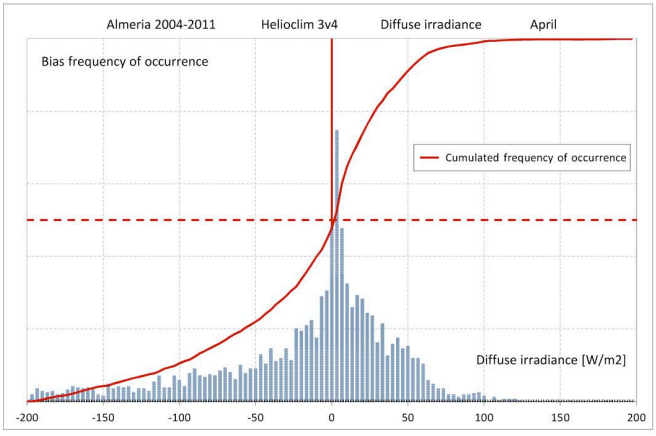

Figure a-12d same as Fig a-10d for April

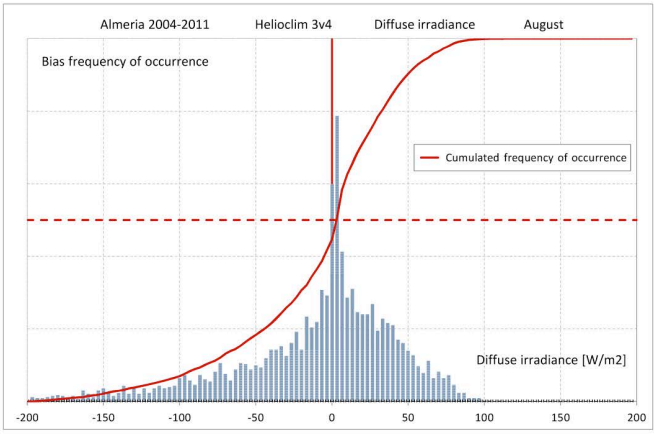

Figure a-13d same as Fig a-10d for August

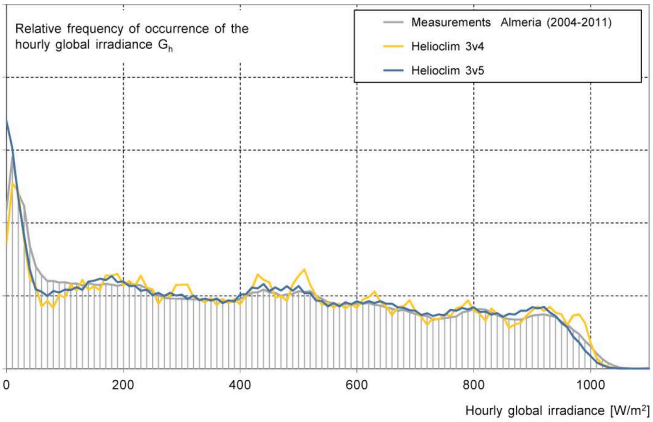

Figure a-14g Relative frequency of occurrence of the hourly global irradiance versus the corresponding irradiance. The measurements are represented in grey.

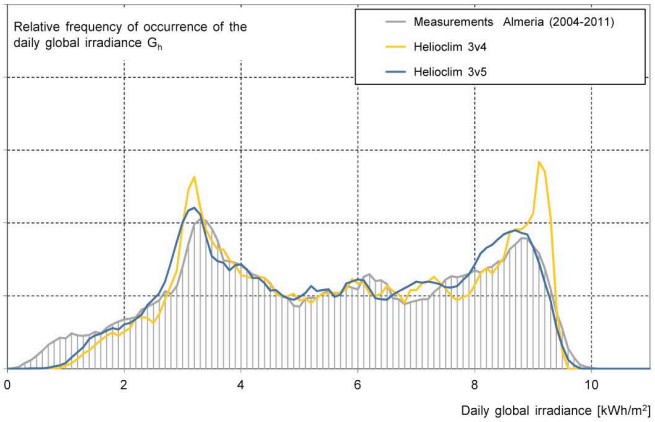

Figure a-15g Relative frequency of occurrence of the daily global irradiance versus the corresponding irradiance. The measurements are represented in grey.

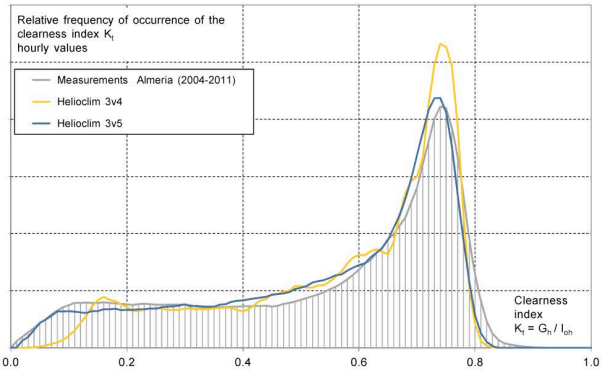

Figure a-16g Relative frequency of occurrence of the global clearness index versus the corresponding clearness index K_t. The measurements are represented in grey.

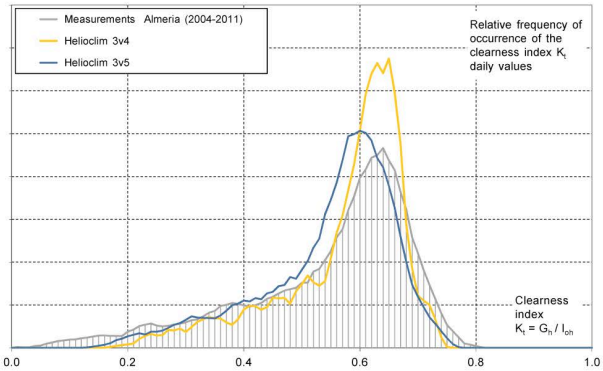

Figure a-17g Relative frequency of occurrence of the daily global clearness index versus the corresponding clearness index. The measurements are represented in grey.

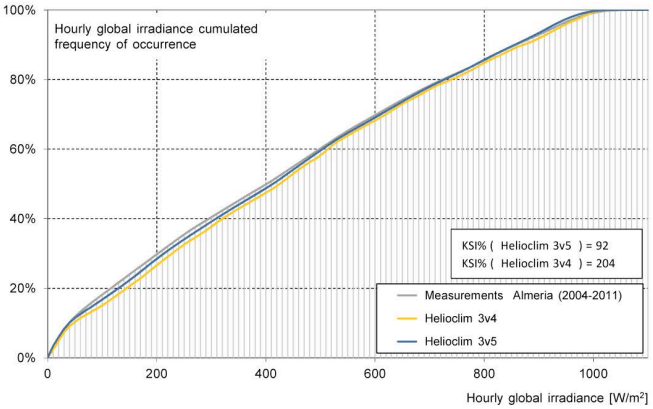

Figure a-18g Cumulated frequency of occurrence of the hourly global irradiance values versus the corresponding irradiance. The measurements are represented in grey.

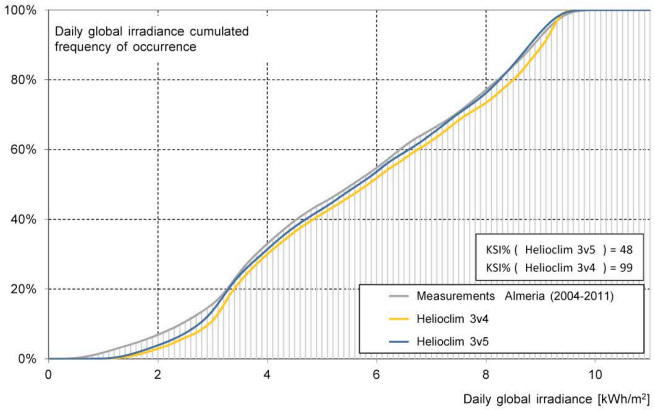

Figure a-19g Cumulated frequency of occurrence of the daily global irradiance values versus the corresponding irradiance. The measurements are represented in grey.

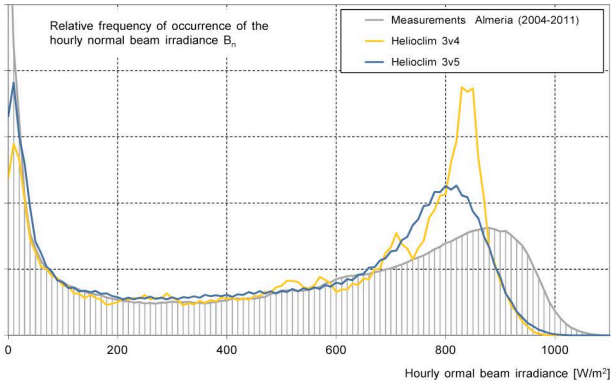

Figure a-14b Relative frequency of occurrence of the hourly normal beam irradiance versus the corresponding irradiance. The measurements are represented in grey.

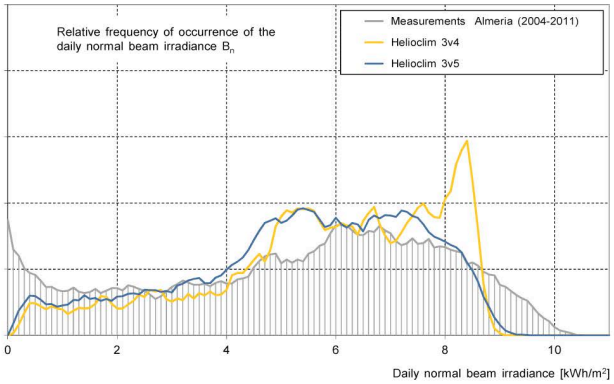

Figure a-15b Relative frequency of occurrence of the daily normal beam irradiance versus the corresponding irradiance. The measurements are represented in grey.

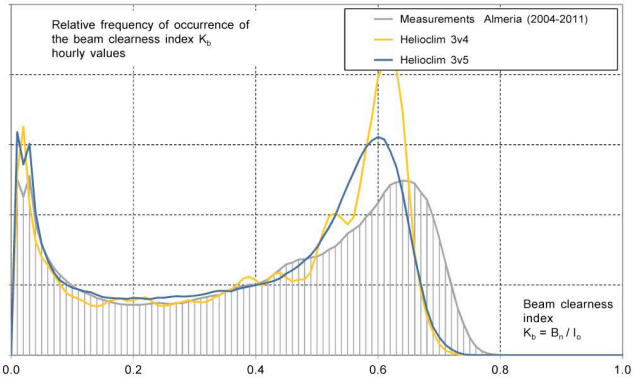

Figure a-16b Relative frequency of occurrence of the normal beam clearness index versus the corresponding clearness index K_t. The measurements are represented in grey.

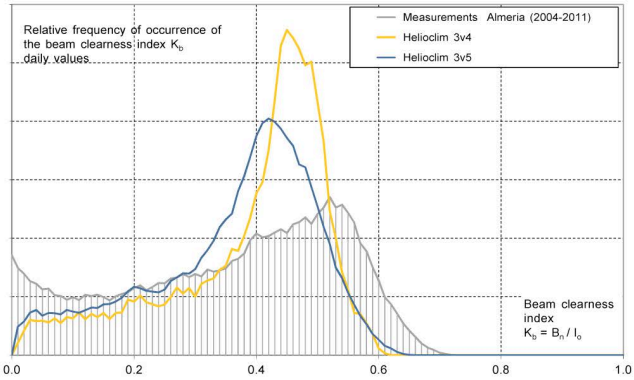

Figure a-17b Relative frequency of occurrence of the daily normal beam clearness index versus the corresponding clearness index. The measurements are represented in grey.

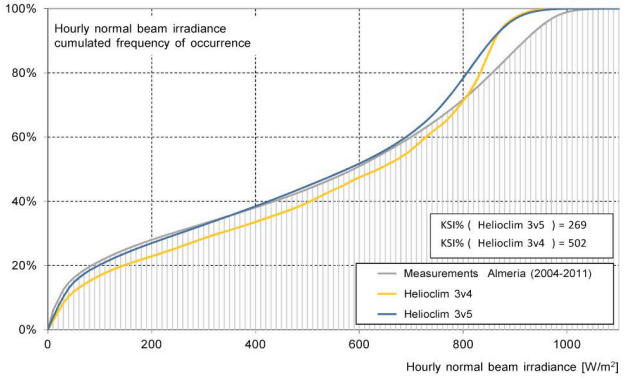

Figure a-18b Cumulated frequency of occurrence of the hourly normal beam irradiance values versus the corresponding irradiance. The measurements are represented in grey.

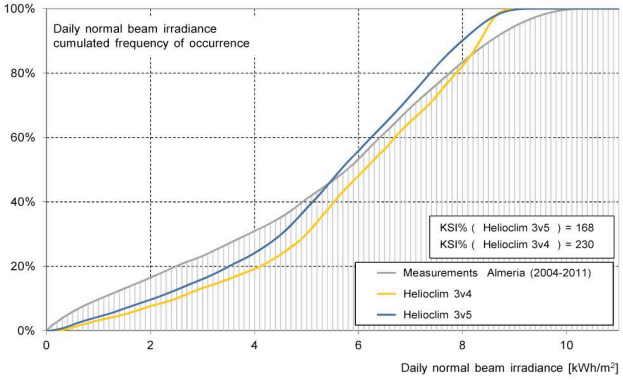

Figure a-19b Cumulated frequency of occurrence of the daily normal beam irradiance values versus the corresponding irradiance. The measurements are represented in grey.

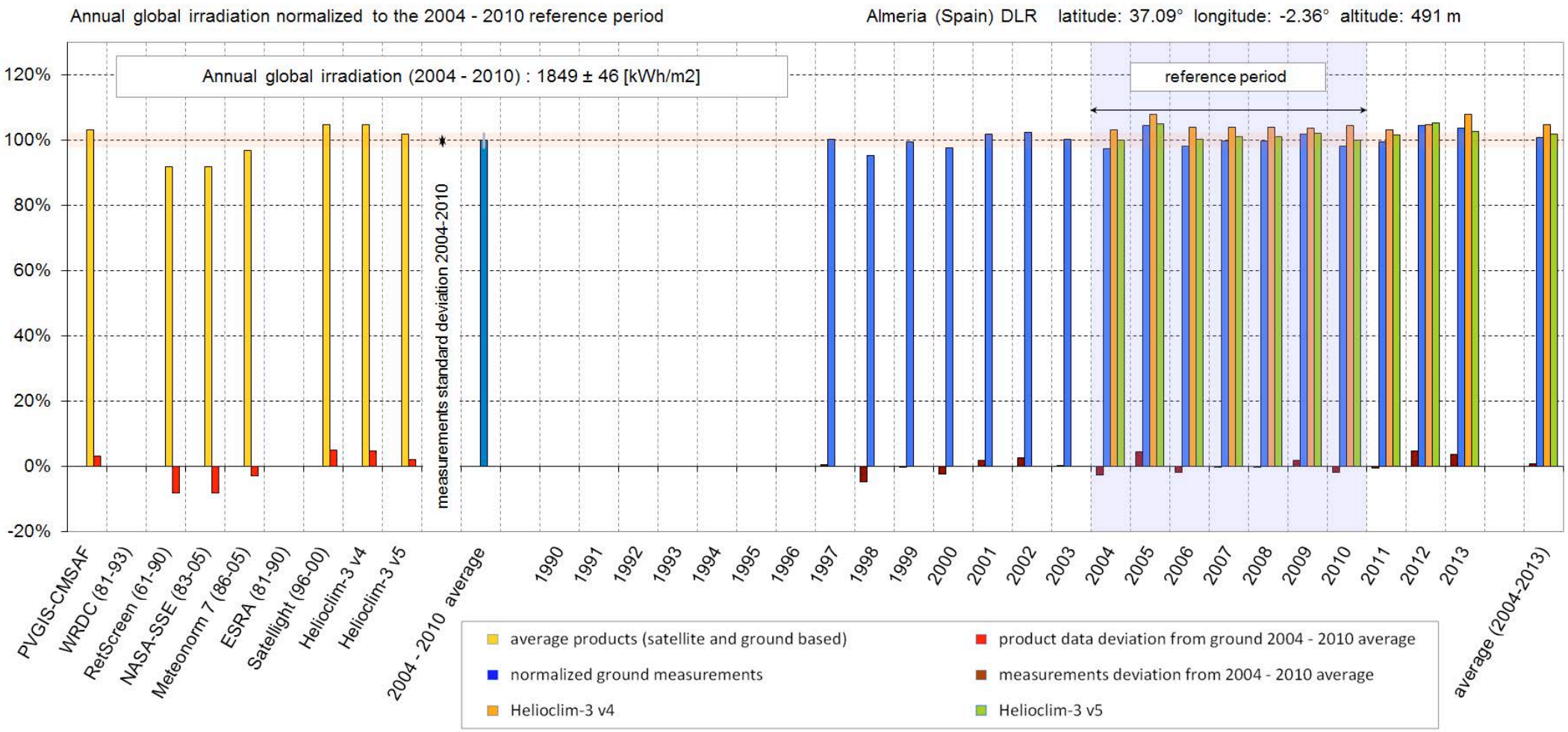

Figure a-20g Interannual variability of the global irradiation for the measurements, the average models, and the nowcasting products. The values are normalized to the 2004-2010 reference period average.

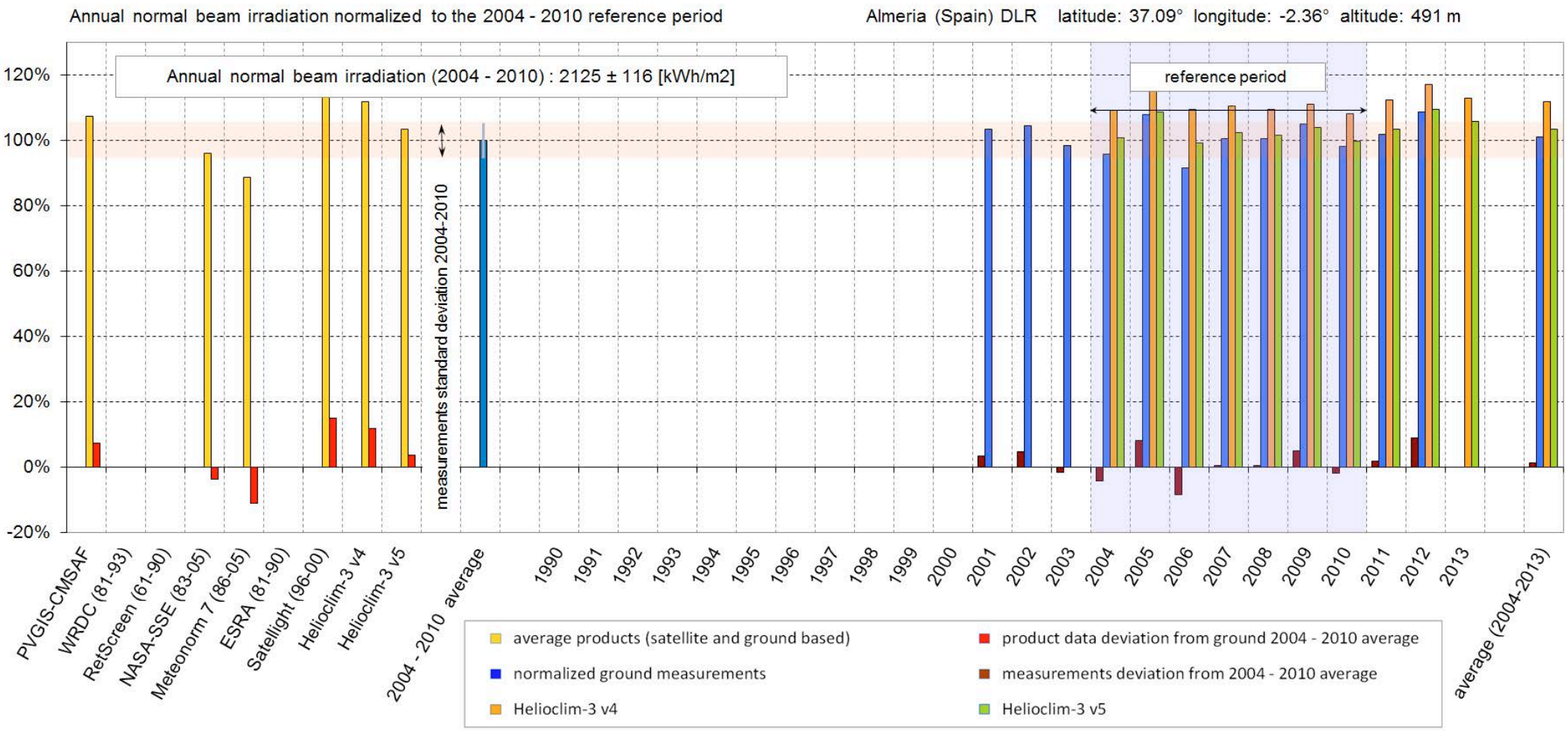

Figure a-20b Interannual variability of the normal beam irradiation for the measurements, the average models, and the nowcasting products. The values are normalized to the 2004-2010 reference period average.

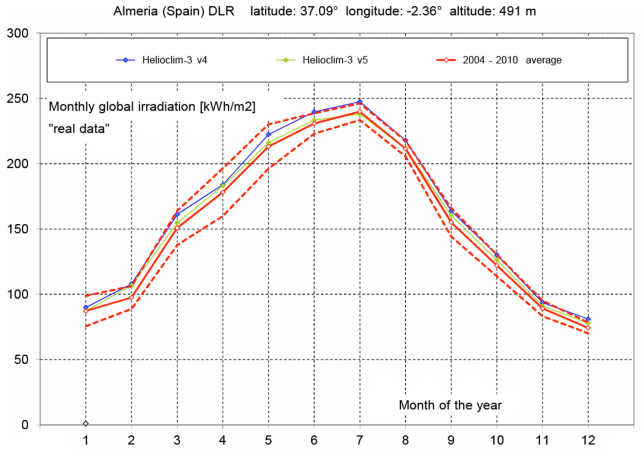

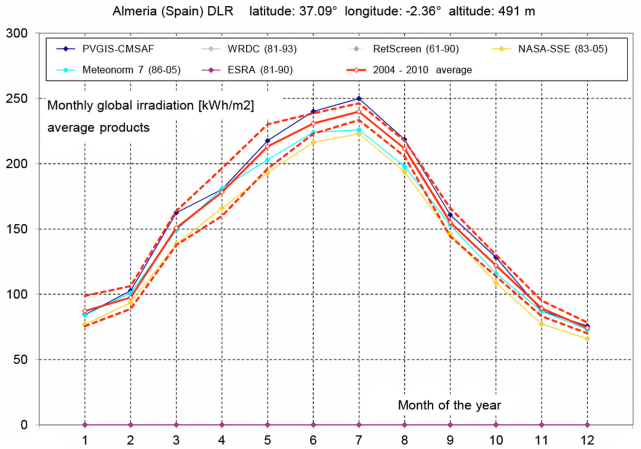

Figure a-21g Comparison of the monthly values for all the models. In red, the measurements, the red dashed lines represent ± one standard deviation.

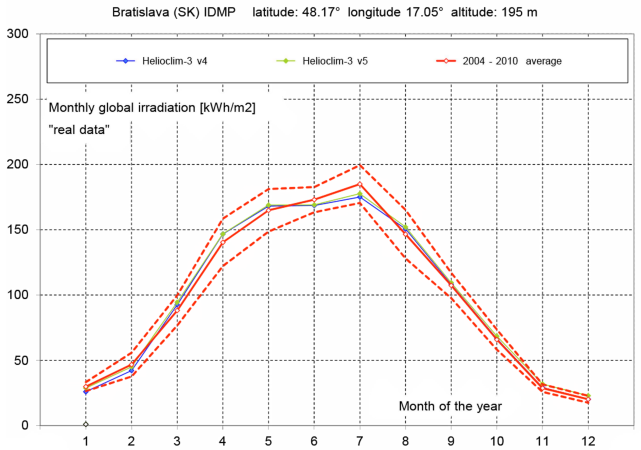

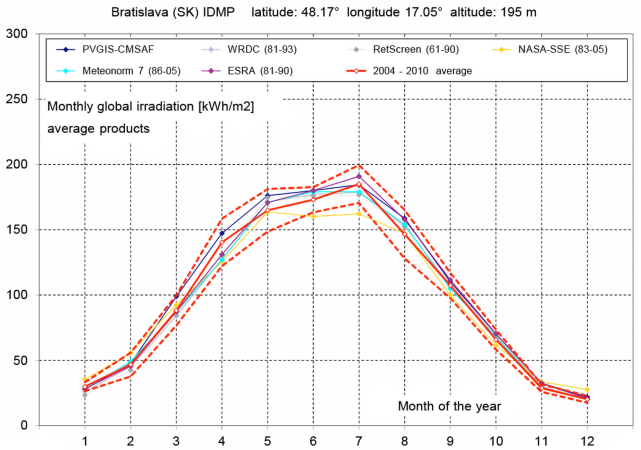

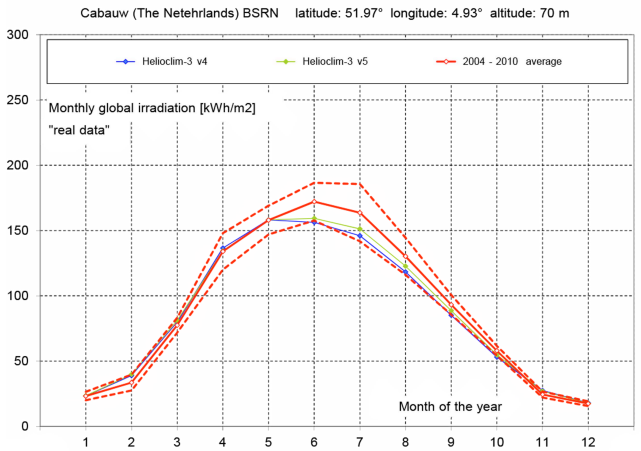

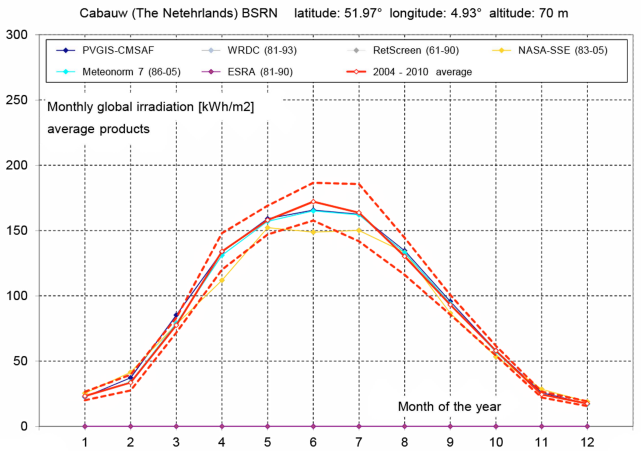

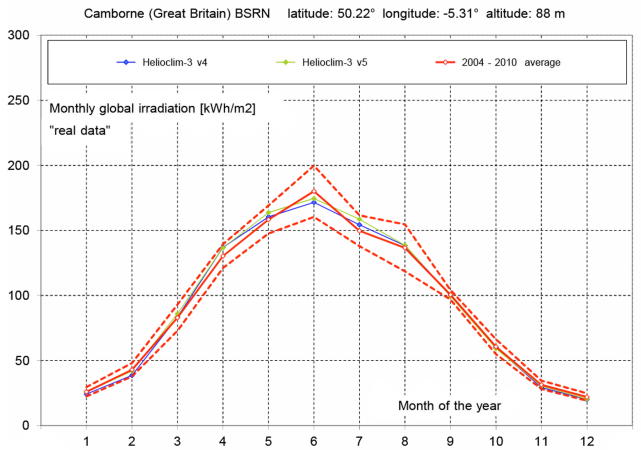

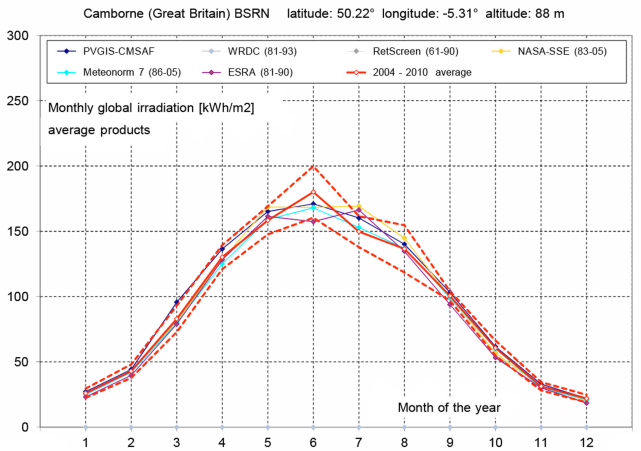

Carpentras (F) BSRN latitude: 44.08° longitude: 5.06° altitude: 100 m

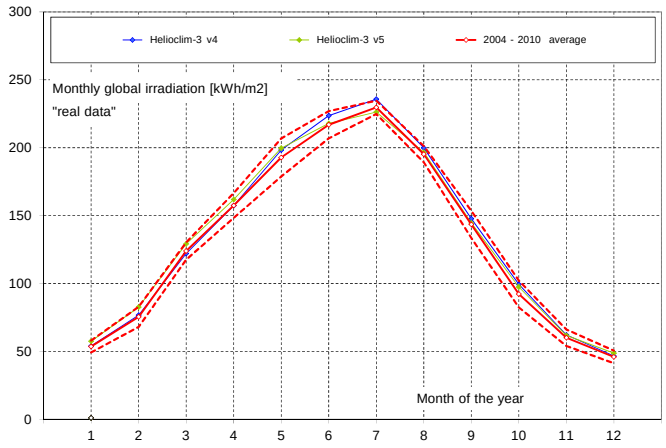

Carpentras (F) BSRN latitude: 44.08° longitude: 5.06° altitude: 100 m

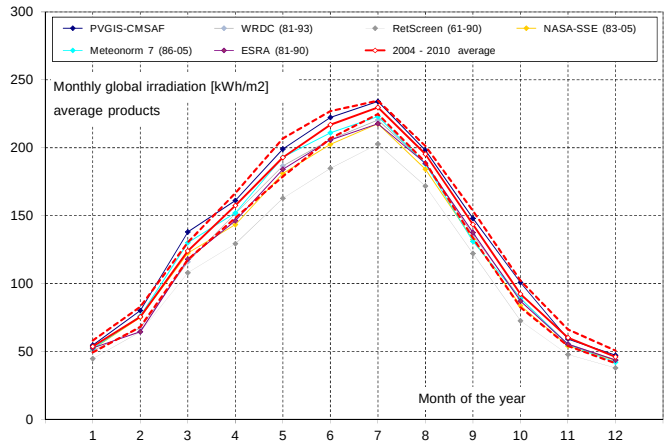

Davos (CH) LSF-PMOD latitude: 46.81° longitude: 9.84° altitude: 1586 m

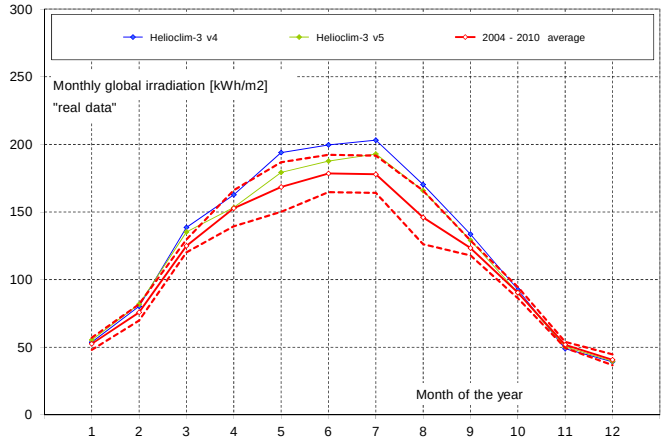

Davos (CH) LSF-PMOD latitude: 46.81° longitude: 9.84° altitude: 1586 m

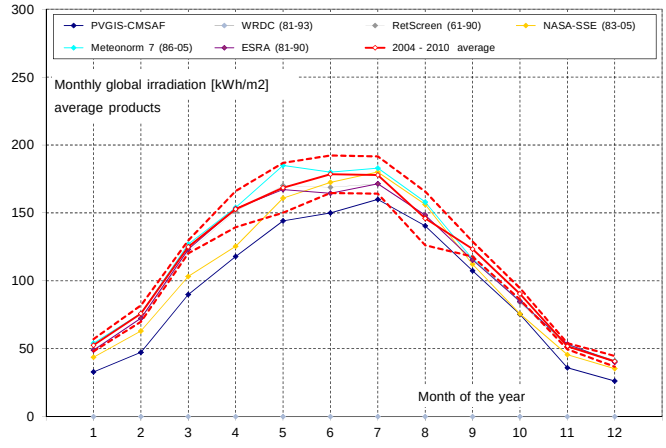

Geneva (CH) CIE-IDMP latitude: 46.20° longitude: 6.13° altitude: 420 m

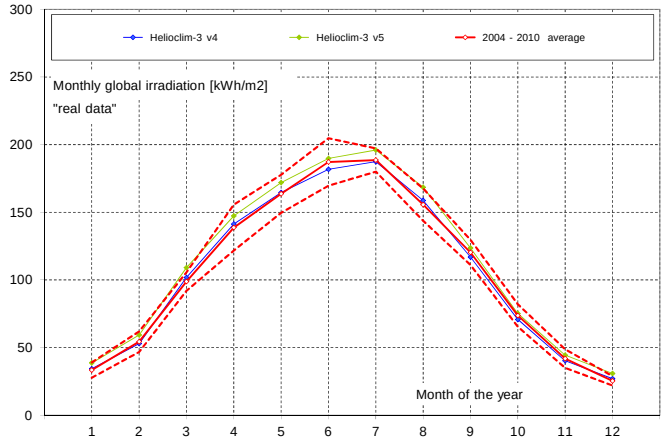

Geneva (CH) CIE-IDMP latitude: 46.20° longitude: 6.13° altitude: 420 m

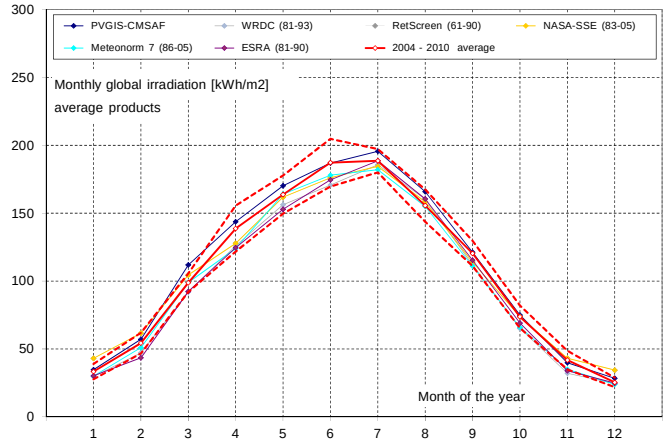

Kassel (D) FHG latitude: 51.312° longitude: 9.478° altitude: 173 m

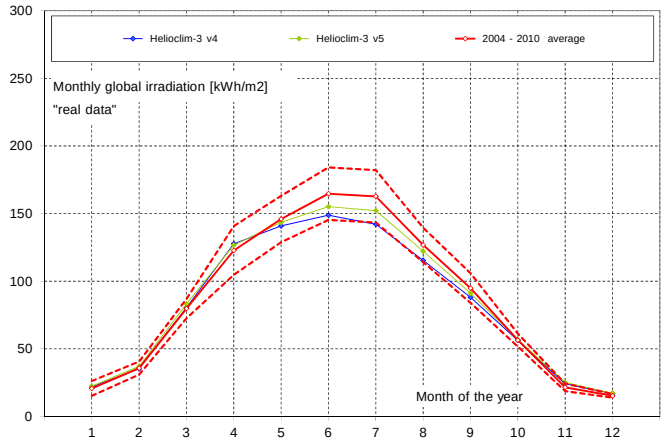

Kassel (D) FHG latitude: 51.312° longitude: 9.478° altitude: 173 m

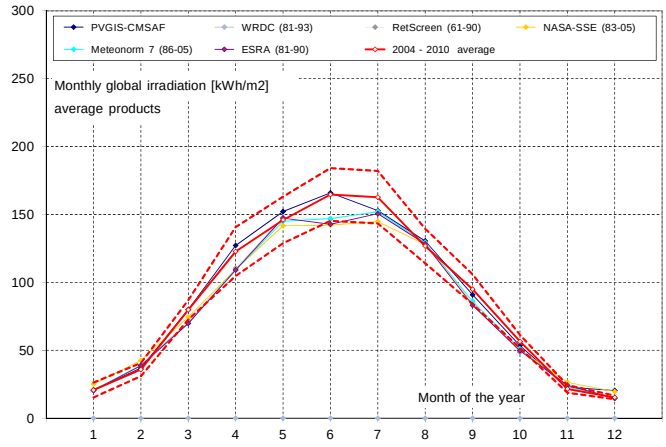

Kishinev (Moldavia) GAW latitude: 47.00° longitude: 28.82° altitude: 205 m

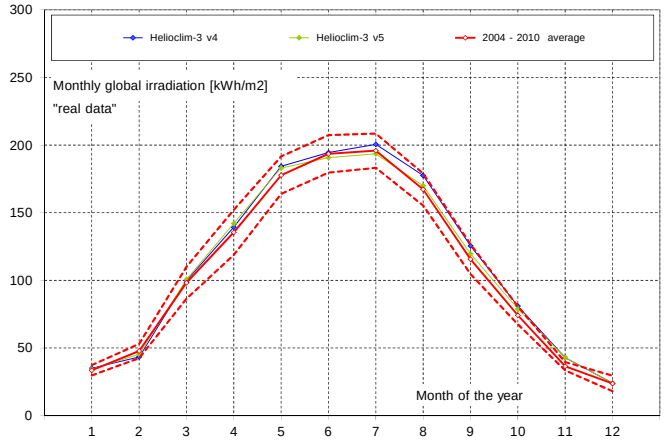

Kishinev (Moldavia) GAW latitude: 47.00° longitude: 28.82° altitude: 205 m

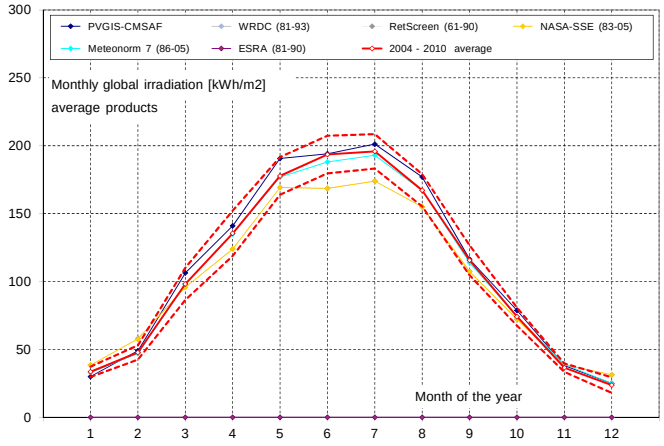

Lerwick (UK) BSRN-GAW latitude: 60.13° longitude: -1.18° altitude: 82 m

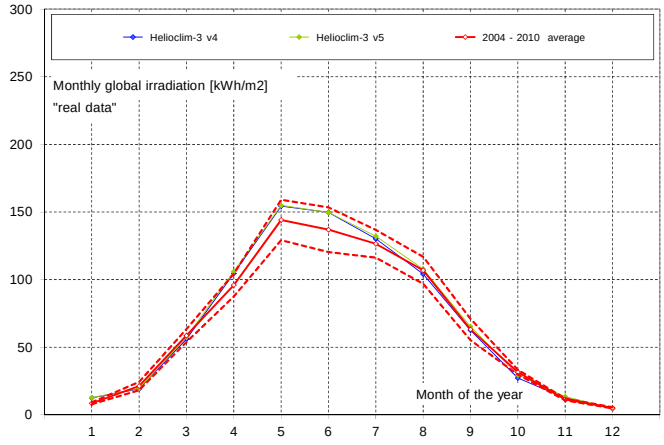

Lerwick (UK) BSRN-GAW latitude: 60.13° longitude: -1.18° altitude: 82 m

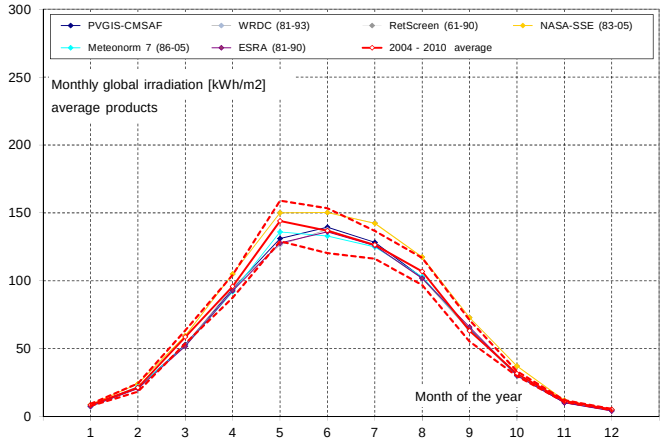

Lindenberg (D) BSRN latitude: 52.22° longitude: 14.12° altitude: 125 m

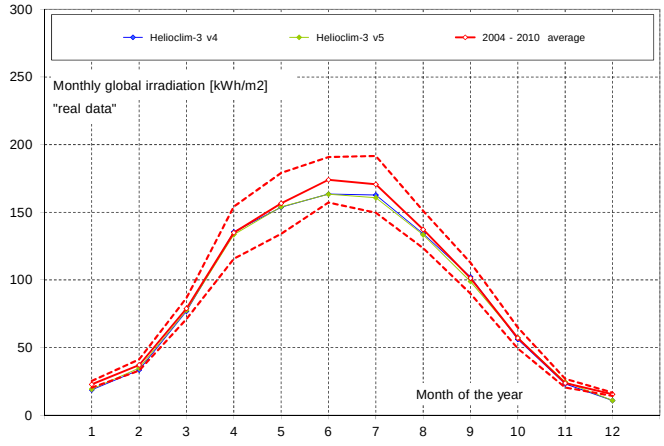

Lindenberg (D) BSRN latitude: 52.22° longitude: 14.12° altitude: 125 m

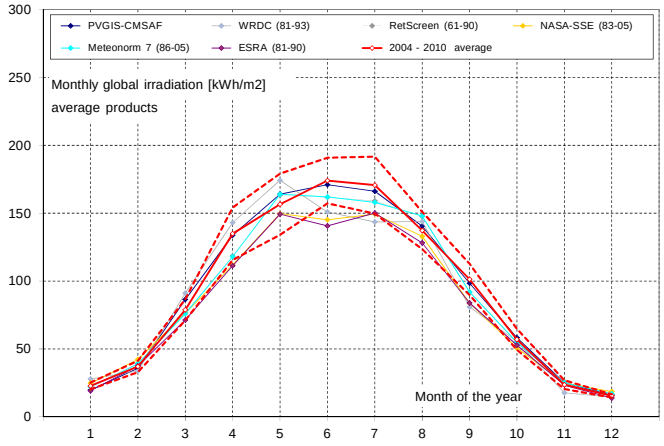

Madrid (SP) UMP latitude: 40.45° longitude: -3.73° altitude: 650 m

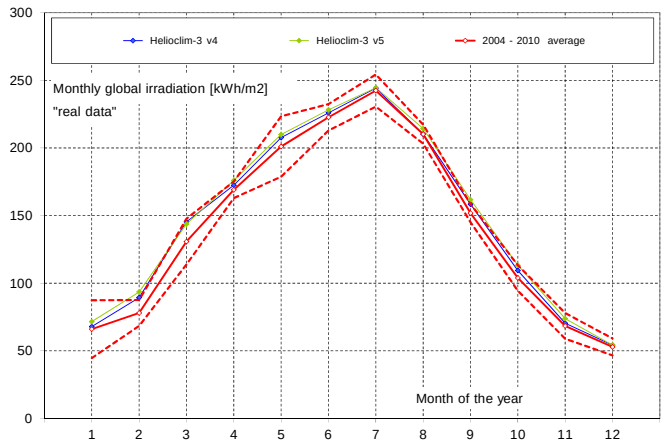

Madrid (SP) UMP latitude: 40.45° longitude: -3.73° altitude: 650 m

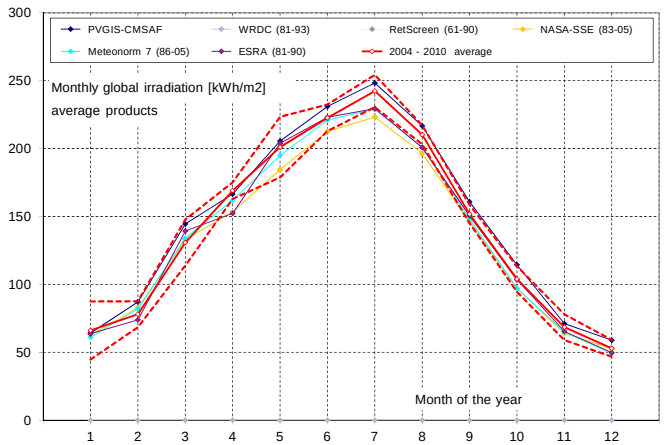

Nantes (F) CSTB - IDMP latitude: 47.25° longitude: -1.55° altitude: 30 m

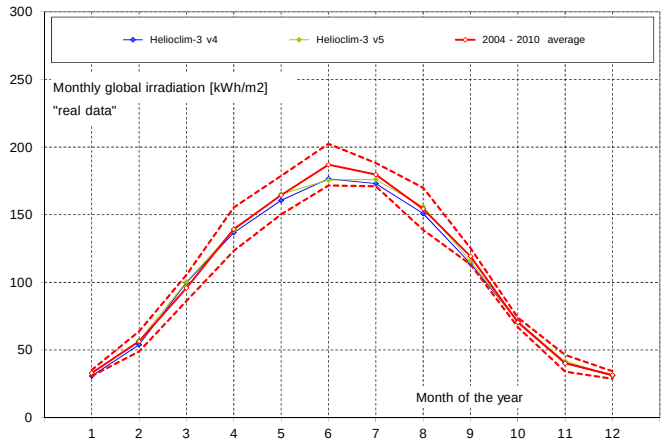

Nantes (F) CSTB - IDMP latitude: 47.25° longitude: -1.55° altitude: 30 m

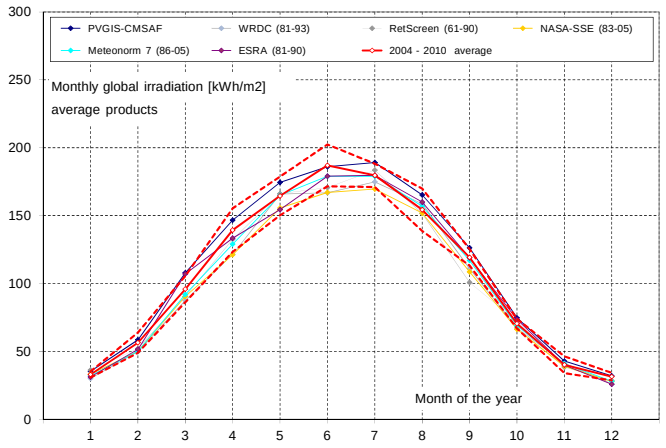

Payerne (CH) BSRN latitude: 46.82° longitude: 6.95° altitude: 490 m

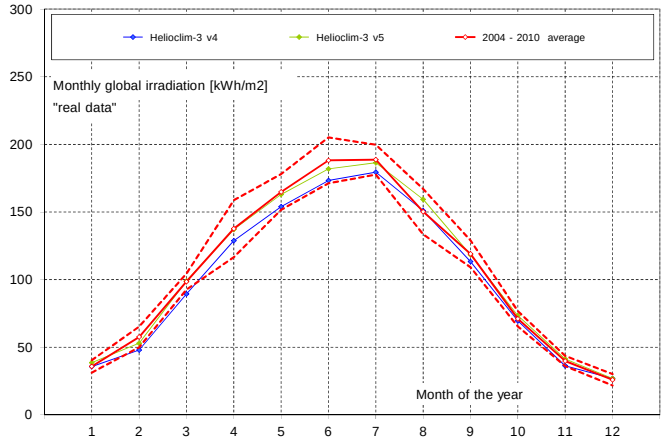

Payerne (CH) BSRN latitude: 46.82° longitude: 6.95° altitude: 490 m

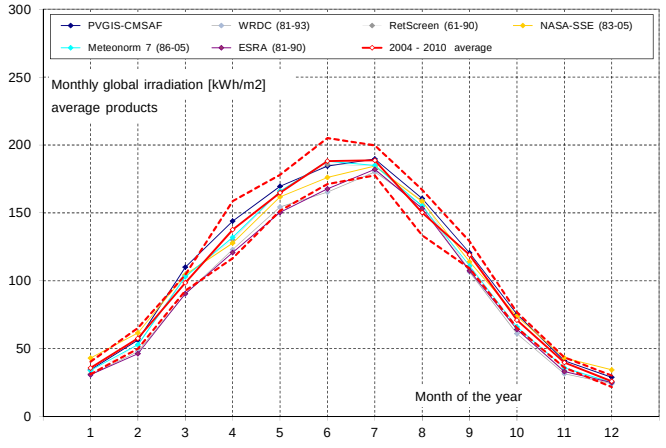

Sede Boqer (Israel) BSRN latitude: 30.91° longitude: 34.78° altitude: 457 m

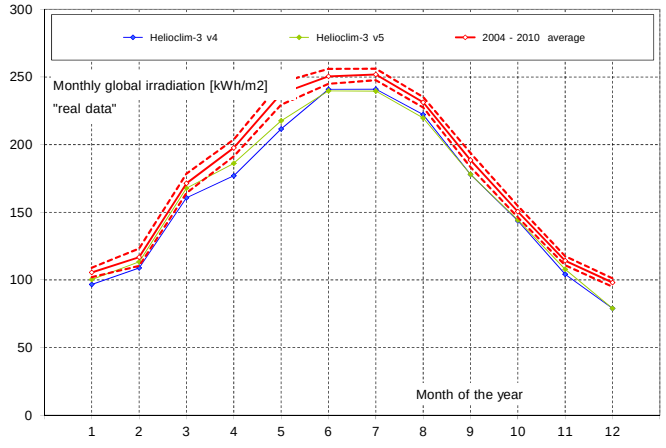

Sede Boqer (Israel) BSRN latitude: 30.91° longitude: 34.78° altitude: 457 m

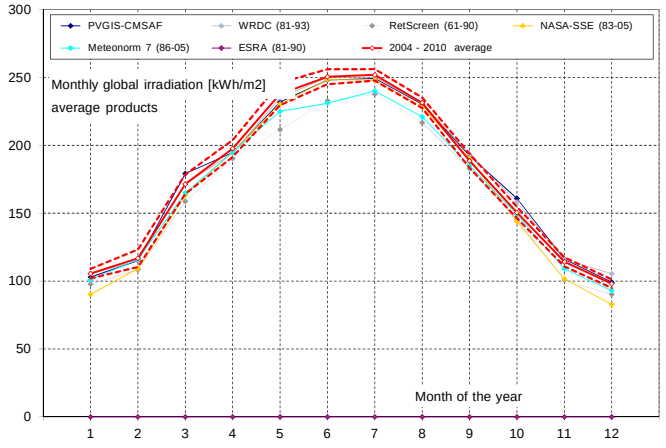

Tamanrasset (Algeria) BSRN latitude: 22.78° longitude: 5.52° altitude: 1400 m

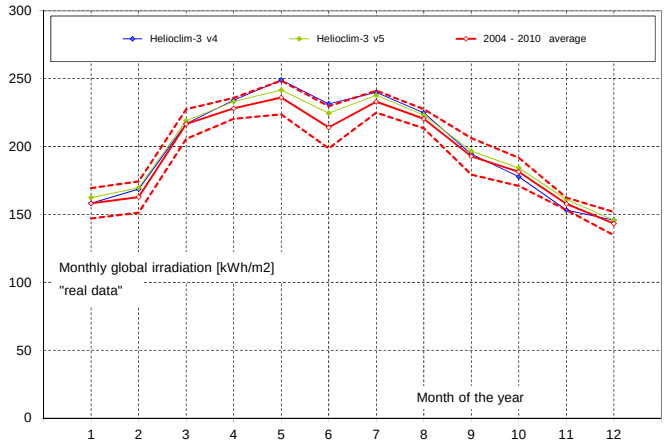

Tamanrasset (Algeria) BSRN latitude: 22.78° longitude: 5.52° altitude: 1400 m

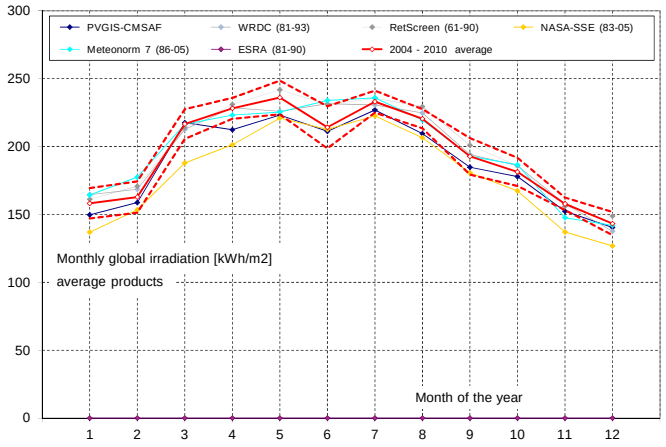

Toravere (Estonia) BSRN latitude: 58.27° longitude: 26.47 altitude: 70 m

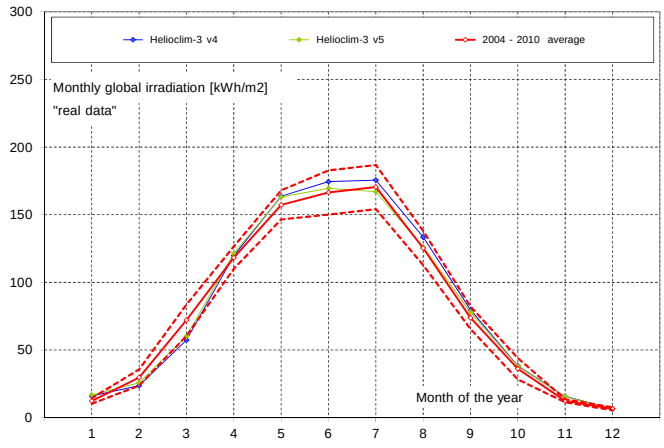

Toravere (Estonia) BSRN latitude: 58.27° longitude: 26.47 altitude: 70 m

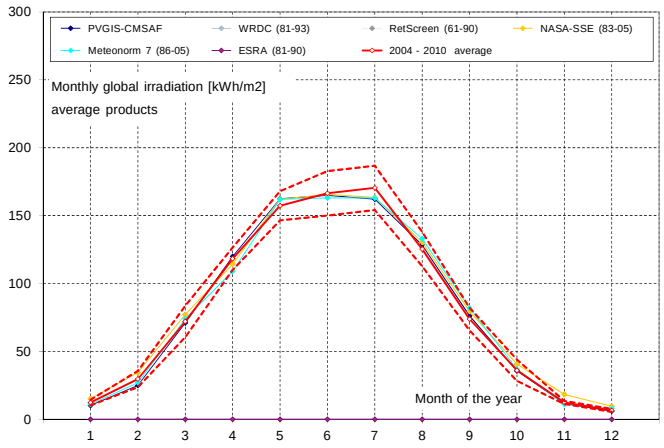

Valentia (Ireland) WRDC latitude: 51.93° longitude: -10.25° altitude: 14 m

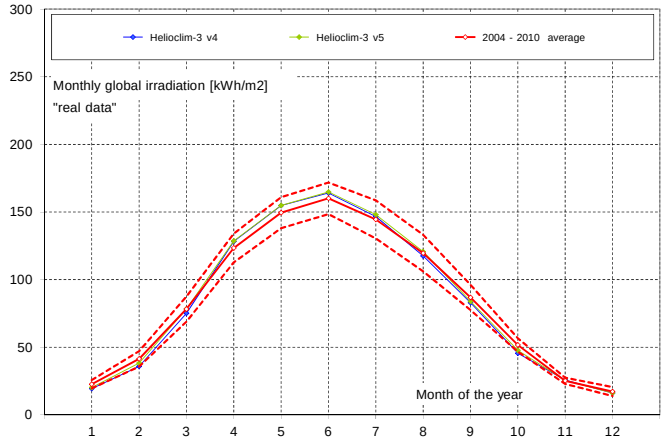

Valentia (Ireland) WRDC latitude: 51.93° longitude: -10.25° altitude: 14 m

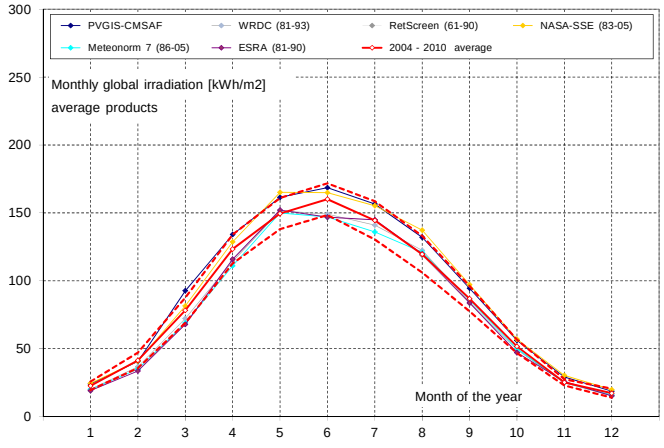

Vaulx-en-Velin (F) ENTPE - IDMP latitude: 45.78° longitude: 4.93° altitude: 170 m

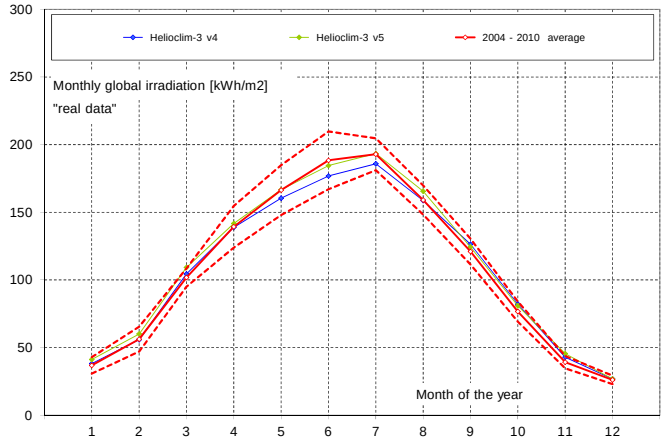

Vaulx-en-Velin (F) ENTPE - IDMP latitude: 45.78° longitude: 4.93° altitude: 170 m

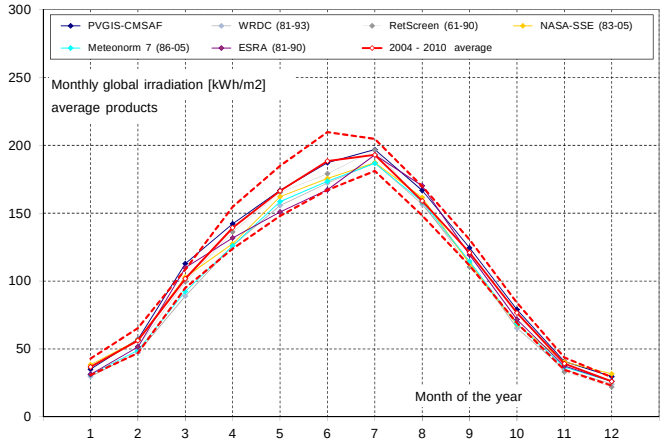

Wien (A) WRDC latitude: 48.25° longitude: 16.35° altitude: 203 m

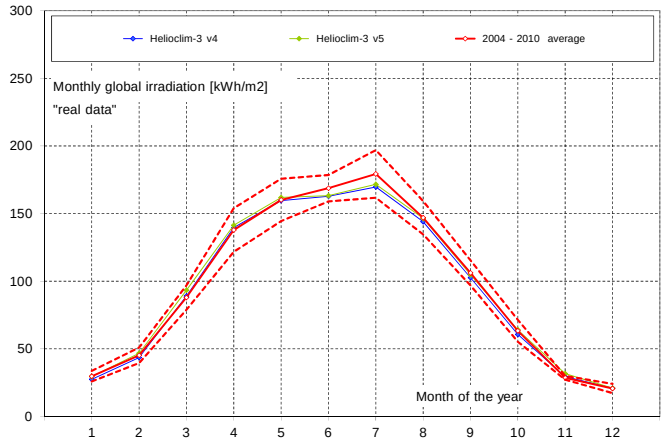

Wien (A) WRDC latitude: 48.25° longitude: 16.35° altitude: 203 m

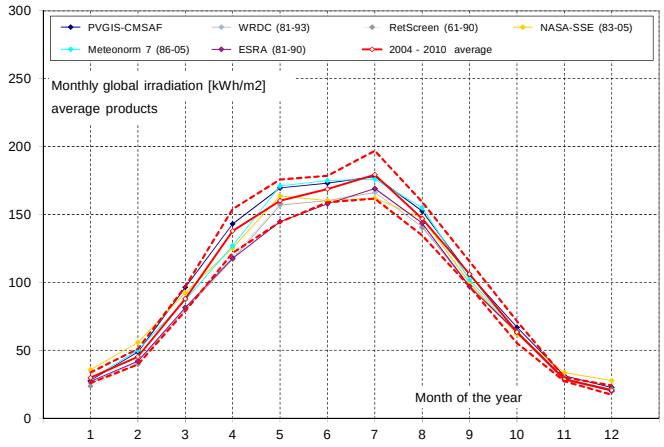

Zilani (Lativa) WRDC latitude: 56.52° longitude 25.92° altitude: 107 m

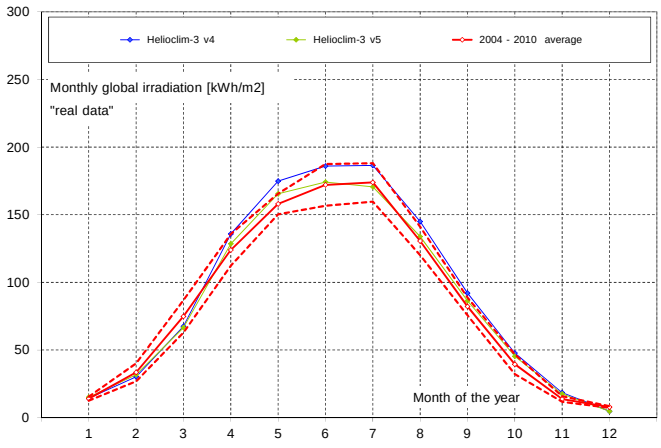

Zilani (Lativa) WRDC latitude: 56.52° longitude 25.92° altitude: 107 m

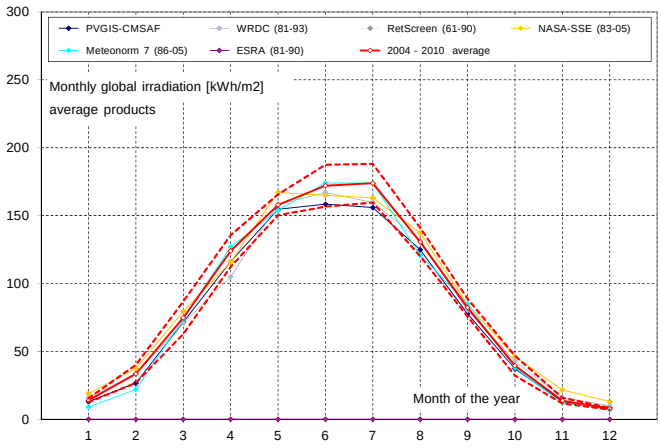

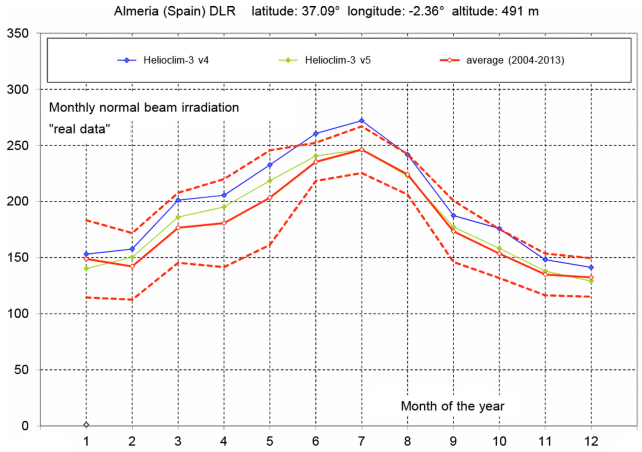

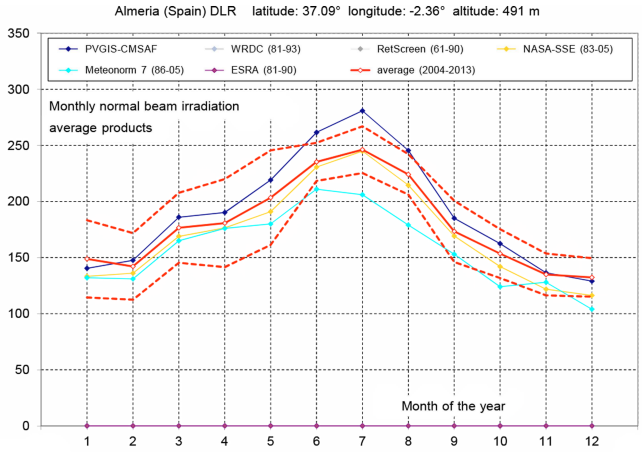

Figure a-21b Comparison of the monthly values for all the models. In red, the measurements, the red dashed lines represent ± one standard deviation.

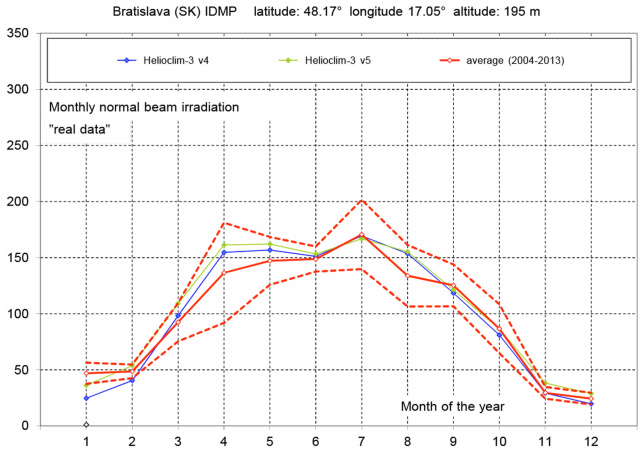

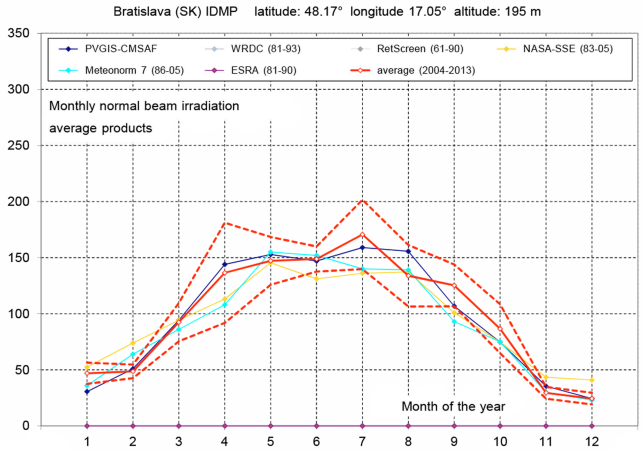

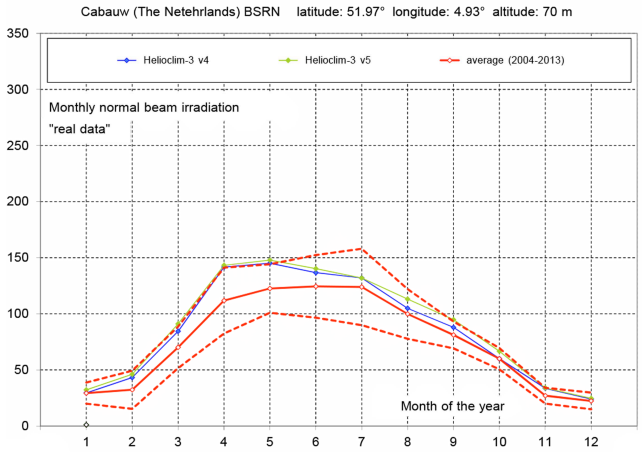

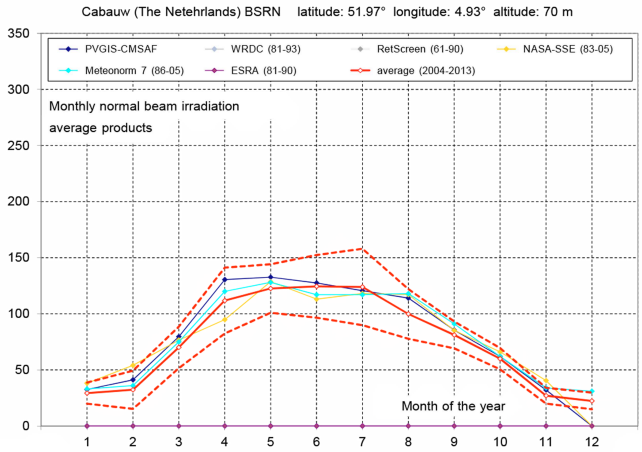

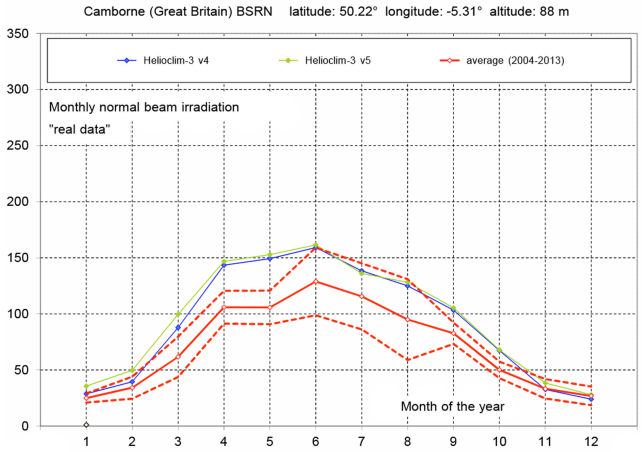

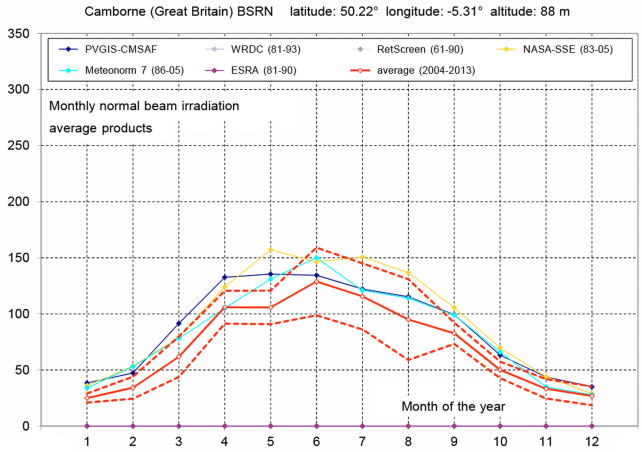

Carpentras (F) BSRN latitude: 44.08° longitude: 5.06° altitude: 100 m

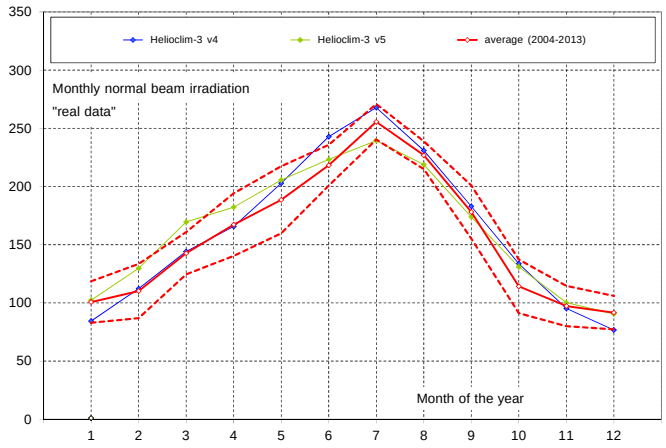

Carpentras (F) BSRN latitude: 44.08° longitude: 5.06° altitude: 100 m

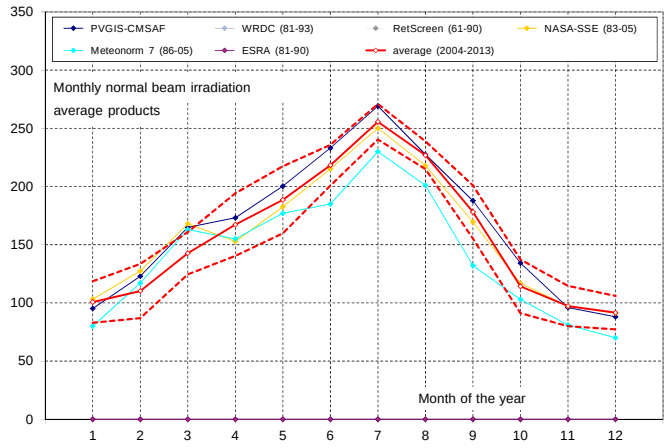

Davos (CH) LSF-PMOD latitude: 46.81° longitude: 9.84° altitude: 1586 m

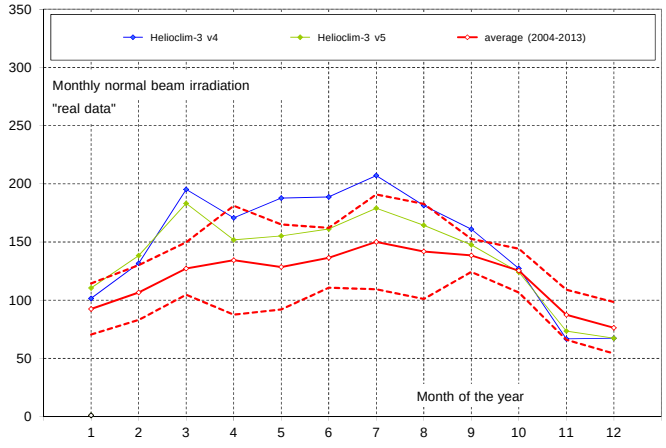

Davos (CH) LSF-PMOD latitude: 46.81° longitude: 9.84° altitude: 1586 m

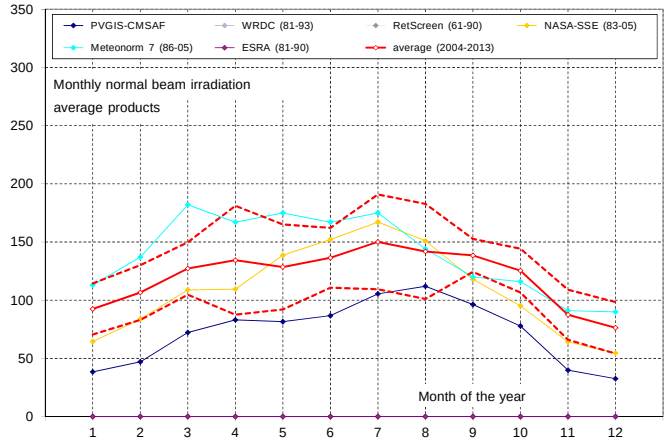

Geneva (CH) CIE-IDMP latitude: 46.20° longitude: 6.13° altitude: 420 m

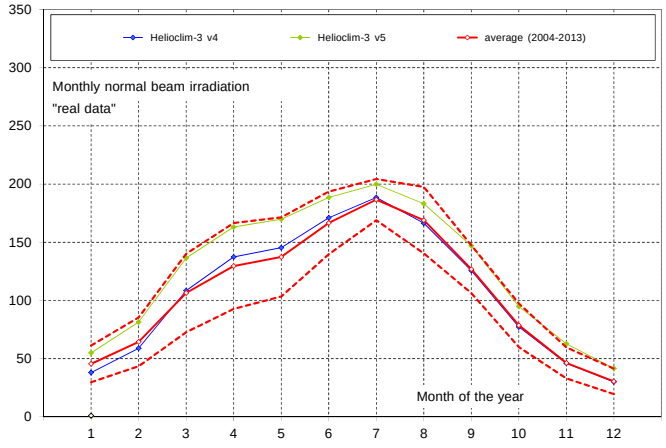

Geneva (CH) CIE-IDMP latitude: 46.20° longitude: 6.13° altitude: 420 m

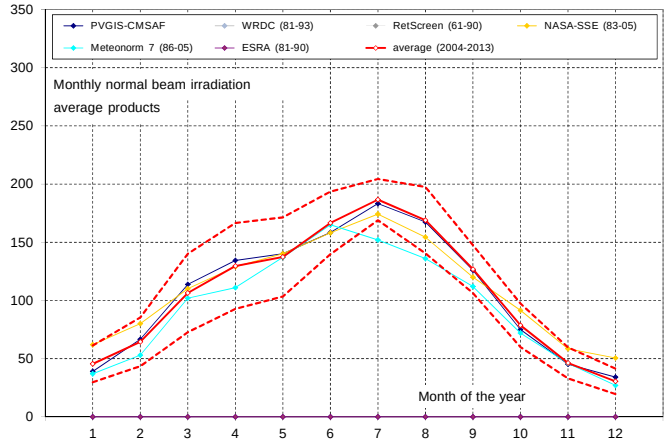

Kassel (D) FHG latitude: 51.312° longitude: 9.478° altitude: 173 m

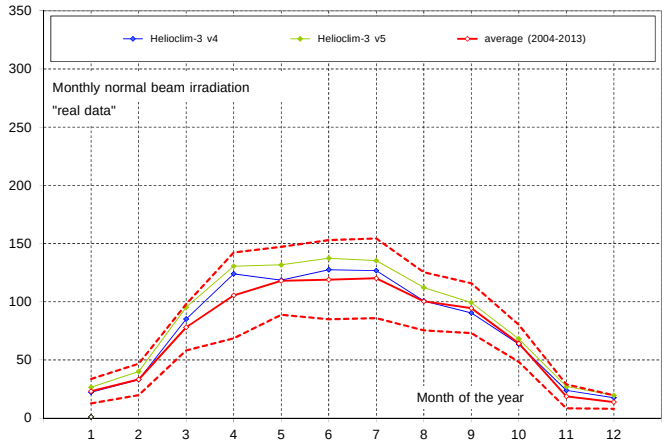

Kassel (D) FHG latitude: 51.312° longitude: 9.478° altitude: 173 m

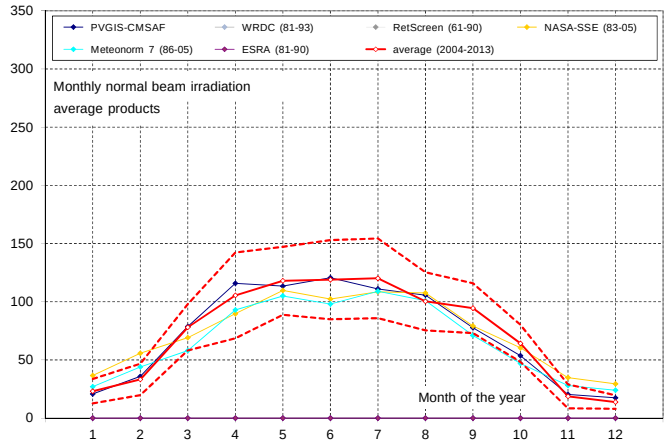

Kishinev (Moldavia) GAW latitude: 47.00° longitude: 28.82° altitude: 205 m

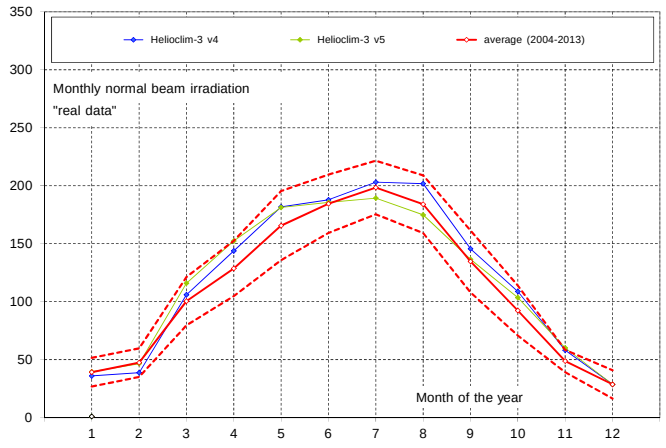

Kishinev (Moldavia) GAW latitude: 47.00° longitude: 28.82° altitude: 205 m

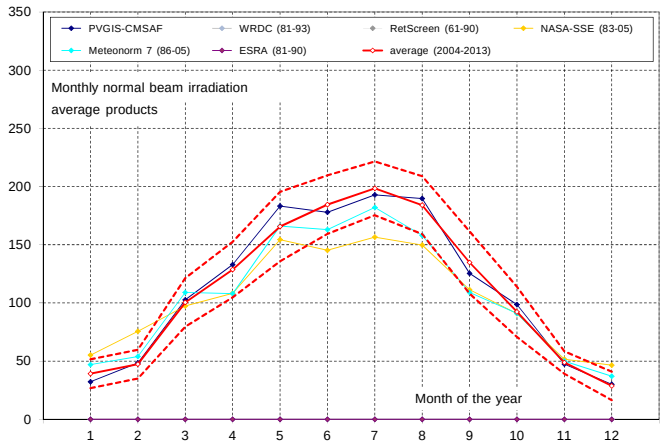

Lerwick (UK) BSRN-GAW latitude: 60.13° longitude: -1.18° altitude: 82 m

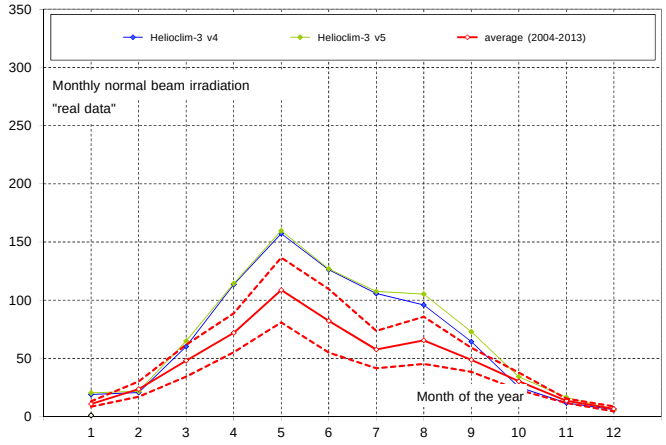

Lerwick (UK) BSRN-GAW latitude: 60.13° longitude: -1.18° altitude: 82 m

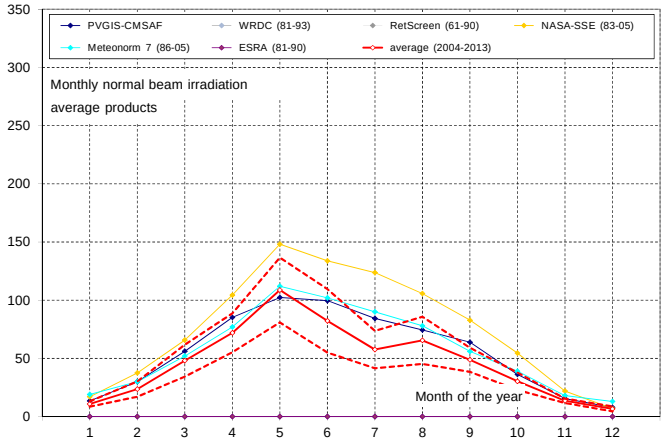

Lindenberg (D) BSRN latitude: 52.22° longitude: 14.12° altitude: 125 m

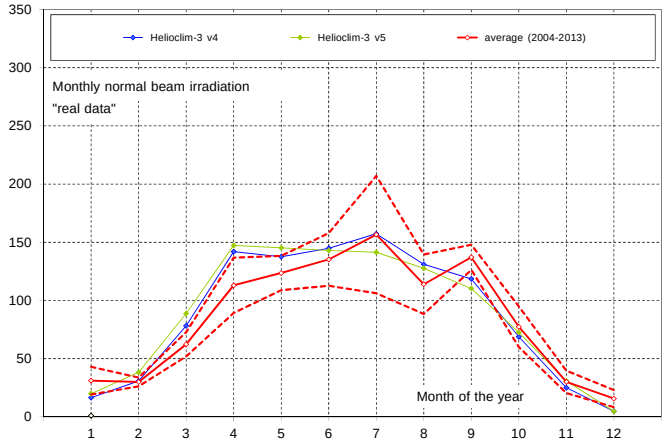

Lindenberg (D) BSRN latitude: 52.22° longitude: 14.12° altitude: 125 m

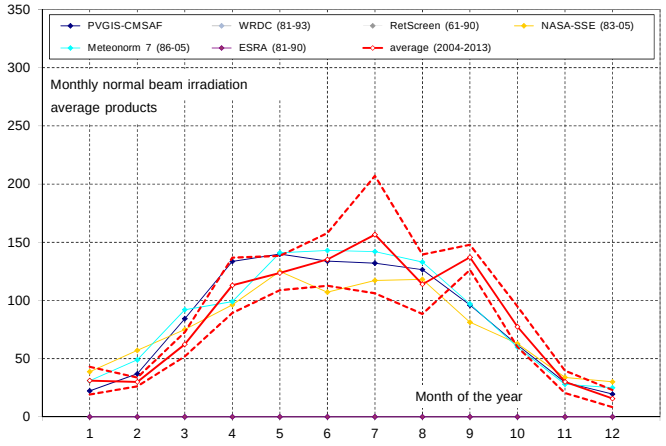

Madrid (SP) UMP latitude: 40.45° longitude: -3.73° altitude: 650 m

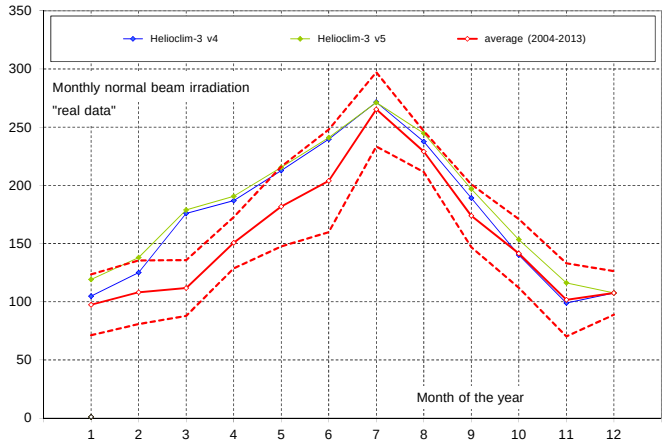

Madrid (SP) UMP latitude: 40.45° longitude: -3.73° altitude: 650 m

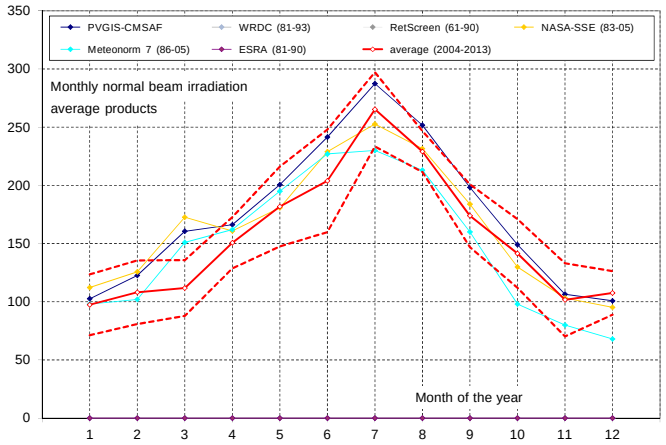

Nantes (F) CSTB - IDMP latitude: 47.25° longitude: -1.55° altitude: 30 m

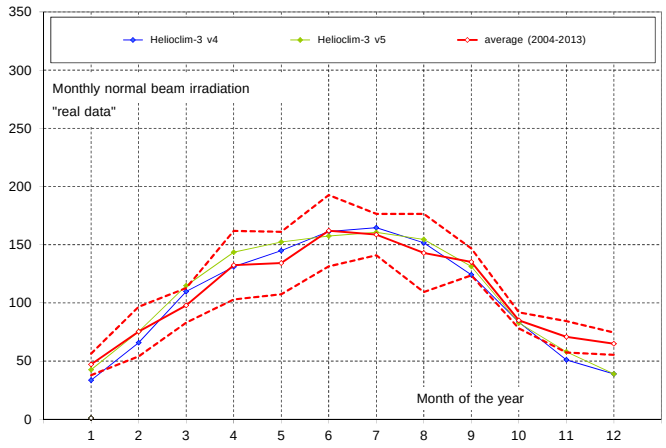

Nantes (F) CSTB - IDMP latitude: 47.25° longitude: -1.55° altitude: 30 m

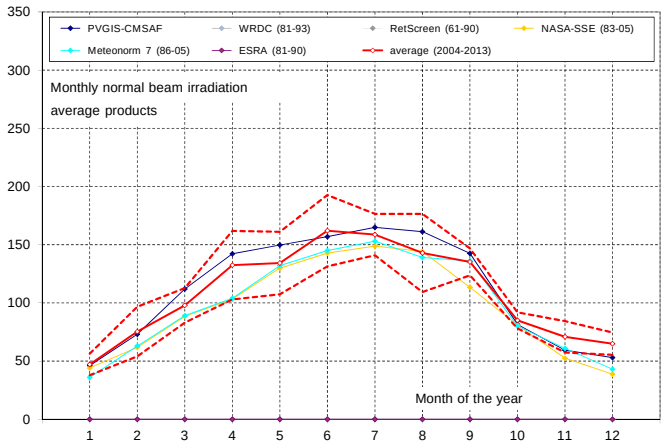

Payerne (CH) BSRN latitude: 46.82° longitude: 6.95° altitude: 490 m

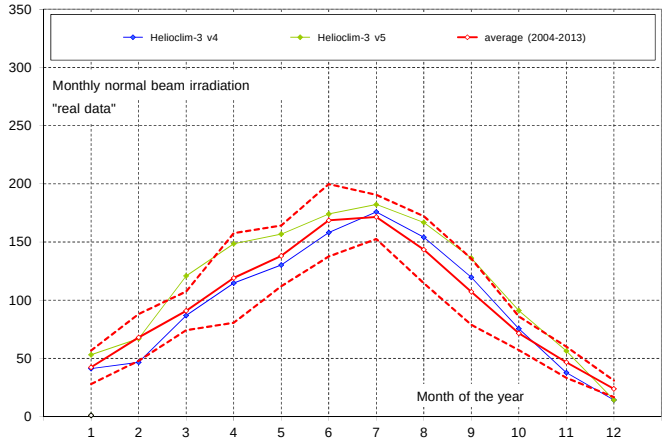

Payerne (CH) BSRN latitude: 46.82° longitude: 6.95° altitude: 490 m

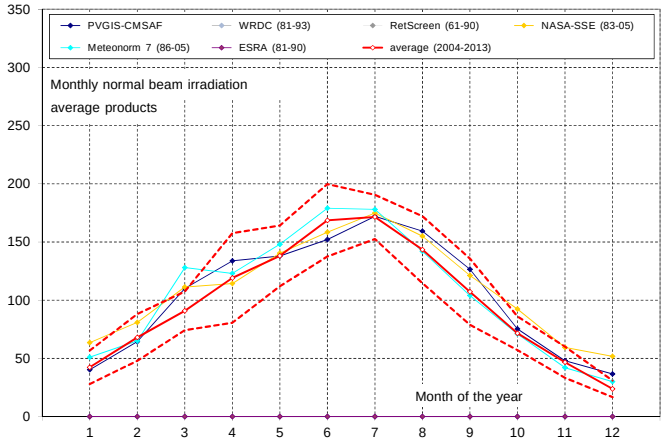

Sede Boqer (Israel) BSRN latitude: 30.91° longitude: 34.78° altitude: 457 m

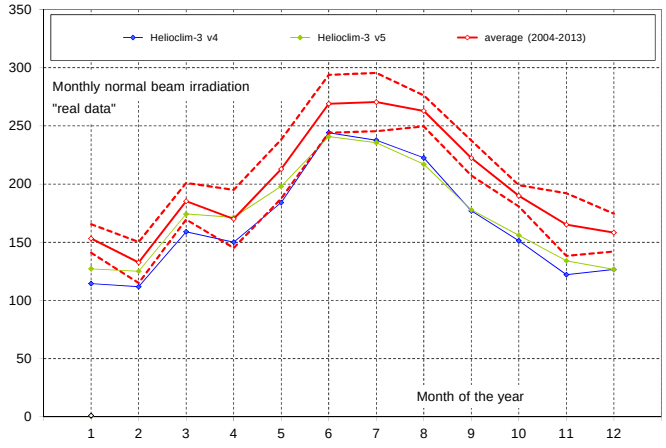

Sede Boqer (Israel) BSRN latitude: 30.91° longitude: 34.78° altitude: 457 m

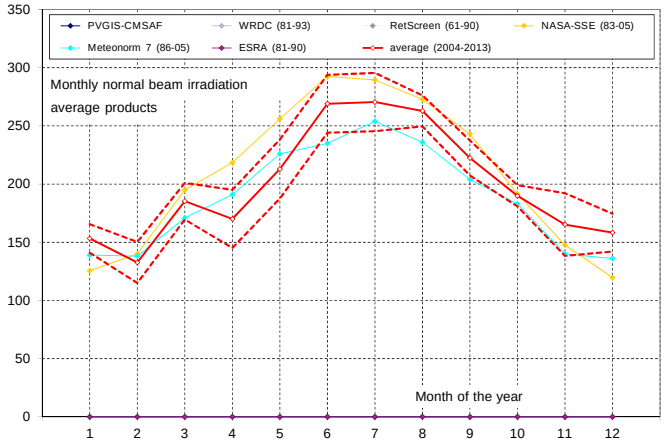

Tamanrasset (Algeria) BSRN latitude: 22.78° longitude: 5.52° altitude: 1400 m

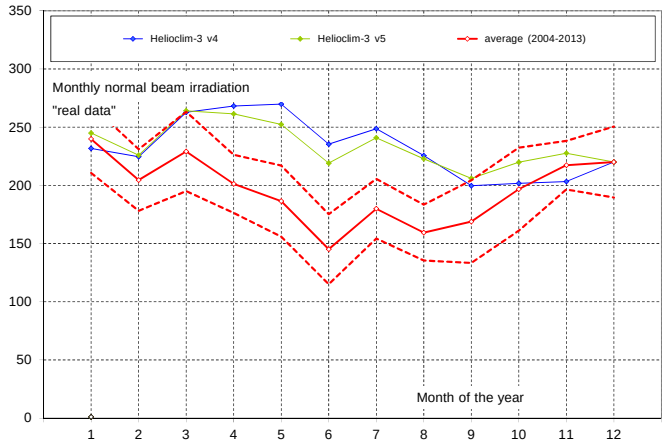

Tamanrasset (Algeria) BSRN latitude: 22.78° longitude: 5.52° altitude: 1400 m

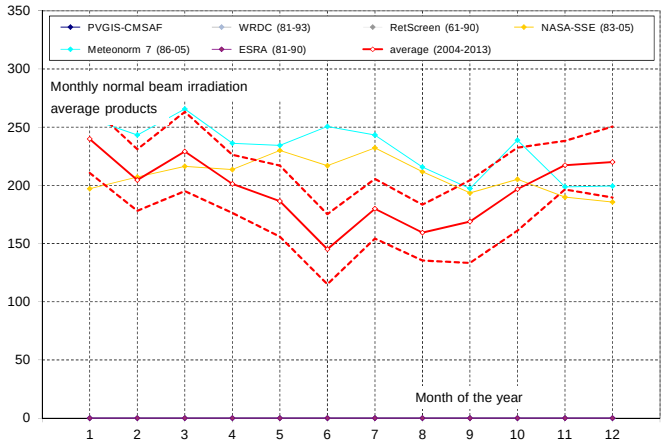

Toravere (Estonia) BSRN latitude: 58.27° longitude: 26.47 altitude: 70 m

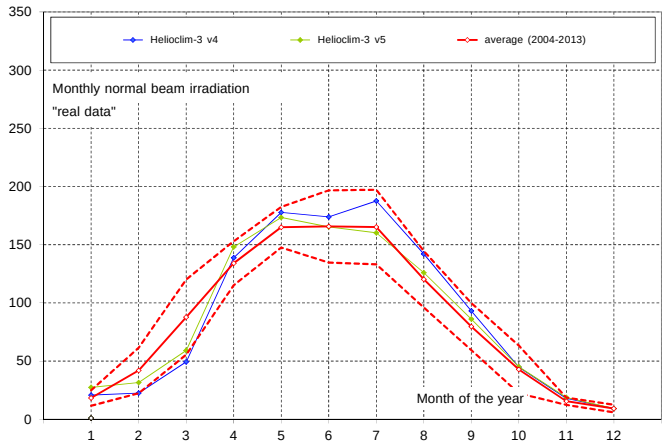

Toravere (Estonia) BSRN latitude: 58.27° longitude: 26.47 altitude: 70 m

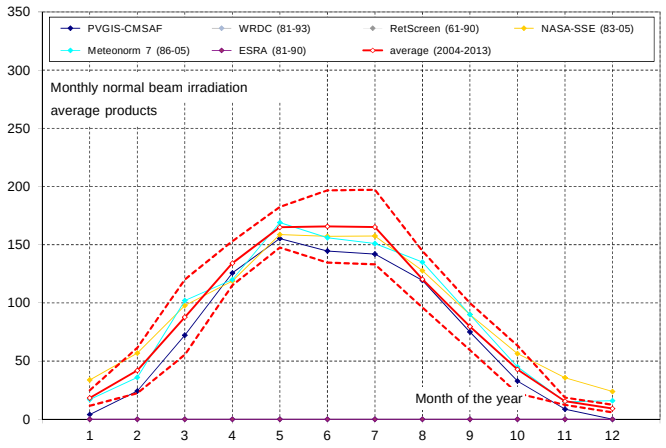

Valentia (Ireland) WRDC latitude: 51.93° longitude: -10.25° altitude: 14 m

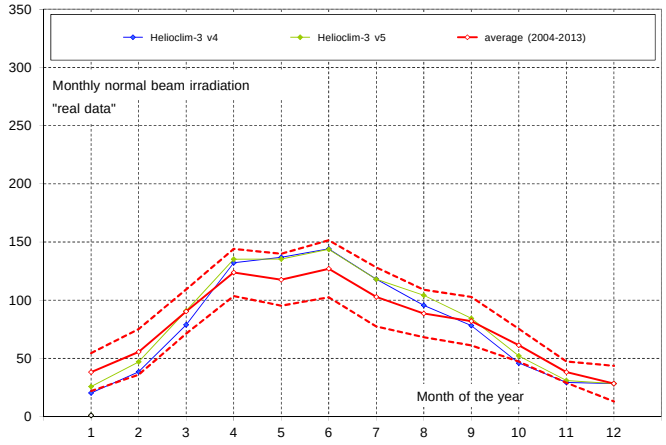

Valentia (Ireland) WRDC latitude: 51.93° longitude: -10.25° altitude: 14 m

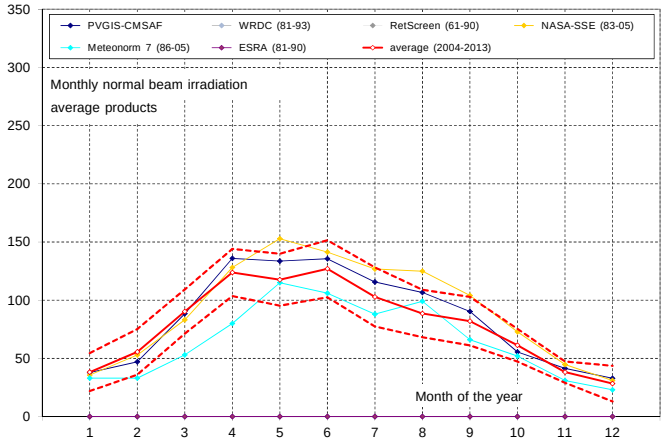

Vaulx-en-Velin (F) ENTPE - IDMP latitude: 45.78° longitude: 4.93° altitude: 170 m

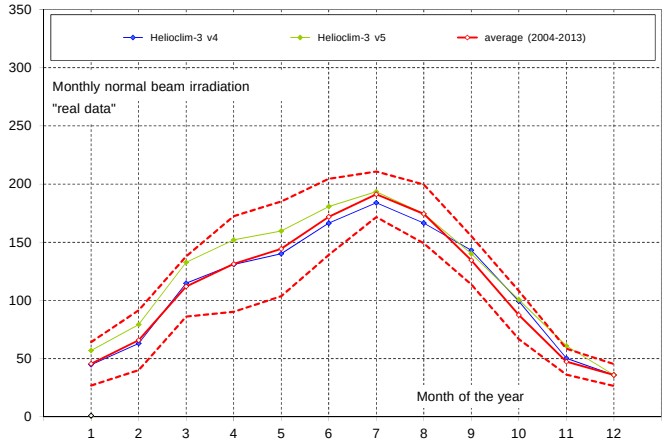

Vaulx-en-Velin (F) ENTPE - IDMP latitude: 45.78° longitude: 4.93° altitude: 170 m

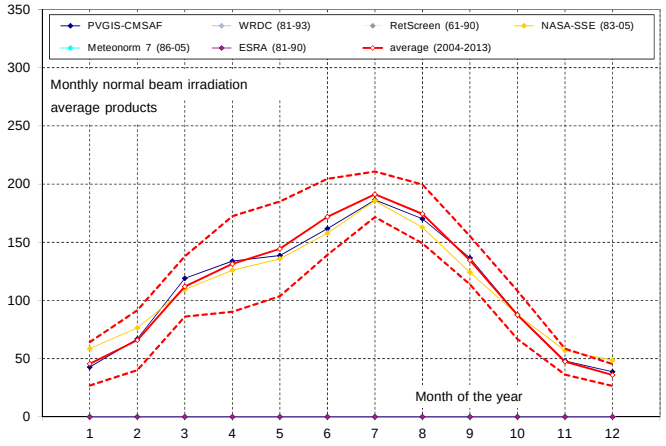

Wien (A) WRDC latitude: 48.25° longitude: 16.35° altitude: 203 m

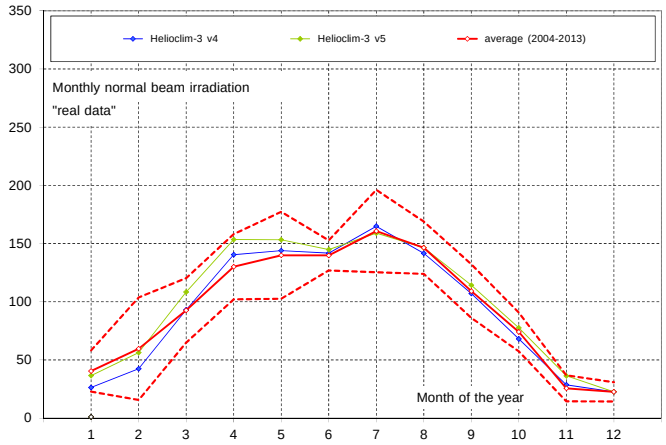

Wien (A) WRDC latitude: 48.25° longitude: 16.35° altitude: 203 m

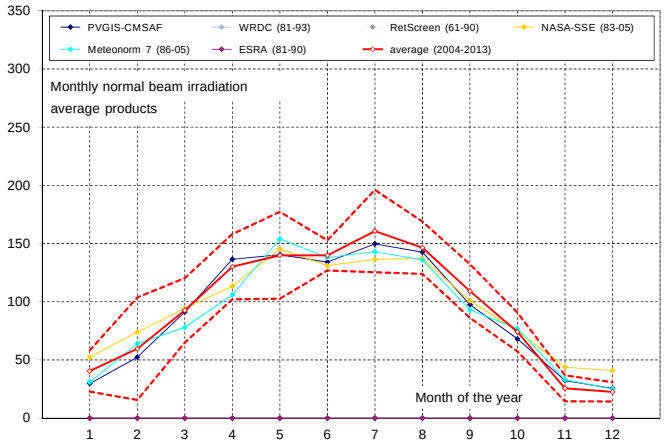

Zilani (Lativa) WRDC latitude: 56.52° longitude 25.92° altitude: 107 m

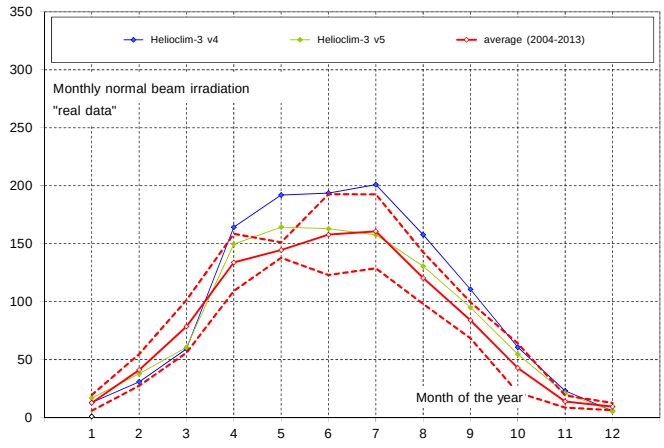

Zilani (Lativa) WRDC latitude: 56.52° longitude 25.92° altitude: 107 m

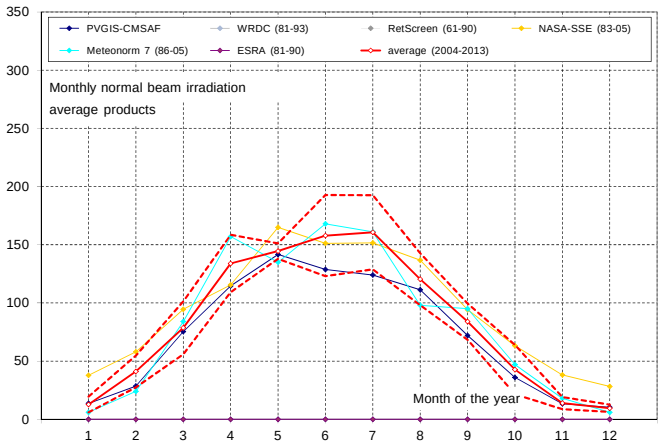

Global irradiance	Hourly values									
	HelioClim-3v4					HelioClim-3v5				
	Gh	nb	R	mbd	sd	Gh	nb	R	mbd	sd
Almeria 2004 - 2011	416	34772	0.981	5%	14%	416	34769	0.983	2%	13%
Bratislava 2004 - 2007	255	18120	0.971	0%	23%	257	17958	0.971	2%	24%
Cabauw 2004 - 2013	253	36243	0.967	-4%	23%	253	36209	0.969	-3%	22%
Camborne 2004 - 2013	254	32920	0.971	0%	22%	254	32911	0.972	2%	22%
Carpentras 2004 - 2013	401	36075	0.985	0%	12%	400	36101	0.986	1%	11%
Davos 2004 - 2011	339	23924	0.933	9%	29%	339	23927	0.938	5%	28%
Geneva 2004 - 2013	286	44421	0.975	-1%	20%	286	44389	0.976	6%	21%
Kassel 2004 - 2011	236	34177	0.964	-5%	26%	237	34162	0.966	-1%	25%
Kishinev 2004-2013	296	43100	0.971	2%	21%	297	43082	0.972	1%	21%
Lerwick 2004-2013	200	31517	0.864	3%	49%	200	31510	0.867	5%	49%
Lindenberg 2004-2010	298	10527	0.964	-5%	20%	299	10509	0.965	-4%	20%
Madrid 2004-2013	401	34445	0.982	3%	14%	404	34197	0.983	5%	14%
Nantes 2004-2010	272	26956	0.978	-2%	18%	276	26519	0.978	-1%	18%
Payerne 2004-2011	341	26119	0.962	-8%	20%	341	26093	0.964	-2%	20%
Sede Boqer 2004-2012	538	30366	0.979	-7%	11%	538	30366	0.982	-5%	10%
Skukuza 2004-2007	423	10865	0.899	8%	32%	423	10863	0.899	3%	31%
Tamanrasset 2004-2013	562	35657	0.978	0%	12%	562	35651	0.982	1%	11%
Toravere 2004 - 2013	255	37016	0.952	0%	26%	255	36989	0.957	-1%	25%
Valentia 2004-2013	219	45517	0.966	0%	25%	224	44399	0.967	2%	25%
Vaulx-en-Velin 2004-2013	291	42612	0.974	1%	20%	294	42025	0.975	5%	20%
Wien 2004-2013	266	41926	0.969	-4%	23%	266	41879	0.969	-1%	23%
Zilani 2004-2009	262	21260	0.952	9%	27%	263	21198	0.955	3%	25%
All sites	317	31753		0.0%	21%	319	31624		1.2%	20%
All sites absolute bias				3.1%					2.7%	
Standard dev. of the bias				4.4%					3.4%	

Beam irradiance	Hourly values									
	HelioClim-3v4					HelioClim-3v5				
	Bn	nb	R	mbd	sd	Bn	nb	R	mbd	sd
Almeria 2004 - 2011	473	34772	0.886	12%	34%	473	34769	0.904	4%	32%
Bratislava 2004 - 2007	265	18120	0.895	-4%	48%	267	17958	0.903	2%	48%
Cabauw 2004 - 2013	217	36243	0.887	17%	57%	217	36209	0.901	14%	56%
Camborne 2004 - 2013	204	32920	0.886	23%	63%	204	32911	0.895	30%	64%
Carpentras 2004 - 2013	484	36075	0.882	1%	32%	483	36101	0.897	3%	30%
Davos 2004 - 2011	366	23924	0.789	17%	65%	366	23927	0.820	10%	61%
Geneva 2004 - 2013	285	44421	0.915	2%	46%	285	44389	0.919	20%	47%
Kassel 2004 - 2011	197	34177	0.909	7%	57%	197	34162	0.916	17%	58%
Kishinev 2004-2013	306	43100	0.897	7%	47%	306	43082	0.907	5%	45%
Lerwick 2004-2013	136	31517	0.660	46%	142%	136	31510	0.669	54%	148%
Lindenberg 2004-2010	284	10527	0.874	2%	50%	285	10509	0.879	2%	49%
Madrid 2004-2013	447	34445	0.895	6%	34%	450	34197	0.914	12%	31%
Nantes 2004-2010	270	26956	0.910	-1%	44%	273	26519	0.916	4%	43%
Payerne 2004-2011	329	26119	0.882	-6%	46%	329	26093	0.892	13%	46%
Sede Boqer 2004-2012	622	30366	0.772	-17%	29%	622	30366	0.808	-14%	28%
Skukuza 2004-2007	415	10865	0.670	19%	63%	415	10863	0.692	8%	60%
Tamanrasset 2004-2013	578	35657	0.749	13%	38%	579	35651	0.822	15%	33%
Toravere 2004 - 2013	268	37016	0.842	3%	62%	268	36989	0.865	0%	58%
Valentia 2004-2013	206	45517	0.887	-2%	59%	211	44399	0.899	4%	57%
Vaulx-en-Velin 2004-2013	300	42612	0.914	2%	42%	303	42025	0.918	12%	43%
Wien 2004-2013	245	41926	0.900	2%	51%	245	41879	0.907	11%	52%
Zilani 2004-2009	245	21260	0.846	27%	68%	246	21198	0.863	12%	62%
All sites	322	31753		6%	48%	323	31624		9%	46%
All sites absolute bias				9.4%					11.1%	
Standard dev. of the bias				13.1%					13.7%	

Diffuse irradiance	Hourly values									
	HelioClim-3v4					HelioClim-3v5				
	Dh	nb	R	mbd	sd	Dh	nb	R	mbd	sd
Almeria 2004 - 2011	128	34772	0.800	-11%	49%	128	34769	0.841	-7%	44%
Bratislava 2004 - 2007	113	18120	0.888	-4%	38%	114	17958	0.896	-7%	37%
Cabauw 2004 - 2013	138	36243	0.907	-22%	41%	138	36209	0.914	-19%	36%
Camborne 2004 - 2013	141	32920	0.897	-18%	41%	141	32911	0.894	-21%	41%
Carpentras 2004 - 2013	123	36075	0.851	-6%	44%	123	36101	0.857	-9%	43%
Davos 2004 - 2011	134	23924	0.748	-3%	59%	134	23927	0.779	0%	56%
Geneva 2004 - 2013	121	44421	0.871	-6%	45%	121	44389	0.879	-14%	44%
Kassel 2004 - 2011	118	34177	0.900	-7%	38%	118	34162	0.909	-11%	37%
Kishinev 2004-2013	121	43100	0.862	-7%	42%	121	43082	0.870	-8%	40%
Lerwick 2004-2013	133	31517	0.824	-19%	49%	133	31510	0.814	-21%	50%
Lindenberg 2004-2010	147	10527	0.895	-14%	33%	147	10509	0.893	-15%	33%
Madrid 2004-2013	117	34445	0.815	4%	48%	117	34197	0.842	-3%	45%
Nantes 2004-2010	130	26956	0.924	-9%	32%	132	26519	0.923	-12%	32%
Payerne 2004-2011	151	26119	0.863	-14%	37%	151	26093	0.885	-21%	35%
Sede Boqer 2004-2012	137	30366	0.638	10%	52%	137	30366	0.692	3%	49%
Skukuza 2004-2007	163	10865	0.766	-18%	47%	163	10863	0.815	-13%	42%
Tamanrasset 2004-2013	170	35657	0.680	-32%	62%	170	35651	0.796	-35%	56%
Toravere 2004 - 2013	115	37016	0.859	-4%	39%	115	36989	0.871	-5%	37%
Valentia 2004-2013	114	45517	0.920	-4%	33%	117	44399	0.919	-7%	33%
Vaulx-en-Velin 2004-2013	118	42612	0.879	0%	38%	119	42025	0.884	-6%	37%
Wien 2004-2013	127	41926	0.867	-12%	41%	127	41879	0.875	-16%	40%
Zilani 2004-2009	125	21260	0.825	-8%	42%	125	21198	0.862	-6%	37%
All sites	129	31753		-10%	45%	129	31624		-12%	43%
All sites absolute bias				10.9%					12.5%	
Standard dev. of the bias				14.5%					16.2%	

Global irradiance	Hourly values									
	HelioClim-3v4					HelioClim-3v5				
	Gh	nb	R	mbd	sd	Gh	nb	R	mbd	sd
Almeria 2004 - 2011	416	34772	0.981	19.5	56.8	416	34769	0.983	7.2	54.3
Bratislava 2004 - 2007	255	18120	0.971	0.7	58.5	257	17958	0.971	6.3	60.4
Cabauw 2004 - 2013	253	36243	0.967	-10.0	57.5	253	36209	0.969	-6.8	55.7
Camborne 2004 - 2013	254	32920	0.971	-0.1	56.0	254	32911	0.972	4.0	55.3
Carpentras 2004 - 2013	401	36075	0.985	1.8	47.9	400	36101	0.986	3.5	45.6
Davos 2004 - 2011	339	23924	0.933	30.0	98.5	339	23927	0.938	18.6	95.7
Geneva 2004 - 2013	286	44421	0.975	-3.0	58.0	286	44389	0.976	16.5	59.2
Kassel 2004 - 2011	236	34177	0.964	-11.1	61.0	237	34162	0.966	-2.9	59.6
Kishinev 2004-2013	296	43100	0.971	5.9	62.5	297	43082	0.972	3.6	61.2
Lerwick 2004-2013	200	31517	0.864	6.8	97.6	200	31510	0.867	10.2	98.4
Lindenberg 2004-2010	298	10527	0.964	-13.9	60.4	299	10509	0.965	-13.4	59.3
Madrid 2004-2013	401	34445	0.982	11.3	55.8	404	34197	0.983	20.1	54.9
Nantes 2004-2010	272	26956	0.978	-6.4	50.0	276	26519	0.978	-2.2	49.6
Payerne 2004-2011	341	26119	0.962	-28.4	69.5	341	26093	0.964	-5.4	69.6
Sede Boqer 2004-2012	538	30366	0.979	-35.2	59.2	538	30366	0.982	-25.4	56.2
Skukuza 2004-2007	423	10865	0.899	31.9	133.7	423	10863	0.899	12.4	131.7
Tamanrasset 2004-2013	562	35657	0.978	-0.5	69.0	562	35651	0.982	3.9	62.7
Toravere 2004 - 2013	255	37016	0.952	0.5	67.5	255	36989	0.957	-3.2	64.1
Valentia 2004-2013	219	45517	0.966	1.0	55.3	224	44399	0.967	4.6	55.9
Vaulx-en-Velin 2004-2013	291	42612	0.974	3.0	57.3	294	42025	0.975	14.9	57.9
Wien 2004-2013	266	41926	0.969	-9.3	60.3	266	41879	0.969	-1.7	60.9
Zilani 2004-2009	262	21260	0.952	22.7	70.8	263	21198	0.955	8.4	66.7
All sites	317	31753		-0.1	65.2	319	31624		3.7	64.1
All sites absolute bias				9.7					8.5	
Standard dev. of the bias				14.1					10.7	

Beam irradiance	Hourly values									
	HelioClim-3v4					HelioClim-3v5				
	Bn	nb	R	mbd	sd	Bn	nb	R	mbd	sd
Almeria 2004 - 2011	473	34772	0.886	55.1	162.7	473	34769	0.904	16.6	150.3
Bratislava 2004 - 2007	265	18120	0.895	-10.4	126.0	267	17958	0.903	4.9	128.5
Cabauw 2004 - 2013	217	36243	0.887	36.9	123.8	217	36209	0.901	30.3	121.2
Camborne 2004 - 2013	204	32920	0.886	47.6	129.1	204	32911	0.895	60.3	130.3
Carpentras 2004 - 2013	484	36075	0.882	4.5	153.8	483	36101	0.897	12.8	145.7
Davos 2004 - 2011	366	23924	0.789	63.8	238.8	366	23927	0.820	36.2	223.4
Geneva 2004 - 2013	285	44421	0.915	4.6	129.8	285	44389	0.919	58.3	134.9
Kassel 2004 - 2011	197	34177	0.909	14.2	112.8	197	34162	0.916	34.0	114.0
Kishinev 2004-2013	306	43100	0.897	20.1	142.8	306	43082	0.907	15.1	137.4
Lerwick 2004-2013	136	31517	0.660	61.8	193.0	136	31510	0.669	72.5	200.7
Lindenberg 2004-2010	284	10527	0.874	4.6	141.8	285	10509	0.879	5.4	140.6
Madrid 2004-2013	447	34445	0.895	28.4	152.7	450	34197	0.914	55.0	140.4
Nantes 2004-2010	270	26956	0.910	-1.9	117.8	273	26519	0.916	10.9	118.3
Payerne 2004-2011	329	26119	0.882	-19.4	151.6	329	26093	0.892	42.6	152.4
Sede Boqer 2004-2012	622	30366	0.772	-108.5	180.9	622	30366	0.808	-86.2	174.0
Skukuza 2004-2007	415	10865	0.670	77.3	260.2	415	10863	0.692	31.1	250.9
Tamanrasset 2004-2013	578	35657	0.749	76.6	222.7	579	35651	0.822	89.6	193.0
Toravere 2004 - 2013	268	37016	0.842	7.8	166.9	268	36989	0.865	-0.2	154.8
Valentia 2004-2013	206	45517	0.887	-4.1	121.1	211	44399	0.899	7.5	121.5
Vaulx-en-Velin 2004-2013	300	42612	0.914	6.1	124.9	303	42025	0.918	37.3	129.1
Wien 2004-2013	245	41926	0.900	5.5	125.4	245	41879	0.907	26.6	127.3
Zilani 2004-2009	245	21260	0.846	66.5	167.0	246	21198	0.863	30.5	151.5
All sites	322	31753		18.0	155.4	323	31624		28.3	150.1
All sites absolute bias				30.1					35.8	
Standard dev. of the bias				42.2					44.1	

Diffuse irradiance	Hourly values									
	HelioClim-3v4					HelioClim-3v5				
	Dh	nb	R	mbd	sd	Dh	nb	R	mbd	sd
Almeria 2004 - 2011	128	34772	0.800	-13.7	62.2	128	34769	0.841	-8.7	56.7
Bratislava 2004 - 2007	113	18120	0.888	-4.8	43.2	114	17958	0.896	-8.5	41.8
Cabauw 2004 - 2013	138	36243	0.907	-30.4	57.0	138	36209	0.914	-26.2	50.3
Camborne 2004 - 2013	141	32920	0.897	-25.1	57.3	141	32911	0.894	-29.2	57.6
Carpentras 2004 - 2013	123	36075	0.851	-7.4	54.1	123	36101	0.857	-10.8	52.2
Davos 2004 - 2011	134	23924	0.748	-4.0	79.1	134	23927	0.779	0.1	75.1
Geneva 2004 - 2013	121	44421	0.871	-6.8	53.9	121	44389	0.879	-17.0	53.6
Kassel 2004 - 2011	118	34177	0.900	-8.4	44.3	118	34162	0.909	-12.8	43.1
Kishinev 2004-2013	121	43100	0.862	-8.1	50.4	121	43082	0.870	-9.7	48.6
Lerwick 2004-2013	133	31517	0.824	-25.3	65.1	133	31510	0.814	-28.5	66.1
Lindenberg 2004-2010	147	10527	0.895	-21.0	48.7	147	10509	0.893	-22.5	48.3
Madrid 2004-2013	117	34445	0.815	4.4	56.0	117	34197	0.842	-3.3	52.7
Nantes 2004-2010	130	26956	0.924	-12.3	41.6	132	26519	0.923	-16.4	41.5
Payerne 2004-2011	151	26119	0.863	-20.9	56.1	151	26093	0.885	-32.3	53.5
Sede Boqer 2004-2012	137	30366	0.638	13.4	71.1	137	30366	0.692	4.7	67.3
Skukuza 2004-2007	163	10865	0.766	-28.6	76.1	163	10863	0.815	-21.9	68.7
Tamanrasset 2004-2013	170	35657	0.680	-54.3	105.0	170	35651	0.796	-59.1	94.8
Toravere 2004 - 2013	115	37016	0.859	-5.0	44.6	115	36989	0.871	-5.7	42.6
Valentia 2004-2013	114	45517	0.920	-4.8	38.3	117	44399	0.919	-8.7	38.5
Vaulx-en-Velin 2004-2013	118	42612	0.879	0.5	44.6	119	42025	0.884	-7.0	44.2
Wien 2004-2013	127	41926	0.867	-15.2	51.9	127	41879	0.875	-20.0	51.1
Zilani 2004-2009	125	21260	0.825	-10.5	52.1	125	21198	0.862	-7.1	46.8
All sites	129	31753		-12.3	58.1	129	31624		-15.8	55.3
All sites absolute bias				14.0					16.2	
Standard dev. of the bias				18.7					20.9	

Table a-I Site by site, for the two helioclim-3 versions, hourly global, normal beam and diffuse irradiance validation results expressed in relative and absolute values. The absolute values are given in [Wh/m²h].

For all sites, the overall values, the absolute mean bias and the standard deviation of the bias are given.

Global irradiance	Daily values									
	HelioClim-3v4					HelioClim-3v5				
	Gh	nb	R	mbd	sd	Gh	nb	R	mbd	sd
Almeria 2004 - 2011	5.04	2872	0.993	5%	7%	5.04	2872	0.995	2%	6%
Bratislava 2004 - 2007	3.26	1417	0.994	0%	12%	3.26	1417	0.994	2%	12%
Cabauw 2004 - 2013	2.89	3168	0.990	-4%	12%	2.89	3168	0.991	-3%	11%
Camborne 2004 - 2013	2.99	2793	0.992	0%	11%	2.99	2792	0.993	2%	11%
Carpentras 2004 - 2013	4.47	3229	0.996	1%	6%	4.47	3229	0.996	1%	6%
Davos 2004 - 2011	3.08	2618	0.972	9%	20%	3.08	2618	0.975	5%	19%
Geneva 2004 - 2013	3.52	3609	0.991	-1%	9%	3.52	3609	0.991	6%	10%
Kassel 2004 - 2011	2.83	2855	0.990	-5%	13%	2.83	2855	0.991	-1%	12%
Kishinev 2004-2013	3.56	3591	0.988	2%	11%	3.56	3591	0.989	1%	11%
Lerwick 2004-2013	2.63	2393	0.937	3%	34%	2.63	2393	0.938	5%	34%
Lindenberg 2004-2010	3.29	952	0.995	-5%	10%	3.29	952	0.996	-4%	10%
Madrid 2004-2013	4.47	3083	0.993	3%	8%	4.47	3083	0.994	5%	7%
Nantes 2004-2010	3.48	2106	0.996	-2%	8%	3.47	2106	0.997	-1%	8%
Payerne 2004-2011	3.63	2448	0.991	-8%	11%	3.63	2448	0.992	-2%	11%
Sede Boqer 2004-2012	5.69	2866	0.994	-7%	7%	5.69	2866	0.996	-5%	6%
Skukuza 2004-2007	4.94	932	0.973	8%	22%	4.94	932	0.973	3%	22%
Tamanrasset 2004-2013	6.22	3223	0.982	0%	8%	6.22	3223	0.988	1%	7%
Toravere 2004 - 2013	3.20	2950	0.986	0%	14%	3.20	2950	0.989	-1%	13%
Valentia 2004-2013	2.76	3610	0.987	0%	13%	2.76	3610	0.988	2%	12%
Vaulx-en-Velin 2004-2013	3.45	3589	0.989	1%	10%	3.45	3589	0.990	5%	10%
Wien 2004-2013	3.31	3368	0.990	-4%	11%	3.31	3368	0.989	-1%	11%
Zilani 2004-2009	3.11	1794	0.985	10%	19%	3.12	1784	0.989	3%	15%
All sites	3.73	2704		0.0%	12%	3.73	2704		1.2%	11%
All sites absolute bias				3.1%					2.7%	
Standard dev. of the bias				4.3%					3.3%	

Beam irradiance	Daily values									
	HelioClim-3v4					HelioClim-3v5				
	Bn	nb	R	mbd	sd	Bn	nb	R	mbd	sd
Almeria 2004 - 2011	5.73	2872	0.937	12%	24%	5.73	2872	0.960	4%	20%
Bratislava 2004 - 2007	3.38	1417	0.972	-4%	29%	3.38	1417	0.981	2%	23%
Cabauw 2004 - 2013	2.48	3168	0.946	17%	37%	2.48	3168	0.963	14%	31%
Camborne 2004 - 2013	2.40	2793	0.948	23%	41%	2.40	2792	0.957	30%	38%
Carpentras 2004 - 2013	5.40	3229	0.962	3%	19%	5.40	3229	0.962	3%	19%
Davos 2004 - 2011	3.31	2617	0.885	17%	49%	3.31	2617	0.907	10%	44%
Geneva 2004 - 2013	3.51	3609	0.956	2%	28%	3.51	3609	0.965	20%	25%
Kassel 2004 - 2011	2.36	2855	0.963	7%	34%	2.36	2855	0.970	17%	31%
Kishinev 2004-2013	3.67	3591	0.945	7%	29%	3.67	3591	0.958	5%	26%
Lerwick 2004-2013	1.79	2393	0.788	46%	101%	1.79	2393	0.794	54%	103%
Lindenberg 2004-2010	3.14	952	0.968	2%	33%	3.14	952	0.971	2%	31%
Madrid 2004-2013	4.99	3083	0.943	6%	25%	4.99	3083	0.963	12%	20%
Nantes 2004-2010	3.45	2106	0.972	-1%	25%	3.44	2106	0.980	4%	21%
Payerne 2004-2011	3.51	2448	0.961	-6%	30%	3.51	2448	0.968	13%	27%
Sede Boqer 2004-2012	6.59	2866	0.939	-17%	21%	6.59	2866	0.962	-14%	18%
Skukuza 2004-2007	4.84	932	0.909	19%	45%	4.84	932	0.914	8%	43%
Tamanrasset 2004-2013	6.40	3223	0.818	13%	32%	6.40	3223	0.893	15%	25%
Toravere 2004 - 2013	3.36	2950	0.935	3%	39%	3.36	2950	0.955	0%	32%
Valentia 2004-2013	2.60	3610	0.945	-2%	34%	2.60	3610	0.959	4%	30%
Vaulx-en-Velin 2004-2013	3.56	3589	0.964	2%	26%	3.55	3589	0.972	12%	21%
Wien 2004-2013	3.05	3368	0.957	2%	30%	3.05	3368	0.967	11%	26%
Zilani 2004-2009	2.90	1794	0.939	30%	48%	2.92	1784	0.954	12%	39%
All sites	3.78	2704		6%	33%	3.78	2703		9%	29%
All sites absolute bias				9.5%					11.1%	
Standard dev. of the bias				13.0%					13.5%	

Diffuse irradiance	Daily values									
	HelioClim-3v4					HelioClim-3v5				
	Dh	nb	R	mbd	sd	Dh	nb	R	mbd	sd
Almeria 2004 - 2011	1.55	2872	0.893	-11%	34%	1.55	2872	0.918	-7%	30%
Bratislava 2004 - 2007	1.45	1417	0.969	-4%	26%	1.45	1417	0.975	-7%	24%
Cabauw 2004 - 2013	1.58	3168	0.956	-22%	29%	1.58	3168	0.968	-19%	25%
Camborne 2004 - 2013	1.66	2793	0.961	-18%	26%	1.66	2792	0.962	-21%	26%
Carpentras 2004 - 2013	1.37	3229	0.900	-9%	31%	1.37	3229	0.900	-9%	31%
Davos 2004 - 2011	1.21	2617	0.892	-3%	41%	1.21	2617	0.904	0%	39%
Geneva 2004 - 2013	1.49	3609	0.883	-6%	30%	1.49	3609	0.913	-14%	28%
Kassel 2004 - 2011	1.41	2855	0.959	-7%	25%	1.41	2855	0.969	-11%	24%
Kishinev 2004-2013	1.45	3591	0.904	-7%	28%	1.45	3591	0.915	-8%	26%
Lerwick 2004-2013	1.76	2393	0.943	-19%	31%	1.76	2393	0.941	-21%	32%
Lindenberg 2004-2010	1.62	952	0.982	-14%	23%	1.62	952	0.983	-15%	23%
Madrid 2004-2013	1.30	3083	0.877	4%	36%	1.30	3083	0.907	-3%	32%
Nantes 2004-2010	1.66	2106	0.978	-9%	20%	1.66	2106	0.981	-12%	20%
Payerne 2004-2011	1.61	2448	0.952	-14%	26%	1.61	2448	0.969	-21%	23%
Sede Boqer 2004-2012	1.45	2866	0.800	10%	42%	1.45	2866	0.832	3%	39%
Skukuza 2004-2007	1.90	932	0.957	-18%	30%	1.90	932	0.966	-13%	27%
Tamanrasset 2004-2013	1.88	3223	0.745	-32%	48%	1.88	3223	0.855	-35%	42%
Toravere 2004 - 2013	1.44	2950	0.951	-4%	23%	1.44	2950	0.958	-5%	21%
Valentia 2004-2013	1.44	3610	0.953	-4%	22%	1.44	3610	0.956	-7%	21%
Vaulx-en-Velin 2004-2013	1.40	3589	0.898	0%	27%	1.40	3589	0.921	-6%	25%
Wien 2004-2013	1.58	3368	0.925	-12%	26%	1.58	3368	0.937	-16%	25%
Zilani 2004-2009	1.48	1794	0.959	-8%	29%	1.49	1784	0.971	-6%	24%
All sites	1.51	2704		-10%	31%	1.51	2703		-12%	29%
All sites absolute bias				11.0%					12.5%	
Standard dev. of the bias				14.4%					16.1%	

Global irradiance	Daily values									
	HelioClim-3v4					HelioClim-3v5				
	Gh	nb	R	mbd	sd	Gh	nb	R	mbd	sd
Almeria 2004 - 2011	5.04	2872	0.993	0.24	0.37	5.04	2872	0.995	0.09	0.33
Bratislava 2004 - 2007	3.26	1417	0.994	0.01	0.39	3.26	1417	0.994	0.08	0.39
Cabauw 2004 - 2013	2.89	3168	0.990	-0.11	0.35	2.89	3168	0.991	-0.08	0.33
Camborne 2004 - 2013	2.99	2793	0.992	0.00	0.34	2.99	2792	0.993	0.05	0.33
Carpentras 2004 - 2013	4.47	3229	0.996	0.04	0.25	4.47	3229	0.996	0.04	0.25
Davos 2004 - 2011	3.08	2618	0.972	0.27	0.62	3.08	2618	0.975	0.17	0.57
Geneva 2004 - 2013	3.52	3609	0.991	-0.04	0.33	3.52	3609	0.991	0.20	0.34
Kassel 2004 - 2011	2.83	2855	0.990	-0.13	0.37	2.83	2855	0.991	-0.03	0.35
Kishinev 2004-2013	3.56	3591	0.988	0.07	0.39	3.56	3591	0.989	0.04	0.38
Lerwick 2004-2013	2.63	2393	0.937	0.09	0.90	2.63	2393	0.938	0.13	0.90
Lindenberg 2004-2010	3.29	952	0.995	-0.15	0.34	3.29	952	0.996	-0.15	0.33
Madrid 2004-2013	4.47	3083	0.993	0.13	0.35	4.47	3083	0.994	0.22	0.32
Nantes 2004-2010	3.48	2106	0.996	-0.08	0.29	3.47	2106	0.997	-0.03	0.27
Payerne 2004-2011	3.63	2448	0.991	-0.30	0.39	3.63	2448	0.992	-0.06	0.40
Sede Boqer 2004-2012	5.69	2866	0.994	-0.37	0.38	5.69	2866	0.996	-0.27	0.33
Skukuza 2004-2007	4.94	932	0.973	0.37	1.11	4.94	932	0.973	0.14	1.10
Tamanrasset 2004-2013	6.22	3223	0.982	-0.01	0.51	6.22	3223	0.988	0.04	0.41
Toravere 2004 - 2013	3.20	2950	0.986	0.01	0.45	3.20	2950	0.989	-0.04	0.40
Valentia 2004-2013	2.76	3610	0.987	0.01	0.35	2.76	3610	0.988	0.06	0.34
Vaulx-en-Velin 2004-2013	3.45	3589	0.989	0.04	0.36	3.45	3589	0.990	0.17	0.33
Wien 2004-2013	3.31	3368	0.990	-0.12	0.36	3.31	3368	0.989	-0.02	0.37
Zilani 2004-2009	3.11	1794	0.985	0.30	0.58	3.12	1784	0.989	0.10	0.48
All sites	3.73	2704		0.00	0.45	3.73	2704		0.04	0.42
All sites absolute bias				0.12					0.10	
Standard dev. of the bias				0.16					0.12	

Beam irradiance	Daily values									
	HelioClim-3v4					HelioClim-3v5				
	Bn	nb	R	mbd	sd	Bn	nb	R	mbd	sd
Almeria 2004 - 2011	5.73	2872	0.937	0.67	1.38	5.73	2872	0.960	0.20	1.15
Bratislava 2004 - 2007	3.38	1417	0.972	-0.13	0.97	3.38	1417	0.981	0.06	0.79
Cabauw 2004 - 2013	2.48	3168	0.946	0.42	0.91	2.48	3168	0.963	0.35	0.77
Camborne 2004 - 2013	2.40	2793	0.948	0.56	0.98	2.40	2792	0.957	0.71	0.91
Carpentras 2004 - 2013	5.40	3229	0.962	0.14	1.03	5.40	3229	0.962	0.14	1.03
Davos 2004 - 2011	3.31	2617	0.885	0.58	1.62	3.31	2617	0.907	0.32	1.46
Geneva 2004 - 2013	3.51	3609	0.956	0.06	0.97	3.51	3609	0.965	0.72	0.87
Kassel 2004 - 2011	2.36	2855	0.963	0.17	0.80	2.36	2855	0.970	0.41	0.73
Kishinev 2004-2013	3.67	3591	0.945	0.24	1.08	3.67	3591	0.958	0.18	0.95
Lerwick 2004-2013	1.79	2393	0.788	0.81	1.80	1.79	2393	0.794	0.96	1.84
Lindenberg 2004-2010	3.14	952	0.968	0.05	1.02	3.14	952	0.971	0.06	0.96
Madrid 2004-2013	4.99	3083	0.943	0.31	1.27	4.99	3083	0.963	0.61	0.99
Nantes 2004-2010	3.45	2106	0.972	-0.02	0.87	3.44	2106	0.980	0.14	0.72
Payerne 2004-2011	3.51	2448	0.961	-0.21	1.06	3.51	2448	0.968	0.45	0.95
Sede Boqer 2004-2012	6.59	2866	0.939	-1.15	1.40	6.59	2866	0.962	-0.91	1.17
Skukuza 2004-2007	4.84	932	0.909	0.90	2.19	4.84	932	0.914	0.36	2.08
Tamanrasset 2004-2013	6.40	3223	0.818	0.85	2.07	6.40	3223	0.893	0.99	1.60
Toravere 2004 - 2013	3.36	2950	0.935	0.10	1.29	3.36	2950	0.955	0.00	1.08
Valentia 2004-2013	2.60	3610	0.945	-0.05	0.88	2.60	3610	0.959	0.09	0.79
Vaulx-en-Velin 2004-2013	3.56	3589	0.964	0.07	0.92	3.55	3589	0.972	0.44	0.76
Wien 2004-2013	3.05	3368	0.957	0.07	0.90	3.05	3368	0.967	0.33	0.79
Zilani 2004-2009	2.90	1794	0.939	0.86	1.38	2.92	1784	0.954	0.36	1.13
All sites	3.78	2704		0.22	1.24	3.78	2703		0.33	1.08
All sites absolute bias				0.36					0.42	
Standard dev. of the bias				0.49					0.51	

Diffuse irradiance	Daily values									
	HelioClim-3v4					HelioClim-3v5				
	Dh	nb	R	mbd	sd	Dh	nb	R	mbd	sd
Almeria 2004 - 2011	1.55	2872	0.893	-0.17	0.52	1.55	2872	0.918	-0.11	0.47
Bratislava 2004 - 2007	1.45	1417	0.969	-0.06	0.37	1.45	1417	0.975	-0.11	0.35
Cabauw 2004 - 2013	1.58	3168	0.956	-0.35	0.46	1.58	3168	0.968	-0.30	0.39
Camborne 2004 - 2013	1.66	2793	0.961	-0.30	0.43	1.66	2792	0.962	-0.34	0.44
Carpentras 2004 - 2013	1.37	3229	0.900	-0.12	0.42	1.37	3229	0.900	-0.12	0.42
Davos 2004 - 2011	1.21	2617	0.892	-0.04	0.50	1.21	2617	0.904	0.00	0.47
Geneva 2004 - 2013	1.49	3609	0.883	-0.08	0.44	1.49	3609	0.913	-0.21	0.42
Kassel 2004 - 2011	1.41	2855	0.959	-0.10	0.36	1.41	2855	0.969	-0.15	0.34
Kishinev 2004-2013	1.45	3591	0.904	-0.10	0.40	1.45	3591	0.915	-0.12	0.38
Lerwick 2004-2013	1.76	2393	0.943	-0.33	0.54	1.76	2393	0.941	-0.37	0.55
Lindenberg 2004-2010	1.62	952	0.982	-0.23	0.37	1.62	952	0.983	-0.25	0.37
Madrid 2004-2013	1.30	3083	0.877	0.05	0.47	1.30	3083	0.907	-0.04	0.42
Nantes 2004-2010	1.66	2106	0.978	-0.16	0.34	1.66	2106	0.981	-0.21	0.33
Payerne 2004-2011	1.61	2448	0.952	-0.22	0.42	1.61	2448	0.969	-0.34	0.38
Sede Boqer 2004-2012	1.45	2866	0.800	0.14	0.61	1.45	2866	0.832	0.05	0.56
Skukuza 2004-2007	1.90	932	0.957	-0.33	0.57	1.90	932	0.966	-0.26	0.50
Tamanrasset 2004-2013	1.88	3223	0.745	-0.60	0.90	1.88	3223	0.855	-0.65	0.78
Toravere 2004 - 2013	1.44	2950	0.951	-0.06	0.33	1.44	2950	0.958	-0.07	0.31
Valentia 2004-2013	1.44	3610	0.953	-0.06	0.31	1.44	3610	0.956	-0.11	0.31
Vaulx-en-Velin 2004-2013	1.40	3589	0.898	0.01	0.37	1.40	3589	0.921	-0.08	0.35
Wien 2004-2013	1.58	3368	0.925	-0.19	0.42	1.58	3368	0.937	-0.25	0.40
Zilani 2004-2009	1.48	1794	0.959	-0.12	0.42	1.49	1784	0.971	-0.08	0.36
All sites	1.51	2704		-0.15	0.47	1.51	2703		-0.18	0.44
All sites absolute bias				0.17					0.19	
Standard dev. of the bias				0.22					0.24	

Table a-II Site by site, for the two helioclim-3 versions, daily global, normal beam and diffuse irradiation validation results expressed in relative and absolute values. The absolute values are given in [kWh/m²h day].

For all sites, the overall values, the absolute mean bias and the standard deviation of the bias are given.

Global irradiance	Monthly values									
	HelioClim-3v4					HelioClim-3v5				
	Gh	nb	R	mbd	sd	Gh	nb	R	mbd	sd
Almeria 2004 - 2011	152.3	95	0.999	5%	3%	152.3	95	0.999	2%	2%
Bratislava 2004 - 2007	98.2	47	0.999	0%	5%	98.2	47	0.999	2%	5%
Cabauw 2004 - 2013	85.6	107	0.996	-4%	7%	85.6	107	0.997	-3%	6%
Camborne 2004 - 2013	85.3	98	0.999	0%	4%	85.3	98	0.999	2%	4%
Carpentras 2004 - 2013	123.6	117	0.999	1%	2%	123.6	117	0.999	1%	2%
Davos 2004 - 2011	85.4	95	0.994	9%	11%	85.4	95	0.996	5%	8%
Geneva 2004 - 2013	106.8	119	0.999	-1%	3%	106.8	119	0.999	6%	3%
Kassel 2004 - 2011	85.1	95	0.998	-5%	7%	85.1	95	0.998	-1%	6%
Kishinev 2004-2013	107.4	119	0.997	2%	5%	107.4	119	0.998	1%	4%
Lerwick 2004-2013	65.7	96	0.993	3%	12%	65.7	96	0.994	5%	12%
Lindenberg 2004-2010	89.7	35	0.999	-5%	4%	89.7	35	0.999	-4%	5%
Madrid 2004-2013	125.5	110	0.998	3%	4%	125.5	110	0.998	5%	4%
Nantes 2004-2010	103.1	71	0.999	-2%	3%	103.0	71	1.000	-1%	3%
Payerne 2004-2011	101.1	88	0.997	-8%	6%	101.1	88	0.999	-2%	4%
Sede Boqer 2004-2012	163.3	100	0.997	-7%	4%	163.3	100	0.999	-5%	4%
Skukuza 2004-2007	127.8	36	0.998	8%	6%	127.8	36	0.998	3%	6%
Tamanrasset 2004-2013	187.3	107	0.994	0%	4%	187.3	107	0.996	1%	3%
Toravere 2004 - 2013	86.5	109	0.993	0%	10%	86.5	109	0.995	-1%	8%
Valentia 2004-2013	83.7	119	0.997	0%	6%	83.6	119	0.999	2%	5%
Vaulx-en-Velin 2004-2013	104.0	119	0.996	1%	6%	104.0	119	0.997	5%	4%
Wien 2004-2013	99.5	112	0.998	-4%	4%	99.5	112	0.998	-1%	5%
Zilani 2004-2009	85.7	65	0.997	10%	10%	88.4	63	0.997	3%	7%
All sites	107.7	95		0.0%	6%	107.7	95		1.2%	5%
All sites absolute bias				3.1%					2.7%	
Standard dev. of the bias				4.3%					3.3%	

Beam irradiance	Monthly values									
	HelioClim-3v4					HelioClim-3v5				
	Bn	nb	R	mbd	sd	Bn	nb	R	mbd	sd
Almeria 2004 - 2011	173.3	95	0.986	12%	9%	173.3	95	0.991	4%	7%
Bratislava 2004 - 2007	102.0	47	0.994	-4%	10%	102.0	47	0.996	2%	9%
Cabauw 2004 - 2013	73.5	107	0.983	17%	16%	73.5	107	0.986	14%	14%
Camborne 2004 - 2013	68.4	98	0.984	23%	23%	68.4	98	0.984	30%	22%
Carpentras 2004 - 2013	149.2	117	0.981	3%	8%	149.2	117	0.981	3%	8%
Davos 2004 - 2011	92.1	95	0.923	17%	29%	92.1	95	0.942	10%	22%
Geneva 2004 - 2013	106.4	119	0.990	2%	8%	106.4	119	0.987	20%	9%
Kassel 2004 - 2011	70.9	95	0.992	7%	11%	70.9	95	0.991	17%	12%
Kishinev 2004-2013	110.7	119	0.987	7%	10%	110.7	119	0.981	5%	11%
Lerwick 2004-2013	44.5	96	0.942	46%	53%	44.5	96	0.947	54%	53%
Lindenberg 2004-2010	85.4	35	0.993	2%	14%	85.4	35	0.988	2%	16%
Madrid 2004-2013	139.9	110	0.975	6%	12%	139.9	110	0.983	12%	9%
Nantes 2004-2010	102.4	71	0.992	-1%	10%	102.1	71	0.995	4%	8%
Payerne 2004-2011	97.7	88	0.990	-6%	10%	97.7	88	0.990	13%	12%
Sede Boqer 2004-2012	188.8	100	0.986	-17%	8%	188.8	100	0.989	-14%	8%
Skukuza 2004-2007	125.3	36	0.987	19%	17%	125.3	36	0.990	8%	13%
Tamanrasset 2004-2013	192.8	107	0.867	13%	20%	192.8	107	0.935	15%	14%
Toravere 2004 - 2013	90.9	109	0.966	3%	22%	90.9	109	0.978	0%	16%
Valentia 2004-2013	78.9	119	0.969	-2%	18%	78.8	119	0.982	4%	15%
Vaulx-en-Velin 2004-2013	107.3	119	0.986	2%	10%	107.0	119	0.988	12%	8%
Wien 2004-2013	91.7	112	0.988	2%	10%	91.7	112	0.986	11%	11%
Zilani 2004-2009	80.2	65	0.987	30%	27%	82.7	63	0.987	12%	17%
All sites	109.1	95		5.8%	16%	109.2	95		8.8%	13%
All sites absolute bias				9.6%					11.1%	
Standard dev. of the bias				12.8%					13.5%	

Diffuse irradiance	Monthly values									
	HelioClim-3v4					HelioClim-3v5				
	Dh	nb	R	mbd	sd	Dh	nb	R	mbd	sd
Almeria 2004 - 2011	46.9	95	0.985	-11%	11%	46.9	95	0.987	-7%	10%
Bratislava 2004 - 2007	43.7	47	0.995	-4%	10%	43.7	47	0.996	-7%	11%
Cabauw 2004 - 2013	46.8	107	0.996	-22%	18%	46.8	107	0.997	-19%	16%
Camborne 2004 - 2013	47.4	98	0.997	-18%	14%	47.4	98	0.996	-21%	15%
Carpentras 2004 - 2013	37.9	117	0.964	-9%	12%	37.9	117	0.964	-9%	12%
Davos 2004 - 2011	33.7	95	0.963	-3%	22%	33.7	95	0.964	0%	21%
Geneva 2004 - 2013	45.1	119	0.979	-6%	11%	45.1	119	0.978	-14%	13%
Kassel 2004 - 2011	42.4	95	0.995	-7%	12%	42.4	95	0.995	-11%	14%
Kishinev 2004-2013	43.9	119	0.989	-7%	10%	43.9	119	0.982	-8%	11%
Lerwick 2004-2013	43.8	96	0.996	-19%	16%	43.8	96	0.996	-21%	18%
Lindenberg 2004-2010	44.3	35	0.997	-14%	12%	44.3	35	0.996	-15%	14%
Madrid 2004-2013	36.5	110	0.956	4%	15%	36.5	110	0.964	-3%	13%
Nantes 2004-2010	49.2	71	0.997	-9%	10%	49.2	71	0.997	-12%	10%
Payerne 2004-2011	44.9	88	0.993	-14%	10%	44.9	88	0.991	-21%	13%
Sede Boqer 2004-2012	41.5	100	0.932	10%	19%	41.5	100	0.913	3%	21%
Skukuza 2004-2007	49.1	36	0.993	-18%	16%	49.1	36	0.996	-13%	12%
Tamanrasset 2004-2013	56.7	107	0.853	-32%	30%	56.7	107	0.941	-35%	25%
Toravere 2004 - 2013	39.0	109	0.993	-4%	9%	39.0	109	0.994	-5%	8%
Valentia 2004-2013	43.8	119	0.997	-4%	8%	43.7	119	0.997	-7%	9%
Vaulx-en-Velin 2004-2013	42.2	119	0.978	0%	10%	42.1	119	0.975	-6%	13%
Wien 2004-2013	47.5	112	0.989	-12%	12%	47.5	112	0.988	-16%	14%
Zilani 2004-2009	41.0	65	0.995	-8%	12%	42.2	63	0.997	-6%	9%
All sites	43.7	95		-9.7%	15%	43.8	95		-12.2%	15%
All sites absolute bias				11.0%					12.5%	
Standard dev. of the bias				14.5%					16.1%	

Global irradiance	Monthly values									
	HelioClim-3v4					HelioClim-3v5				
	Gh	nb	R	mbd	sd	Gh	nb	R	mbd	sd
Almeria 2004 - 2011	152.3	95	0.999	7.13	4.17	152.3	95	0.999	2.65	3.29
Bratislava 2004 - 2007	98.2	47	0.999	0.29	4.63	98.2	47	0.999	2.40	4.61
Cabauw 2004 - 2013	85.6	107	0.996	-3.38	6.20	85.6	107	0.997	-2.29	5.45
Camborne 2004 - 2013	85.3	98	0.999	-0.02	3.35	85.3	98	0.999	1.34	3.32
Carpentras 2004 - 2013	123.6	117	0.999	1.08	2.46	123.6	117	0.999	1.08	2.46
Davos 2004 - 2011	85.4	95	0.994	7.57	9.11	85.4	95	0.996	4.69	6.44
Geneva 2004 - 2013	106.8	119	0.999	-1.11	3.19	106.8	119	0.999	6.15	3.27
Kassel 2004 - 2011	85.1	95	0.998	-3.99	6.36	85.1	95	0.998	-1.03	4.77
Kishinev 2004-2013	107.4	119	0.997	2.15	5.00	107.4	119	0.998	1.31	4.64
Lerwick 2004-2013	65.7	96	0.993	2.24	7.93	65.7	96	0.994	3.35	7.72
Lindenberg 2004-2010	89.7	35	0.999	-4.18	3.92	89.7	35	0.999	-4.01	4.22
Madrid 2004-2013	125.5	110	0.998	3.53	4.72	125.5	110	0.998	6.24	4.68
Nantes 2004-2010	103.1	71	0.999	-2.42	3.14	103.0	71	1.000	-0.84	2.66
Payerne 2004-2011	101.1	88	0.997	-8.43	5.79	101.1	88	0.999	-1.61	4.20
Sede Boqer 2004-2012	163.3	100	0.997	-10.68	6.90	163.3	100	0.999	-7.70	5.88
Skukuza 2004-2007	127.8	36	0.998	9.64	8.22	127.8	36	0.998	3.75	8.05
Tamanrasset 2004-2013	187.3	107	0.994	-0.15	8.08	187.3	107	0.996	1.29	6.53
Toravere 2004 - 2013	86.5	109	0.993	0.16	8.37	86.5	109	0.995	-1.10	6.61
Valentia 2004-2013	83.7	119	0.997	0.38	5.19	83.6	119	0.999	1.73	4.20
Vaulx-en-Velin 2004-2013	104.0	119	0.996	1.07	6.25	104.0	119	0.997	5.27	4.43
Wien 2004-2013	99.5	112	0.998	-3.50	4.22	99.5	112	0.998	-0.62	4.75
Zilani 2004-2009	85.7	65	0.997	8.21	8.78	88.4	63	0.997	2.81	6.52
All sites	107.7	95		0.03	5.99	107.7	95		1.26	5.05
All sites absolute bias				3.34					2.86	
Standard dev. of the bias				4.60					3.55	

Beam irradiance	Monthly values									
	HelioClim-3v4					HelioClim-3v5				
	Bn	nb	R	mbd	sd	Bn	nb	R	mbd	sd
Almeria 2004 - 2011	173.3	95	0.986	20.18	14.96	173.3	95	0.991	6.09	12.35
Bratislava 2004 - 2007	102.0	47	0.994	-3.99	10.13	102.0	47	0.996	1.89	9.15
Cabauw 2004 - 2013	73.5	107	0.983	12.49	11.58	73.5	107	0.986	10.24	10.26
Camborne 2004 - 2013	68.4	98	0.984	16.01	15.94	68.4	98	0.984	20.23	15.02
Carpentras 2004 - 2013	149.2	117	0.981	3.94	12.27	149.2	117	0.981	3.94	12.27
Davos 2004 - 2011	92.1	95	0.923	16.07	27.09	92.1	95	0.942	9.11	20.50
Geneva 2004 - 2013	106.4	119	0.990	1.71	8.40	106.4	119	0.987	21.74	9.98
Kassel 2004 - 2011	70.9	95	0.992	5.12	7.48	70.9	95	0.991	12.23	8.58
Kishinev 2004-2013	110.7	119	0.987	7.26	11.30	110.7	119	0.981	5.48	12.16
Lerwick 2004-2013	44.5	96	0.942	20.30	23.66	44.5	96	0.947	23.81	23.48
Lindenberg 2004-2010	85.4	35	0.993	1.38	11.87	85.4	35	0.988	1.61	13.93
Madrid 2004-2013	139.9	110	0.975	8.91	16.37	139.9	110	0.983	17.11	12.65
Nantes 2004-2010	102.4	71	0.992	-0.74	10.15	102.1	71	0.995	4.09	8.39
Payerne 2004-2011	97.7	88	0.990	-5.75	9.94	97.7	88	0.990	12.63	11.24
Sede Boqer 2004-2012	188.8	100	0.986	-32.94	14.93	188.8	100	0.989	-26.17	15.92
Skukuza 2004-2007	125.3	36	0.987	23.32	20.74	125.3	36	0.990	9.40	16.79
Tamanrasset 2004-2013	192.8	107	0.867	25.52	39.24	192.8	107	0.935	29.85	26.75
Toravere 2004 - 2013	90.9	109	0.966	2.64	19.96	90.9	109	0.978	-0.06	14.48
Valentia 2004-2013	78.9	119	0.969	-1.56	14.19	78.8	119	0.982	2.81	11.88
Vaulx-en-Velin 2004-2013	107.3	119	0.986	2.18	10.82	107.0	119	0.988	13.16	8.89
Wien 2004-2013	91.7	112	0.988	2.07	9.26	91.7	112	0.986	9.95	9.83
Zilani 2004-2009	80.2	65	0.987	23.76	21.32	82.7	63	0.987	10.27	14.22
All sites	109.1	95		6.32	17.19	109.2	95		9.56	14.36
All sites absolute bias				10.42					12.11	
Standard dev. of the bias				14.02					14.74	

Diffuse irradiance	Monthly values									
	HelioClim-3v4					HelioClim-3v5				
	Dh	nb	R	mbd	sd	Dh	nb	R	mbd	sd
Almeria 2004 - 2011	46.9	95	0.985	-5.02	5.35	46.9	95	0.987	-3.20	4.74
Bratislava 2004 - 2007	43.7	47	0.995	-1.86	4.44	43.7	47	0.996	-3.24	4.75
Cabauw 2004 - 2013	46.8	107	0.996	-10.29	8.32	46.8	107	0.997	-8.87	7.31
Camborne 2004 - 2013	47.4	98	0.997	-8.43	6.52	47.4	98	0.996	-9.79	7.00
Carpentras 2004 - 2013	37.9	117	0.964	-3.35	4.66	37.9	117	0.964	-3.35	4.66
Davos 2004 - 2011	33.7	95	0.963	-1.02	7.39	33.7	95	0.964	0.03	6.96
Geneva 2004 - 2013	45.1	119	0.979	-2.53	4.81	45.1	119	0.978	-6.36	5.98
Kassel 2004 - 2011	42.4	95	0.995	-3.03	5.13	42.4	95	0.995	-4.60	5.95
Kishinev 2004-2013	43.9	119	0.989	-2.93	4.49	43.9	119	0.982	-3.52	4.85
Lerwick 2004-2013	43.8	96	0.996	-8.30	7.07	43.8	96	0.996	-9.34	7.67
Lindenberg 2004-2010	44.3	35	0.997	-6.33	5.50	44.3	35	0.996	-6.75	6.05
Madrid 2004-2013	36.5	110	0.956	1.36	5.34	36.5	110	0.964	-1.03	4.89
Nantes 2004-2010	49.2	71	0.997	-4.65	4.72	49.2	71	0.997	-6.14	5.04
Payerne 2004-2011	44.9	88	0.993	-6.19	4.68	44.9	88	0.991	-9.58	6.01
Sede Boqer 2004-2012	41.5	100	0.932	4.06	7.77	41.5	100	0.913	1.41	8.83
Skukuza 2004-2007	49.1	36	0.993	-8.62	7.80	49.1	36	0.996	-6.62	5.82
Tamanrasset 2004-2013	56.7	107	0.853	-18.08	17.14	56.7	107	0.941	-19.69	14.02
Toravere 2004 - 2013	39.0	109	0.993	-1.71	3.34	39.0	109	0.994	-1.93	3.09
Valentia 2004-2013	43.8	119	0.997	-1.85	3.50	43.7	119	0.997	-3.23	3.81
Vaulx-en-Velin 2004-2013	42.2	119	0.978	0.17	4.40	42.1	119	0.975	-2.48	5.28
Wien 2004-2013	47.5	112	0.989	-5.70	5.82	47.5	112	0.988	-7.47	6.45
Zilani 2004-2009	41.0	65	0.995	-3.42	5.12	42.2	63	0.997	-2.39	3.74
All sites	43.7	95		-4.25	6.73	43.8	95		-5.33	6.52
All sites absolute bias				4.81					5.47	
Standard dev. of the bias				6.33					7.04	

Table a-III Site by site, for the two helioclim-3 versions, monthly global, normal beam and diffuse irradiation validation results expressed in relative and absolute values. The absolute values are given in [kWh/m²h day].

For all sites, the overall values, the absolute mean bias and the standard deviation of the bias are given.